

รายงานวิจัยฉบับสมบูรณ์

แบบจำลองทางคณิตศาสตร์สำหรับคำนวณการ
เคลื่อนที่ของตะกอนและการเปลี่ยนแปลงของพื้น
ท้องทะเลภายใต้การกระทำของคลื่น
(ส่วนที่ 1 Hydrodynamics)

โดย นายวิญญู รัตนปิติกรณ์

กุมภาพันธ์ 2544

Final Report

Mathematical Modeling for Cross Shore Sediment

Transport and Beach Deformation under Regular and

Irregular Waves (Part 1 Hydrodynamics)

By Mr. Winyu Rattanapitikon

February, 2001

รายงานวิจัยฉบับสมบูรณ์

แบบจำลองทางคณิตศาสตร์สำหรับคำนวณการเคลื่อนที่ของ ตะกอนและ การเปลี่ยนแปลงของพื้นท้องทะเลภายใต้การ กระทำของคลื่น (ส่วนที่ 1 Hydrodynamics)

นายวิญญู รัตนปิติกรณ์
ภาควิชาวิศวกรรมโยธา สถาบันเทคโนโลยีนานาชาติสิรินธร
มหาวิทยาลัยธรรมศาสตร์

สนับสนุนโดย สำนักงานกองทุนสนับสนุนการวิจัย

Acknowledgments

The author wishes to express his gratitude and sincere appreciation to his mentor, Prof. Tomoya Shibayama for his comments, and encouragement made throughout this study.

The author is thankful to the Thailand Research Fund and Sirindhorn International Institute of Technology for providing the financial support which enabled him to perform this research.

Sincere appreciation is expressed to the previous researchers, listed in Table 5.1 on page 110, for supplying the valuable experimental results to the public.

The author wishes to thank his graduate students (Ms. Piyamam Leangruxa, Mr. Thirapat Vivattanasirisak, and Ms. Romanee Karunchintadit) for their help in preparing some parts of this report.

To his wife, for her patience and understanding.

Abstract

Project Code: PDF/78/2540

Project Title: Mathematical Modeling for Cross Shore Sediment Transport and Beach

Deformation under Regular and Irregular Waves

Investigator: Mr. Winyu Rattanapitikon, D.Eng., Asst. Prof., Dept. of Civil Engineering,

Sirindhorn International Institute of Technology, Thammasat University,

E-mail Address: winyu@siit.tu.ac.th

Project Period: 3.5 years (1 Sep. 1997 – 28 Feb. 2001)

Objectives: The main objective of this study is to develop a mathematical model for computing beach deformation under the action of regular and irregular waves. The beach deformation model can be separated into two main parts, i.e., hydrodynamics and sediment transport. The present study concentrates only on the hydrodynamics part, which consists of breaker height model, wave model and undertow model.

Methodology: The models are developed based on the analysis of the related existing models. To make the models reliable, wide range and large amount of published experimental results are used to calibrate and verify the models.

Results: Reliable 3 mathematical models, i.e., breaker height model, wave model and undertow model.

Discussion Conclusion: Based on a wide range and large amount of published experimental results, reliable models are developed for computing breaking wave height, wave height transformation, and undertow velocity. The accuracy of the present models and some existing models are also compared. The comparisons show that the present models give better agreement than those of existing models.

Suggestions: It is better to continue part 2 (sediment transport and beach deformation model).

Keywords: wave, wave breaking, energy dissipation, undertow, current.

บทคัดย่อ

Project Code: PDF/78/2540

Project Title: แบบจำลองทางคณิตศาสตร์สำหรับคำนวณการเคลื่อนที่ของตะกอนและ การเปลี่ยน

แปลงของพื้นท้องทะเลภายใต้การกระทำของคลื่น

investigator: ผศ.ดร.วิญญ รัดนปิดิกรณ์ ภาควิชาวิศวกรรมโยชา สถาบันเทคโนโลยีนานาชาติสิริน

ธร มหาวิทยาลัยธรรมศาสตร์ ปทุมธานี

E-mail Address: winyu@siit.tu.ac.th

Project Period: 3.5 ปี (1 ก.ย. 2540 – 28 ก.พ. 2544)

Objectives: วัตถุประสงค์หลักของโครงการคือ พัฒนาแบบจำลองทางคณิตศาสตร์สำหรับคำนวณ การเปลี่ยนแปลงของพื้นท้องทะเล (beach deformation model) ภายใต้การกระทำของคลื่นแบบ regular และ irregular แบบจำลองการเปลี่ยนแปลงของพื้นท้องทะเล สามารถแบ่งออกเป็น 2 ส่วน ใหญ่ ๆคือ Hydrodynamics และ Sediment Transport แต่เนื่องจาก แบบจำลองการเปลี่ยนแปลงของ พื้นท้องทะเล ครอบคลุมเนื้อหาค่อนข้างกว้าง ดังนั้นโครงการนี้จะเน้นเฉพาะส่วนของ Hydrodynamics ซึ่งประกอบด้วย 3 แบบจำลองย่อย ได้แก่ breaker height model, wave model, และ undertow model

Methodology: รวบรวมข้อมูลผลการทดลอง และแบบจำลองทางคณิตศาสตร์ที่นักวิจัยในอดีตใค้ทำ ไว้ เพื่อใช้สำหรับการวิเคราะห์ และ พัฒนาแบบจำลองสำหรับคำนวณ การเปลี่ยนแปลงความสูงคลื่น และความเร็วของกระแสน้ำ ภายใต้การกระทำของคลื่นแบบ regular และ irregular

Results: แบบจำลองทางคณิตศาสตร์ 3 แบบจำลอง คือ breaker height model, wave model, และ undertow model

Discussion Conclusion: การศึกษาครั้งนี้ได้ทำการพัฒนาแบบจำลอง Hydrodynamics ขึ้น จาก ฐานข้อมูลจำนวนมาก และยังได้ทำการเปรียบเทียบแบบจำลองนี้กับแบบจำลองที่นักวิจัยท่านอื่นเคย เสนอไว้ ผลของการเปรียบเทียบแสดงให้เห็นว่าแบบจำลองนี้ให้ผลการการคำนวณดีกว่าแบบจำลอง อื่น ซึ่งทำให้มั่นใจได้ว่าแบบจำลองนี้ สามารถนำไปใช้ได้ในกรณีทั่วๆไป

Suggestions: ควรจะทำต่อใน phase ที่สอง คือส่วนของ Sediment Transport Model และ beach deformation model

Keywords: คลื่น คลื่นแตก การสูญเสียพลังงาน กระแสน้ำ

Executive Summary

The goal of this study is to develop the mathematical model for computing beach deformation under the action of regular and irregular waves. The beach deformation model can be separated into two main parts, i.e., hydrodynamics and sediment transport. Due to the time constrain, the present study concentrates only on the hydrodynamics part. The purpose of the present study is to develop the models for computing breaker height, wave height transformation and undertow velocity under the action of regular and irregular waves.

During the last few decades, many theories have been developed and experimental studies, both in laboratory and in the field, have been carried out to draw a clearer picture of wave and undertow. Considerable amount of knowledge on the mechanism of wave and undertow has been accumulated so far. However, it has not reached to a satisfactory level. Owing to the complexity of the wave breaking mechanism, full description of the mechanism of the wave and undertow has not yet been developed. At the present state of knowledge, clearly any type of mathematical models for computing wave and undertow inside the surf zone have to be based on empirical or semi-empirical formulas. Most of the models were developed with the limited experimental conditions. Therefore their validity is limited according to the range of experimental conditions which were employed in the calibration. The evidence is that there are so many models exist. Also it is logical to expect that a relatively new model based on more experimental results than the previous ones should be the most reliable ones.

The present models for regular waves are developed based on the analysis of the related existing models and then the models are modified for irregular waves. Wide range and large amount of published experimental results are used to calibrate and verify the models. The accuracy of the present models are compared with the 36 existing models (20 models for breaking height, 9 models for wave height, and 7 models for undertow). It appears that the present models give better agreement than those of the existing models.

V.

CONTENTS

A	cknowledgments	iii
Α	bstract	iv
E	xecutive Summary	vi
Li	st of Symbols	ix
Li	st of Figures	xi
Li	st of Tables	xiv
1	INTRODUCTION	1
	1.1 General	1
	1.2 Scope and Objective of Study	3
	1.3 Organization of Report	3
2	WAVE HEIGHT TRANSFORMATION	4
	2.1 Breaker Height Formulas	5
	2.1.1 Formula development	7
	2.1.2 Formula examinations	13
	2.2 Regular Wave Height Transformation	15
	2.2.1 Energy dissipation	15
	2.2.2 Breaking location	23
	2.2.3 Wave model structure and results	24
	2.3 Irregular Wave Height Transformation	28
	2.3.1 Model development	28
	2.3.2 Model calibration	30
	2.3.3 Model verification	35
3	UNDERTOW VELOCITY	39
	3.1 Undertow Velocity Induced by Regular Waves	39
	3.1.1 Governing equation	40
	3.1.2 Shear stress and eddy viscosity coefficient	42
	3.1.3 Mean undertow velocity	50
	3.1.4 Recommended procedure for computation of undertow profile	60
	3.1 5 Model verification	60
	3.2 Undertow Velocity Induced by Irregular Waves	72
	3.2.1 Profile of undertow velocity	73

	3.2.2 Mean undertow velocity	79
4	MODELS COMPARISONS	82
	4.1 Breaker Height Formulas	82
	4.1.1 Description of the breaker height formulas	83
	4.1.2 Comparison of the breaker height formulas	88
	4.2 Wave Models	90
	4.2.1 Energy dissipation for regular breaking waves	92
	4.2.2 Energy dissipation for irregular breaking waves	97
	4.3 Undertow Models	102
	4.3.1 Mean undertow velocity induced by regular waves	103
	4.3.2 Mean undertow velocity induced by irregular waves	106
5	CONCLUSIONS	108
RI	EFERENCES -	111
0	UTPUT	119
ΑI	PPENDIX: PAPER REPRINTS	120
	A.1 Energy Dissipation Model for Regular and Irregular Breaking Waves	120
	A.2 Simple Model for Undertow Profile	141
	A.3 Verification and Modification of Breaker Height Formulas	172

List of Symbols

A cross-sectional area of surface roller coefficient (n = 1, 2, 3, ...) a_{*} R breaker coefficient B_{a} wave shape parameter C_{μ} coefficient (n = 1, 2, 3, ...) phase velocity C C group velocity phase velocity related to the peak spectral wave period Cp $D_{\scriptscriptstyle H}$ rate of energy dissipation due wave breaking d water depth at wave trough E wave energy density E_{-} local mean energy density E_{-} stable energy density ER, root mean square relative error of the data group ER average root mean square relative error ER root mean square relative error g acceleration due to gravity H wave height H_A wave height at breaking point H, incident wave height H_{\bullet} deepwater wave height H. stable wave height H ___ root mean square wave height h water depth h, water depth at breaking still water depth h_ h_ still water depth at breaking point h_ still water depth at transition point K_ coefficient (n = 1, 2, 3, ...) k, coefficient (n = 1, 2, 3, ...) wave number related to the peak spectral wave period k.

- k wave number
- L wavelength
- L_a deepwater wavelength
- L, wavelength at breaking
- L_p wavelength related to the peak spectral wave period
- m local bottom slope
- m_a average bottom slope
- m_h bottom slope at breaking
- Q transport of water across the bore
- Q_h fraction of breaking waves
- rms root mean square
- $S_{\star\star}$ normal radiation stress in x -direction
- T wave period
- T_n peak spectral wave period
- t time
- $U_{m} = x$ -component of mean steady current below trough level
- U_{\star} contribution to U_{\star} from mass flux by surface roller
- U_{\bot} contribution to U_{\bot} from mass flux by wave motion
- U time-averaged velocity component in x -direction
- \hat{u} amplitude of horizontal water particle velocity at the mean water level
- x horizontal coordinate in wave direction
- z vertical coordinate
- z_o height of bottom roughness
- $\vec{\zeta}$ wave set-up or set-down
- θ mean wave angle
- ρ water density
- σ angular frequency
- τ shear stress on x z plane in x direction
- v, \time-averaged eddy viscosity coefficient
- Γ stable wave factor
- Γ_i stable wave factor of irregular wave
- β proportionality constant

List of Figures

Figure		Page
1.1	Basic structure of the beach deformation model	2
2.1	Relationship between $H_{\it b}$ / $L_{\it o}$ and $h_{\it b}$ / $L_{\it o}$ for the case of breaking wave on	8
	horizontal slope (measured data from Hattori and Aono, 1985; Horikawa and	
	Kuo, 1966; and Nagayama, 1983)	
2.2	Relationship between $H_{_b}$ / $L_{_o}$ and $H_{_o}$ / $L_{_o}$ for the case of breaking wave	9
	on horizontal slope (measured data from Hattori and Aono, 1985; Horikawa	
	and Kuo, 1966; and Nagayama, 1983)	
2.3	Relationship between slope effect coefficient ($S_{\scriptscriptstyle \parallel}$) and bottom slope	10
	(measured data from 24 sources shown in Table 2.1)	
2.4	Relationship between slope effect coefficient S_2 and bottom slope	11
	(measured data from 24 sources shown in Table 2.1)	
2.5	Relationship between $H_{\it b}$ / $L_{\it o}$ and $H_{\it o}$ / $L_{\it o}$ (measured data from 24	12
	sources shown in Table 2.1)	
2.6	Comparison between measured and computed breaking wave heights from	14
	the PS1 formula (measured data from 24 sources shown in Table 2.1)	
2.7	Relationship between Γ and h/\sqrt{LH} (laboratory data from Kajima et al.,	21
	1983)	
2.8	Comparison between computed and measured wave heights inside the surf	23
	zone (measured data from Table 2.3)	
2.9	Comparison between computed and measured wave heights (measured	26
	data from Kajima et al., 1983)	
2.10	Examples of computed and measured wave height transformations	26
	(measured data from Kajima et al., 1983, cases 2.1, 2.2, 2.3, and 3.1)	
2.14	Examples of computed and measured wave height transformations	27
	(measured data from Kajima et al., 1983, cases 3.2, 3.4, 4.1, 4.2, 4.3, 5.2,	
	6.1, and 6.2)	
2.12	Comparison between computed and measured rms wave height for 128	31
	cases of large-scale experiments (measured data from Kraus and Smith,	
	1994)	
2.13	Examples of computed and measured rms wave height transformation for	33

	Test No. S110-S160 (measured data from Kraus and Smith, 1994)	
2.14	Examples of computed and measured rms wave height transformation for	34
	Test No. ST70-STKO (measured data from Kraus and Smith, 1994)	
2.15	Comparison between computed and measured rms wave height for 12	36
	cases of small-scale experiments (measured data from Smith and Kraus,	
	1990)	
2.16	Examples of computed and measured rms wave height transformation for	36
	incident rms wave height of 10 cm, peak period of 1.75 s, and four bottom	
	conditions (measured data from Smith and Kraus, 1990)	
2.17	Comparison between computed and measured rms wave height for 8	38
	cases of field experiments (measured data from Smith et al., 1993, and	
	Thornton and Guza, 1986)	
2.18	Examples of computed and measured rms wave height transformation for	38
	cases 1000 and 1600 (measured data from Smith et al., 1993)	
2.19	Examples of computed and measured rms wave height transformation for	38
	cases 3Feb and 5Feb (measured data from Thornton and Guza, 1986)	
3.1	Comparison between measured and computed undertow \boldsymbol{U} inside the surf	46
	zone; the mean velocity $U_{\mbox{\tiny meas}}$ is given data (measured data from 4 sources	
	as shown in Table 3.2)	
3.2	Examples of measured and computed undertow profiles in which the mean	47
	velocity $U_{\mathbf{m}}$ is given data (measured data from Nadaoka et al., 1982;	
	Hansen and Svendsen, 1984; and Cox et al., 1994)	
3.3	Examples of measured and computed undertow profiles in which the mean	48
	velocity U_{m} is given data (measured data from Okayasu et al., 1988)	
3.4	Comparison between measured and computed wave shape parameter $\boldsymbol{B}_{\boldsymbol{\sigma}}$	51
	(measured data from Hansen and Svendsen, 1984; and Okayasu et al.,	
	1988)	
3.5	Comparison between measured and computed mean velocity $\boldsymbol{U}_{\mathrm{m}}$ inside the	58
	surf zone (measured data from 4 sources as shown in Table 3.2)	
3.6	Examples of cross-shore variations of measured and computed mean	59
	velocity, $U_{\mbox{\tiny m}}$, inside the surf zone (measured data from 4 sources as shown	
	in Table 3.2)	
3.7	Comparison between measured and computed U for all points of the data	64
	(measured data from 4 sources of small-scale experiments as shown in	

	Table 3.5)	
3.8	Examples of measured and computed undertow profiles (measured data	65
	from Nadaoka et al., 1982; Hansen and Svendsen, 1984; and Cox et al.,	
	1994)	
3.9	Examples of measured and computed undertow profiles (measured data	66
	from Okayasu et al., 1988)	
3.10	Comparison between measured and computed U for all points of the	69
	measurements (measured data from 2 sources of large-scale experiments	
	as shown in Table 3.6)	
3.11	Measured bottom topography and wave height variation (measured data	70
	from CRIEPI, 1983, case 6.1, time = 53.6 hr)	
3.12	Computed and measured undertow profiles (measured data from CRIEPI,	70
,	1983, case 6.1, time = 53.6 hr)	
3.13	Measured bottom topography and wave height variation (measured data	71
	from SUPERTANK, 1994, case s0510a)	
3.14	Computed and measured undertow profiles (measured data from	71
	SUPERTANK, 1994, case s0510a)	
3.15	Comparison between measured and computed the undertow velocity, \boldsymbol{U} ,	77
	induced by irregular wave actions (measured data from Table 3.8)	
3.16	Examples of measured and computed undertow profiles induced by irregular	78
	wave actions (measured data from Table 3.8)	
3.17	Comparison between measured and computed mean undertow velocity,	80
	$U_{\scriptscriptstyle{ m m}}$, induced by irregular wave actions (measured data from Table 3.8)	
3.18	Examples of cross-shore variations of measured and computed mean	80
	undertow velocity, $U_{\scriptscriptstyle{ m m}}$, induced by irregular wave actions (measured data	
	from Table 3.8, except SUPERTANK data)	
3.19	Examples of cross-shore variations of measured and computed mean	81
X.	undertow velocity, $U_{\hspace{-0.1em}\text{\tiny m}}$, induced by irregular wave actions (measured data	
	from SUPERTANK, 1994)	
4.1	Definition sketch of the bore concept	92

List of Tables

Table		Page
2.1	Summary of collected experimental data used to validate the breaker height	ϵ
	formulas	
2.2	The root mean square relative error ($\it ER$) of each formula for four groups of	14
	bottom slope and all cases	
2.3	Summary of collected experimental data used to validate the present	16
	models	
2.4	Root mean square relative error ($\dot{\it ER}$) of the four possible forms of $D_{\it B}$	20
2.5	Root mean square relative error (ER) of Dally's model and present model	22
2.6	Summary of collected experimental data used to validate the present	28
	models	
2.7	Root mean square relative error ($\it ER$) of the present model comparing with	32
	irregular wave data of Kraus and Smith (1994)	
2.8	Root mean square relative error (ER) of the present model	37
3.1	Summary of collected laboratory data used to validate the present model	41
3.2	Root mean square relative error (ER) of computed undertow from Eq.	49
	(3.14) in which measured $U_{\it m}$ is the given data	
3.3	Results of regression analysis of U_{\star} and rms relative error (ER) of the	53
	four possible forms of $U_{\scriptscriptstyle\mathrm{W}}$ (using measured data at the breaking point)	
3.4	Results of regression analysis of $U_{\rm r}$ and ${\it rms}$ relative error (${\it ER}$) of the ten	57
	possible forms of $\boldsymbol{U}_{\mathbf{r}}$ (using measured data at the breaking point and inner	
	surf zone)	
3.5	Root mean square relative error ($\it ER$) of the present model comparing with	63
	the small-scale experiments	
3.6	Root mean square relative error ($\it ER$) of the present model comparing with	68
	the large-scale laboratory data	
3.7	Summary of root mean square relative error ($\it ER$) of the present model	69
	comparing with measured data of each data source	
3.8	Summary of collected experimental data	72
3.9	Root mean square relative error ($\it ER$) of the Eq. (3.58) comparing with the	74
	experiment performed under irregular wave actions	

3.10	Summary of rms relative error (ER) of each data source	76
3.11	Summary of collected experimental data and $\it rms$ relative error ($\it ER$) of the	79
	Eq. (3.59)	
4.1	Summary of collected experimental data used to validate the formulas	84
4.2	The root mean square relative error (ER) of each formula for four groups	89
	of bottom slope and all cases	
4.3a	Summary of collected experimental data of regular waves	91
4.3b	Summary of collected experimental data of irregular waves	91
4.4	The error $ER_{\rm g}$ for 2 groups of experiment scales, and $ER_{\rm avg}$ of each	96
	model comparing with regular wave data shown in Table 4.3a	
4.5	The error $ER_{\rm g}$ for 3 groups of experiment scales, and $ER_{\rm avg}$ of each	101
	model comparing with irregular wave data shown in Table 4.3b	
4.6a	Summary of collected experimental data for regular breaking waves	103
4.6b	Summary of collected experimental data for irregular breaking waves	103
4.7	Verification results of Eqs. (4.51)-(4.55) (measured data at the breaking	105
	point and inner surf zone from Nadaoka et al., 1982; Hansen and	
	Svendsen, 1984; Okayasu et al., 1988; and Cox et al., 1994)	
4.8	Verification results of Eqs. (4.56) - (4.59) (measured data from Dette and	107
	Uliczka, 1986; Okayasu and Katayama, 1992; SUPERTANK, 1994; Shimisu	
	and Ikeno, 1996; and Rodriguez et al., 1994)	
5.1	Sources and number of collected data for present study	110

Chapter 1: INTRODUCTION

1.1 General

In recent years, the coastal region has become an area of intense human activity for industry and recreation. It is also an important area for tsunami and storm surge protection. The need for reliable predictions of beach response to the changes in hydrodynamic conditions, or to the construction of man-made structures, is increasing due to an increase of human activities on the coast.

Figure 1.1 shows the typical structure of beach deformation model. The calculation of beach deformation is composed of six main parts, i.e., input data, wave, undertow velocity, sediment concentration, sediment transport, and profile change. The wave model is used to compute wave height transformation across beach. From the computed wave height, undertow velocity, sediment concentration and sediment transport rate can be computed. Then new beach profile can be computed from the mass conservation equation. The new beach profile will feed-back into the wave model and causes wave height changes. This yields the loop of dynamic beach deformation.

The beach deformation model can be also separated into two main parts, i.e., hydrodynamics and sediment transport. The present study concentrates only on the hydrodynamics part (wave and undertow models). In the beach deformation model, the hydrodynamics part should be kept as simple as possible because of the frequent updating of wave field for accounting the variability of the change of beach profiles.

During the last few decades, many theories have been developed and experimental studies, both in laboratory and in the field, have been carried out to draw a clearer picture of wave and undertow. Considerable amount of knowledge on the mechanism of wave and undertow has been accumulated so far. However, it has not reached to a satisfactory level. Owing to the complexity of the wave breaking mechanism, full description of the mechanism of the wave and undertow has not yet been developed. At the present state of knowledge, clearly any type of numerical model for computing wave and undertow has to be based on empirical or semi-empirical formulas calibrated with the experimental results. However most of the models were developed with the limited experimental conditions. Therefore their validity is limited according to the range of experimental conditions which were employed in the calibration. The evidence is that there are so many models exist.

In the past, we could not develop a model based on a large amount of experimental results covering a wide range of test conditions, because they did not exist. However, at present, the experimental results obtained by many researchers have been accumulated and a large amount of experimental results have become available. It is a good time to develop models based on the large amount and wide range of experimental results. Also it is logical to expect that a relatively new models based on more experimental results than the previous ones should be the most reliable ones if the accuracy is in the acceptable range.

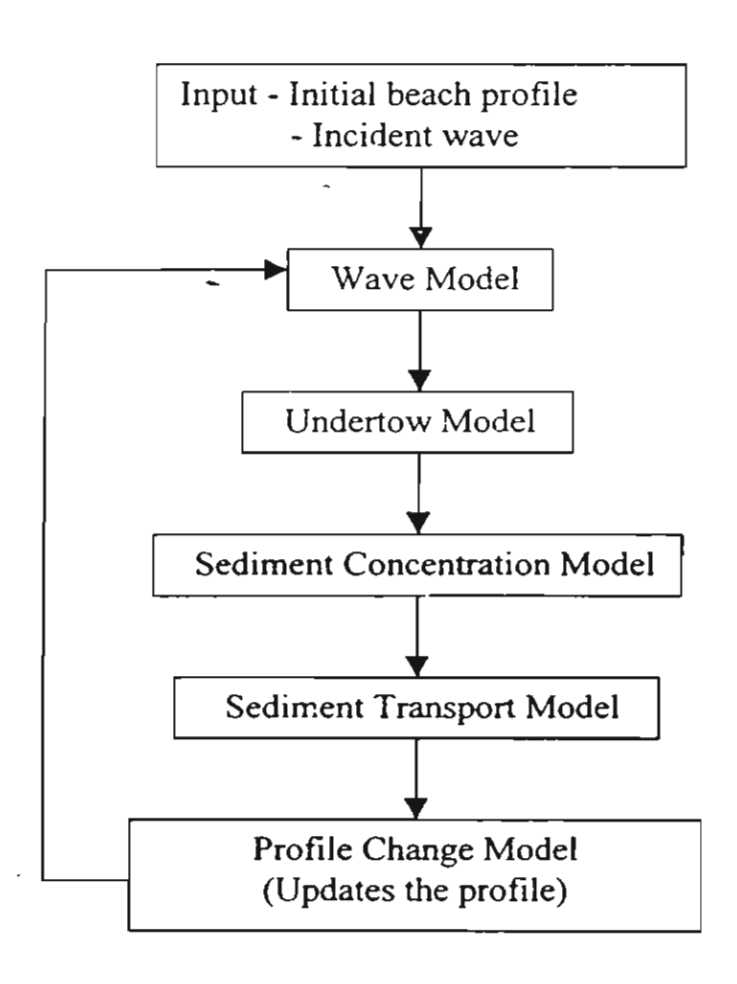


Figure 1.1: Basic structure of the beach deformation model.

1.2 Scope and Objective of Study

The scope and objectives of the present study can be described as follows:

- This study focuses mainly on the two-dimensional (cross-shore) hydrodynamics model for regular and irregular waves.
- Published experimental results are collected for calibration and verification of the present models.
- 3. The main purpose of the present study is to develop simple models for predicting the breaker height, wave height transformation and undertow velocity based on a wide range of published experimental results.
- 4. To confirm the ability of the models, the present models are compared with some existing models.

1.3 Organization of Report

The contents of some parts of this report are substantially the same as a series of papers published in the international journals shown in appendix A. The report updates and extends some material in the papers. The present report is written in the following stages:

Chapter 1 is an introduction and gives a statement of problem and objective and scope of study.

Chapter 2 describes the wave height transformation across beach.

Chapter 3 describes the undertow velocity.

Chapter 4 presents the comparison between the present models and the existing models.

Chapter 5 gives conclusions of the study.

Appendix A presents the paper reprints of this research.

Chapter 2: WAVE HEIGHT TRANSFORMATION

In order to calculate the sediment transport rate and beach profile change, wave height of each location is necessary. During last few decades, a number of studies and experiments have been carried out to develop the wave height transformation models. There is a variety of mathematical model simulating wave propagation and wave decay.

For computing beach transformation, the wave model should be kept as simple as possible because of the frequent updating of wave field for accounting the variability of mean water surface and the change of bottom profiles. For example, if we assume that wave height does not change within the time interval of 30 minutes (although the beach changes), we have to run wave model 96 times for 2-days storm. If the wave model cost 5 minutes to get the solution for a certain beach profile, It spends 8 hours for two-days storm. This calculation time is only for wave model. If the model is extended to include longshore direction or for irregular wave, more computation time will be required. This amount of computation time seems to be not suitable for practical purposes. To avoid this problem, in the present study, wave height transformation in cross-shore direction will be computed from the energy flux conservation. It is

$$\frac{\partial \left(Ec_{R}\cos\theta\right)}{\partial x} = -D_{B} \tag{2.1}$$

where E is the wave energy density, $c_{\rm g}$ is the group velocity, θ is the mean wave angle, x is the distance in cross shore direction, x-axis points onshore, and $D_{\rm g}$ is the energy dissipation rate which is zero outside the surf zone. The energy dissipation due to the bottom friction is neglected.

Snell's law is employed to describe wave refraction as

$$\frac{\sin \theta}{c} = \text{constant}$$
 (2.2)

where c is the phase velocity.

As waves propagate to the nearshore zone, they enter the intermediate-depth region where the wave motions are affected by the sea bed topography or water depth. These effects include decrease of wavelength and increase of wave height (shoaling), and thus change of the wave direction (refraction). The shoaling process continues until the wave becomes unstable and then breaks. The topic of wave breaking point is of considerable interest (see sec. 2.1). Once the waves start to break, a part of wave energy is transformed to turbulence and heat, and wave height decreases towards the shore.

This chapter is divided into three main sections. The first section describes the development of the breaker height formulas. The second section is the development of regular wave model. The third section describes the development of irregular wave model.

2.1 Breaker Height Formulas

The initiation of wave breaking has been a subject of study for a century due to its importance in design of coastal structures, as well as for the prediction of wave height transformation. Owing to the complexity of wave breaking mechanism, most predictions of the breaker heights are based on empirical formulas. To make the empirical formula reliable, it is necessary to calibrate or verify the formula with wide range of experimental data.

Laboratory data of the breaking wave height from 24 sources, including 574 cases, have been collected for calibration and verification of the formulas (see Table 2.1). The data cover wide range of wave and bottom slope conditions. The data include 3 types of beach conditions, i.e., plane beach, barred beach, and stepped beach. All experiments were performed under regular wave actions and the wave propagates normally to the beach. The experiment of Maruyama et al. (1983) was performed in large-scale wave flume and other experiments were performed in small-scale wave flumes.

This section is divided into two main parts. The first part describes the development of the breaker height formulas. The second part is the examination of the formulas.

Table 2.1: Summary of collected experimental data used to validate the breaker height formulas.

Sources	No. of	Beach	Bottom	H_o/L_o
Sources	cases	conditions	siopes	II o / Lo
Galvin (1969)*	19	plane beach	0.05-0.20	0.001-0.051
Hansen and Svendsen (1979)	17	plane beach	0.03	0.002-0.069
Hattori and Aono (1985)	3	stepped beach	0.00	0.006-0.021
Horikawa and Kuo (1966)	98	plane beach	0.01-0.05	0.006-0.073
Holikawa alid Nuo (1900)	60	stepped beach	0.00	0.007-0.100
Hwung et al. (1992)	2	plane beach	0.07	0.026-0.048
lversen (1952)*	63.	plane beach	0.02-0.10	0.003-0.080
Iwagaki et al. (1974)	39	plane beach	0.03-0.10	0.005-0.074
Maruyama et al. (1983)*	1	plane beach	0.03	0.091
Mizuguchi (1980)*	1	plane beach	0.10	0.045
Nadaoka et al. (1982)	12	plane beach	0.05	0.013-0.080
	1	plane beach	0.05	0.027
Nagayama (1983)	5	barred beach	0.05	0.025-0.051
	6	stepped beach	0.00-0.05	0.025-0.055
Okayasu et al. (1986)	2	plane beach	0 05	0.023-0.025
Okayasu et al. (1988)	10	plane beach	0.03-0.05	0.009-0.054
Ozaki et al. (1977)	20	plane beach	0.10	0.005-0.060
Saeki and Sasaki (1973)*	2	plane beach	0.02	0.005-0.039
Sato et al. (1988)	3	plane beach	0.05	0.031-0.050
Sato et al. (1989)	2	plane beach	0.03	0.019-0.036
Sato et al. (1990)	7	plane beach	0.05	0.003-0.073
Singamsetti and Wind (1980)*	95	plane beach	0.03-0.20	0.018-0.079
Smith and Kraus (1990)*	5	plane beach	0.03	0.009-0.092
Child and Mads (1990)	75	barred beach	0.03-0.44	0.008-0.096
Stive (1984)	2	plane beach	0.03	0.010-0.032
Ting and Kirby (1994)	2	plane beach	0.03	0.002-0.020
Visser (1982)*	7	plane beach	0.05-0.10	0.014-0.079
Walker (1974)*	15	plane beach	0.03	0.001-0.037
Total	574		0.00-0.44	0.001-0.100
* data from Smith and Kraus (1990	,			

^{*} data from Smith and Kraus (1990)

2.1.1 Formula development

The majority of the existing formulas represent a relationship between the breaking wave height (H_b) and the variables at the breaking or deepwater conditions, i.e., still water depth at breaking (h_b) , wavelength at breaking (L_b) , local bottom slope (m), deepwater wavelength (L_o) , and deepwater wave height (H_o) . The term "breaker index" is used to describe non-dimensional breaker height. The four common indices are in the form of H_b/h_b , H_b/L_b , H_b/L_o , and H_b/H_o . Either local or deepwater conditions are used to express the breaker indices. There are four dimensionless parameters that often used to express the breaker indices, i.e., m, h_b/L_b , h_b/L_o , and H_o/L_o . The existing breaker indices can be categorized into four general functions as:

$$\frac{H_b}{h_b} = f_1 \left\{ \tilde{m}, \frac{h_b}{L_b}, \frac{h_b}{L_a}, \frac{H_o}{L_a} \right\}$$
 (2.3)

$$\frac{H_b}{L_b} = f_2 \left\{ m, \frac{h_b}{L_b}, \frac{h_b}{L_a}, \frac{H_o}{L_a} \right\}$$
 (2.4)

$$\frac{H_{b}}{L_{a}} = f_{3} \left\{ m, \frac{h_{b}}{L_{b}}, \frac{h_{b}}{L_{a}}, \frac{H_{o}}{L_{a}} \right\}$$
 (2.5)

$$\frac{H_b}{H_o} = f_4 \left\{ m, \frac{h_b}{L_b}, \frac{h_b}{L_o}, \frac{H_o}{L_o} \right\} \tag{2.6}$$

Each breaker index may be the function of four dimensionless parameters as shown in Eqs. (2.3) - (2.6). However not all of the dimensionless parameters are contained in each existing breaker index and it is difficult to consider all these dimensionless parameters simultaneously. A common way for engineers to do is to select one or two as the dominant parameters governing each breaker index. In this study, the selection of dominant parameters is performed by plotting the relationship between each breaker index and each dimensionless parameter. A much simpler relationship is expected for the breaking wave on horizontal slope (m = 0) because the parameter m can be excluded from the formula. Therefore, the development of breaker height formula is separated into two stages. At first, the breaking waves on horizontal slope (m = 0) are analyzed to identify the "basic forms" of breaker indices. After that the bottom slope effect will be included explicitly into the basic formulas obtained from the first stage.

2.1.1.1 First stage of development

To identify the basic form of breaker index, the effect of bottom slope effect is excluded in this sub-section. Only the measured data of the breaking waves on horizontal slope (m=0) are used in this sub-section (i.e., the experiments from Hattori and Aono, 1985; Horikawa

and Kuo, 1966; and Nagayama, 1983). An attempt is made to correlate the breaker indices (i.e., H_b/h_b , H_b/L_b , H_b/L_o , and H_b/H_o) with the possible dimensionless parameters (i.e., h_b/L_b , h_b/L_o , and H_o/L_o). A total of 12 possible relations are plotted (e.g., $H_b/h_b \otimes h_b/L_b$, $H_b/h_b \otimes h_b/L_o$, and $H_b/H_o \otimes H_o/L_o$). Among the 12 possibilities, the relationships of $H_b/L_o \otimes h_b/L_o$, and $H_b/L_o \otimes H_o/L_o$ show better correlation than the others.

The relationship between H_b/L_o and h_b/L_o is shown in Fig. 2.1. A hyperbolic tangent function has been fitted to this relation, with the result

$$\frac{H_b}{L_o} = 0.1 \tanh \left[7.4 \frac{h_b}{L_o} \right] \tag{2.7}$$

Figure 2.2 shows the relationship between $H_{\it b}/L_{\it o}$ and $H_{\it o}/L_{\it o}$. The relation can be fitted with a power function, which is a straight line on logarithmic graph. The equation of fitted line can be expressed as

$$\frac{H_b}{L_o} = 0.46 \left(\frac{H_o}{L_o}\right)^{0.75} \tag{2.8}$$

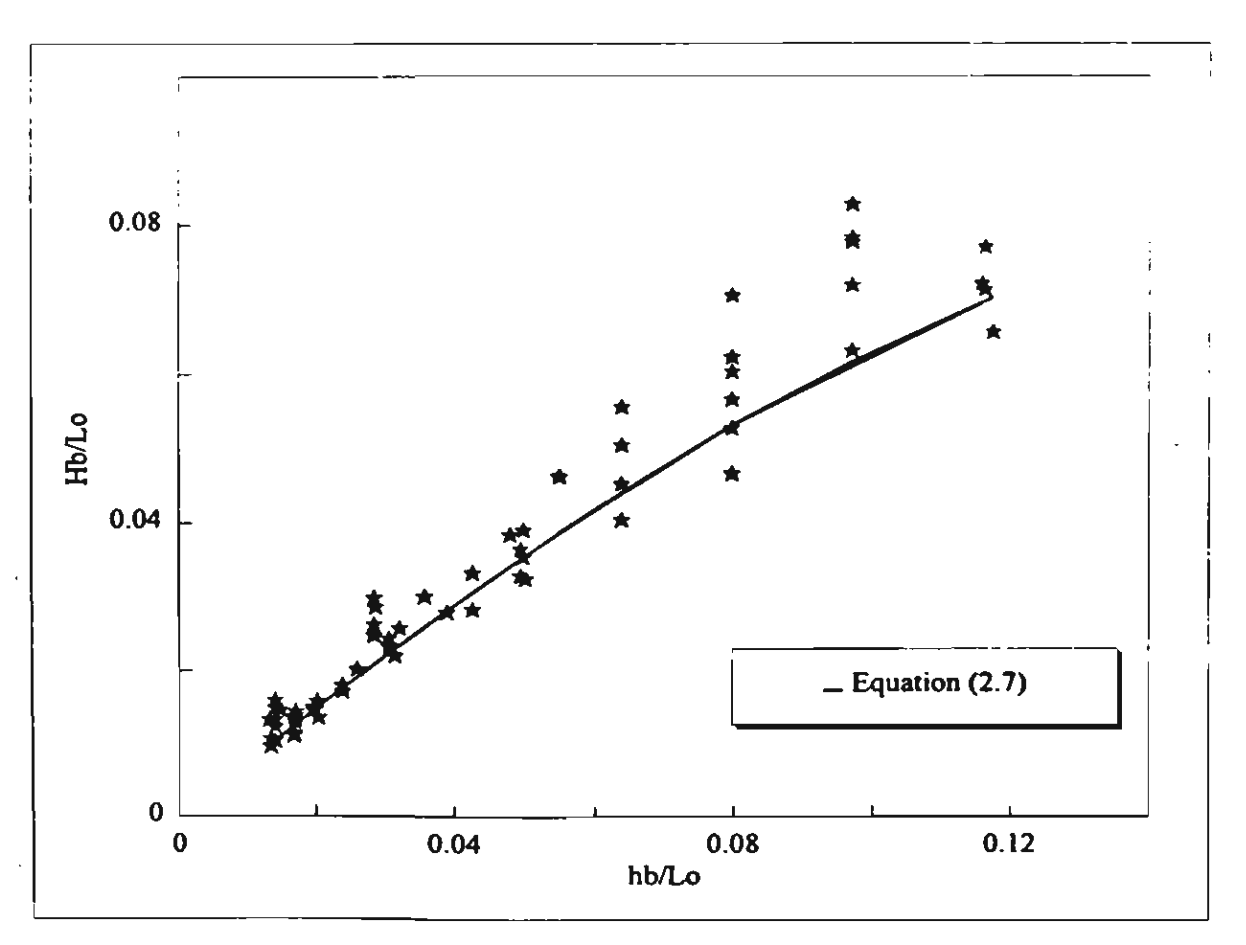


Figure 2.1: Relationship between H_b/L_o and h_b/L_o for the case of breaking wave on horizontal slope (measured data from Hattori and Aono, 1985; Horikawa and Kuo, 1966; and Nagayama, 1983).

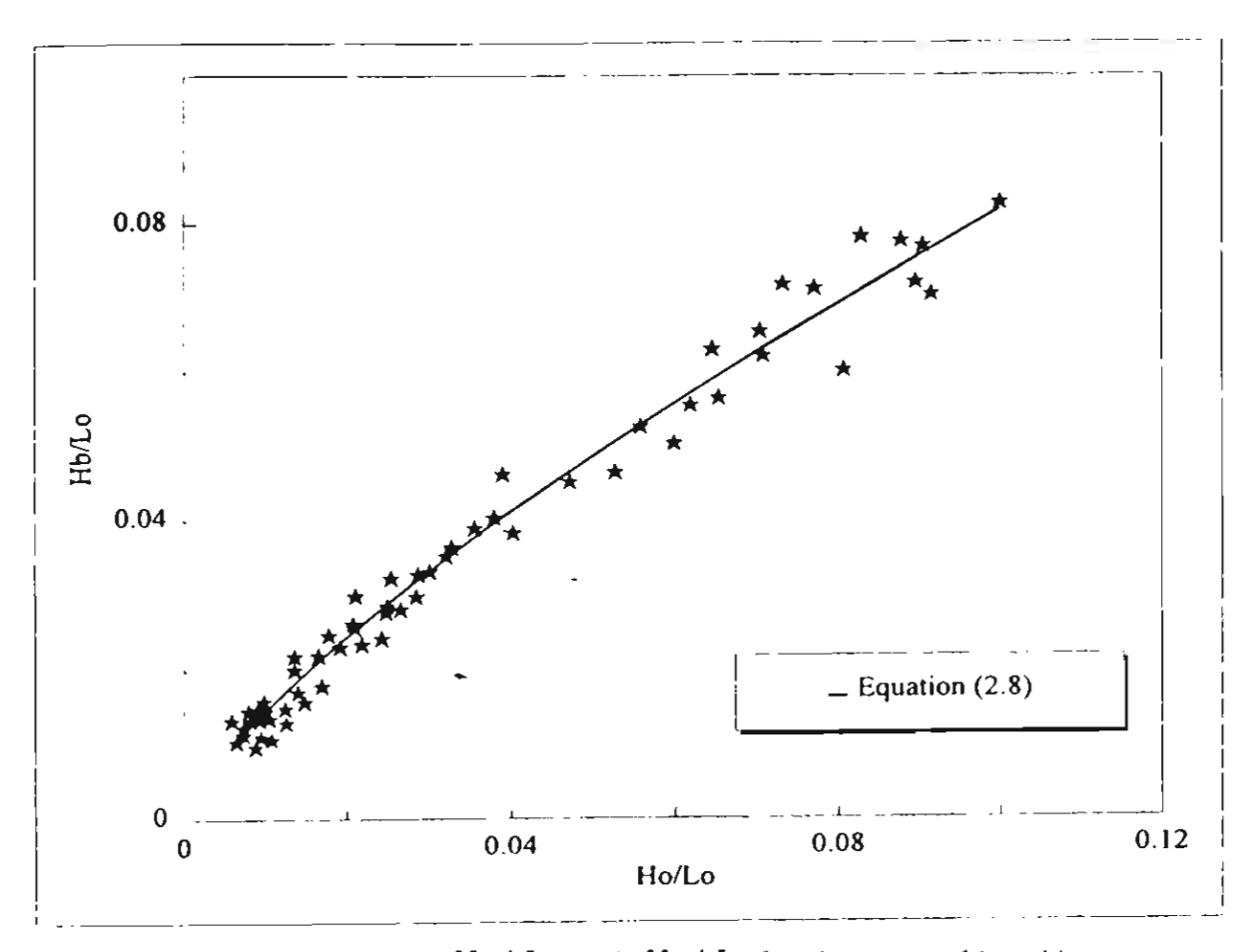


Figure 2.2: Relationship between $H_{\mathfrak{p}}/L_{\mathfrak{p}}$ and $H_{\mathfrak{p}}/L_{\mathfrak{p}}$ for the case of breaking wave on horizontal slope (measured data from Hattori and Aono, 1985; Horikawa and Kuo, 1966; and Nagayama, 1983).

2.1.1.2 Second stage of development

The analysis is extended by incorporating the measured data of the breaking waves on various bottom slopes. The measured data from 24 sources (shown in Table 2.1) are used in this analysis. This revised analysis is based entirely on the basic formulas obtained from the first stage of development (Eqs. 2.7 and 2.8). To include the effect of bottom slope, Eqs. (2.7) and (2.8) can be modified as the following.

a) Modification of equation (2.7)

The bottom slope effect coefficient may be included in Eq. (2.7) by replacing the constant "7.4" as

$$\frac{H_h}{L_o} = 0.1 \tanh \left[S_1 \frac{h_h}{L_o} \right] \tag{2.9}$$

where S_1 is the bottom slope effect coefficient.

From Eq. (2.9), the formula of S_1 can be written as

$$S_1 = \frac{L_o}{h_b} \tanh^{-1} \left(\frac{H_b}{0.1 L_c} \right) \tag{2.10}$$

The measured S_1 of the collected data (shown in Table 2.1) is determined by using Eq. (2.10). The relationship between the measured S_1 and the bottom slope m is shown in Fig. 2.3. It can be seen that the relationship can be fitted with a parabolic function $(S_1 = a_1 m^2 + a_2 m + a_3)$. The coefficients $a_1 - a_3$, in the parabolic function, can be determined from multi-regression analysis. After the analysis, it is found that the best-fit formula for S_1 can be expressed as

$$S_1 = -81.07m^2 + 35.27m + 7.88 \tag{2.11}$$

Substituting Eq. (2.11) into Eq. (2.9), the breaker height formula can be expressed as

$$H_b = 0.1L_o \tanh \left[\left(-81.07m^2 + 35.27m + 7.88 \right) \frac{h_b}{L_o} \right]$$
 (2.12)

Hereafter Eq. (2.12) is referred to as PS1 formula.

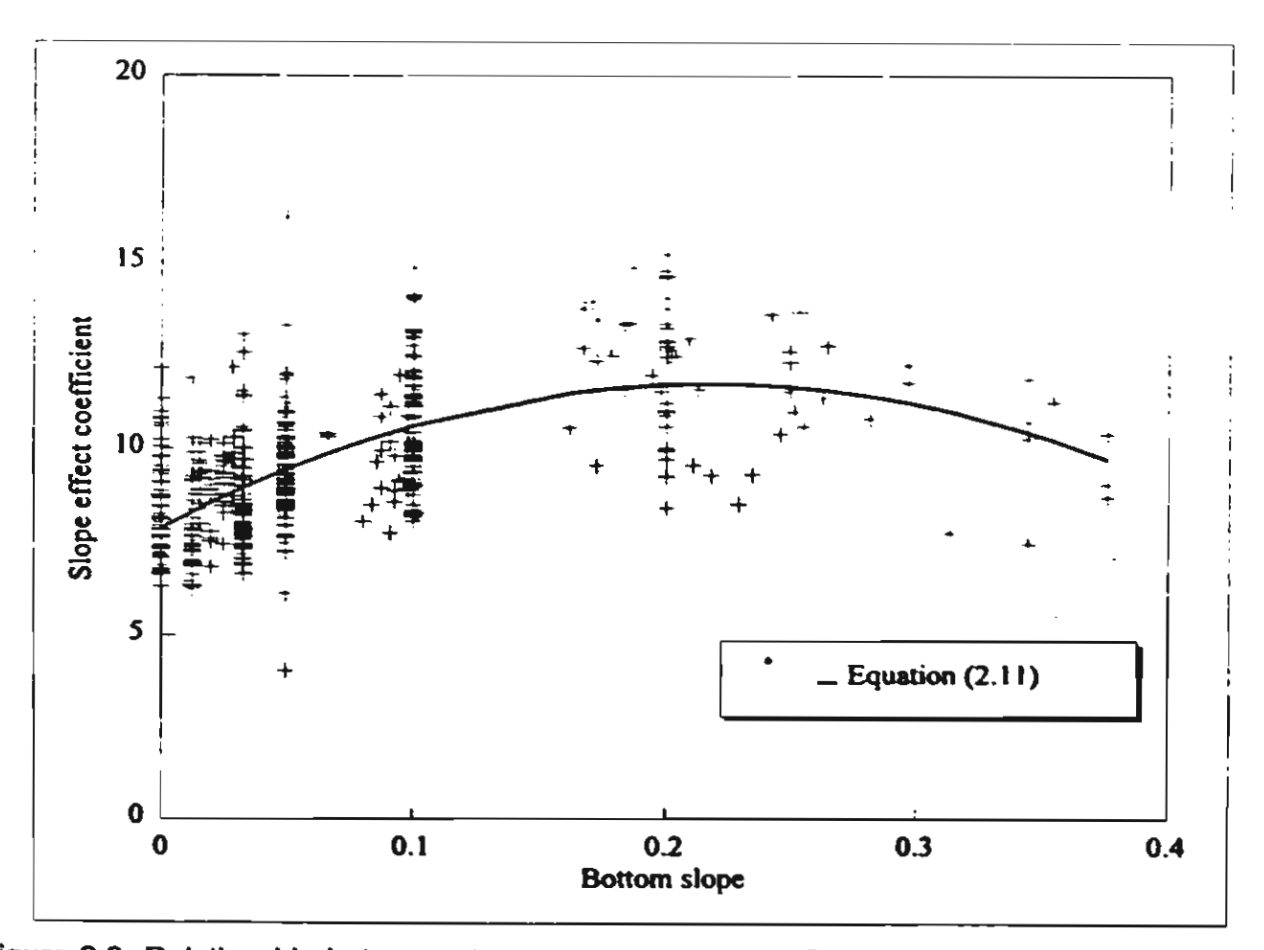


Figure 2.3: Relationship between slope effect coefficient (S_1) and bottom slope (measured data from 24 sources shown in Table 2.1).

b) Modification of equation (2.8)

The slope effect coefficient is included in Eq. (2.8) by replacing the constant "0.46" as

$$\frac{H_b}{L_o} = S_2 \left(\frac{H_o}{L_o}\right)^{0.75} \tag{2.13}$$

where S_2 is the bottom slope effect coefficient.

From Eq. (2.13), the formula of S_2 can be written as

$$S_2 = \frac{H_h}{L_o} \left(\frac{L_o}{H_o}\right)^{0.75} \tag{2.14}$$

The measured S_2 of the collected data (shown in Table 2.1) is determined by using Eq. (2.14). Figure 2.4 shows the relation between measured S_2 and the bottom slope m. The derivation of the formula of S_2 is the same as that of S_1 . After the analysis, it is found the best-fit formula for S_2 can be expressed as

$$S_2 = -2.06m^2 + 0.67m + 0.46 \tag{2.15}$$

Substituting Eq. (2.15) into Eq. (2.13), yields

$$H_b = \left(-2.06m^2 + 0.67m + 0.46\right)L_o\left(\frac{H_o}{L_o}\right)^{0.75}$$
 (2.16)

Hereafter Eq. (2.16) is referred to as PS2 formula.

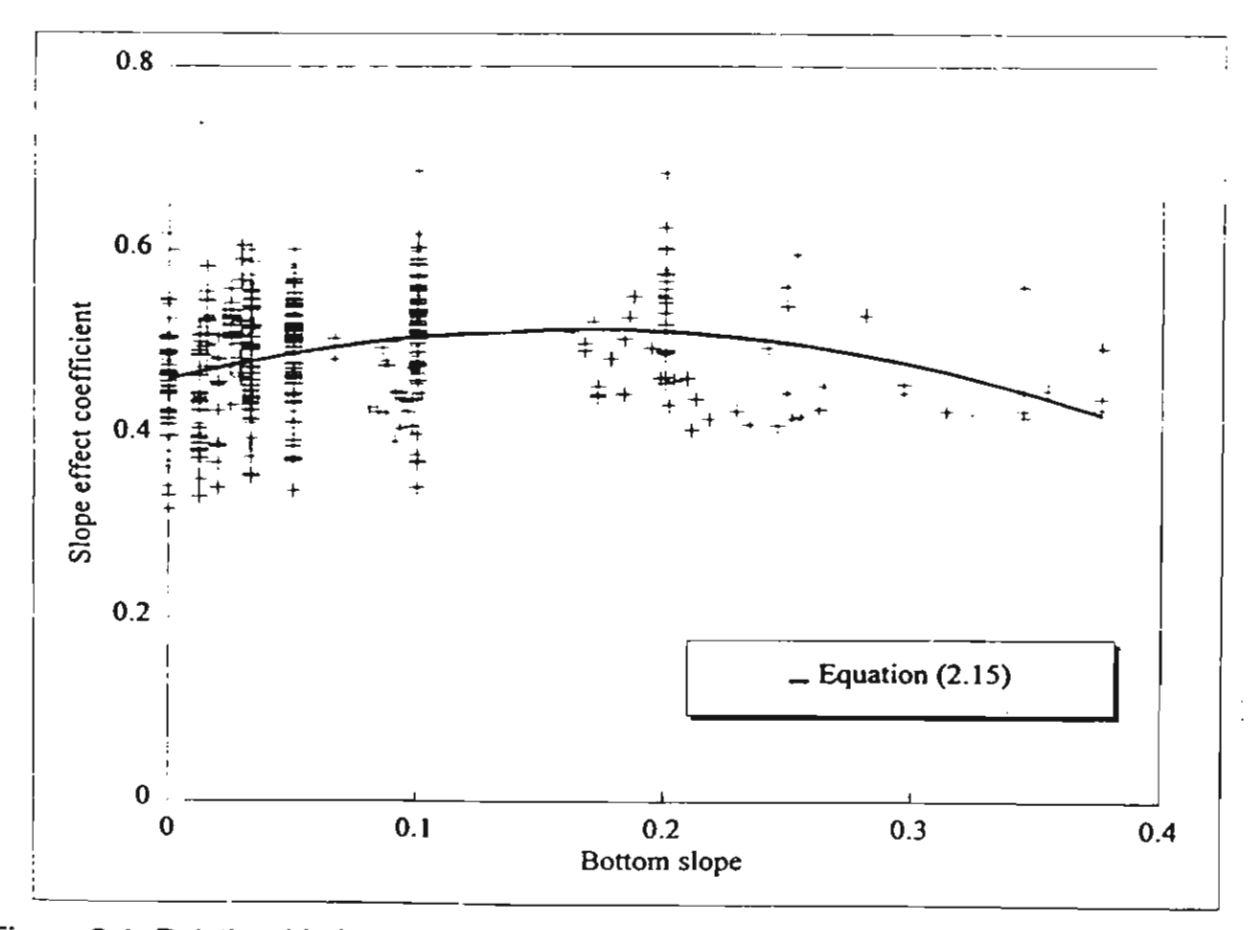


Figure 2.4: Relationship between slope effect coefficient S_2 and bottom slope (measured data from 24 sources shown in Table 2.1).

It can be seen from Fig. 2.4 that the variation of S_2 with m is quite small. It is worth while checking, whether excluding the effect of m is possible. The graph between H_b/L_o and H_o/L_o is plotted to check the effect of m on this relation (see Fig. 2.5). It can be seen from Fig. 2.5 that the effect of bottom slope may not significant for this relationship. The relationship in Fig. 2.5 can be fitted by a power relation of the form

$$\frac{H_b}{L_o} = a_4 \left(\frac{H_o}{L_o}\right)^{a_5} \tag{2.17}$$

where a_4 and a_5 are constants.

Equation (2.17) is a straight line on logarithmic graph. The constants a_4 and a_5 can be determined by the regression analysis between $\log(H_b/L_o)$ and $\log(H_o/L_o)$. Using all collected data for the regression analysis, it is found that $a_4=0.48$ and $a_5=0.75$.

Therefore the breaker height formula becomes

$$\frac{H_b}{L_o} = 0.48 \left(\frac{H_o}{L_o}\right)^{0.75} \tag{2.18}$$

Hereafter Eq. (2.18) is referred to as PS3 formula.

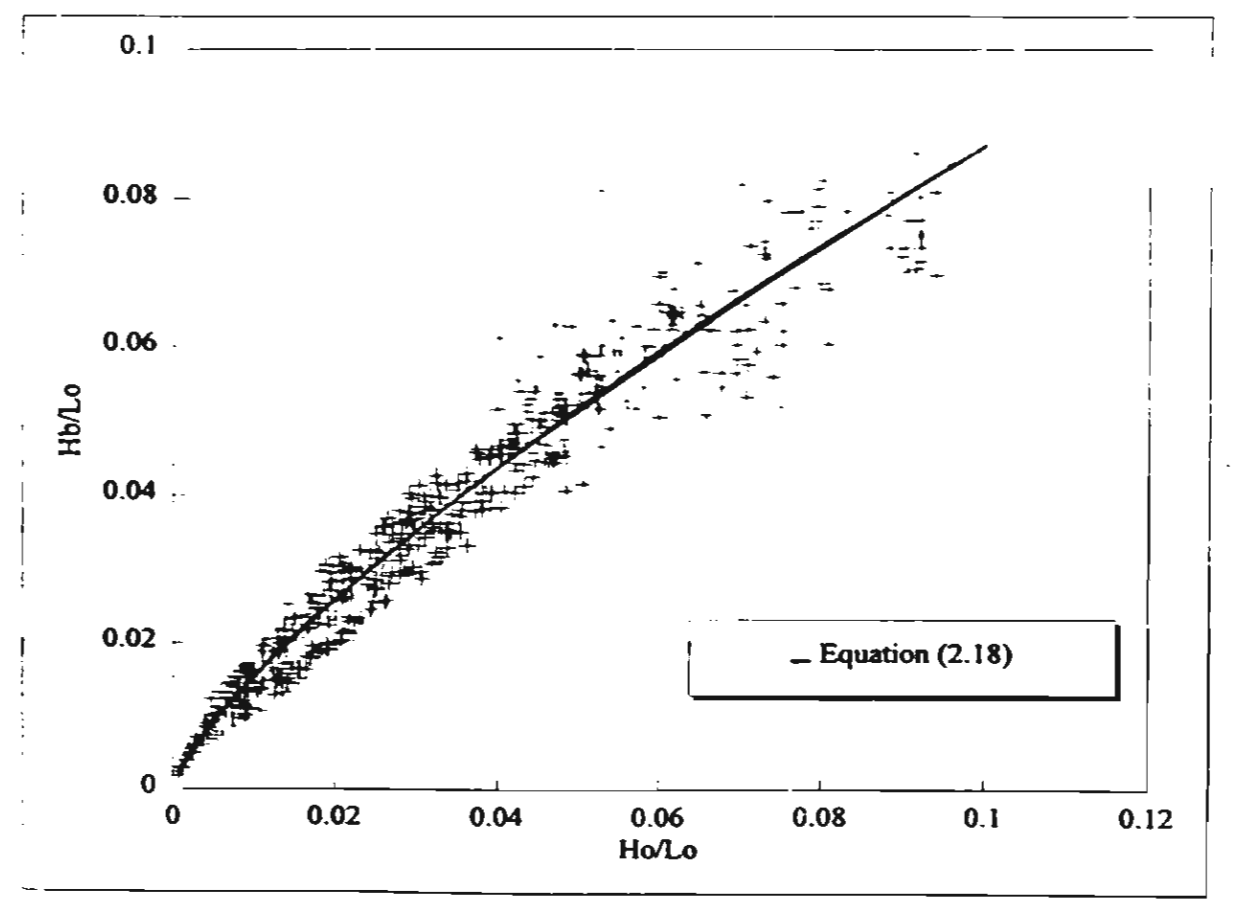


Figure 2.5: Relationship between $H_{\mathfrak{b}}/L_{\mathfrak{o}}$ and $H_{\mathfrak{o}}/L_{\mathfrak{o}}$ (measured data from 24 sources shown in Table 2.1).

2.1.2 Formula examinations

The objective of this subsection is to examine the accuracy of the present formulas (Eqs. 2.12, 2.16 and 2.18). A straightforward way to examine a formula is to compare the computed breaker height with the measured data. In order to evaluate the accuracy of the computation, the examination results are presented in term of root mean square (rms) relative error, ER, which is defined as

$$ER = 100 \sqrt{\frac{\sum_{i=1}^{m} (H_{ci} - H_{mi})^2}{\sum_{i=1}^{m} H_{mi}^2}}$$
 (2.19)

where i is the wave height number, H_{ci} is the computed wave height of number i, H_{mi} is the measured wave height of number i, and tn is the total number of measured wave height. Smaller values of ER correspond to a better prediction.

The measured breaking wave heights from 24 sources are used to examine the validity of each formula. The experiments cover wide range of wave and bottom conditions (0.001 $\leq H_o/L_o \leq 0.100$, and $0 \leq m \leq 0.44$). The bottom slope is classified into 4 groups, i.e., horizontal (m=0), gentle $(0 < m \leq 0.07)$, intermediate $(0.07 < m \leq 0.10)$, and steep (m>0.10). The total number of cases of the collected data for m=0, $0 < m \leq 0.07$, $0.07 < m \leq 0.10$ and m>0.10 are 64, 338, 102 and 70, respectively.

The computations of the breaker height formulas are carried out with 24 sources of collected data (see Table 2.1). Table 2.2 shows the error ER of each formula for 4 groups of bottom slope and all cases. It can be seen that overall, the present formulas (PS1-PS3) give very well prediction for general cases and the PS1 formula (Eq. 2.12) gives the best prediction for general cases. The error ER of the formula is 10.8%.

The comparison between measured and computed breaking wave height from the PS1 formula is shown in Fig. 2.6. One point on the upper right of the figure is the data from large-scale wave flume of Maruyama et al. (1983) and other points are the data from small-scale wave flumes. The solid line in the figure is the line of perfect agreement.

Table 2.2: The root mean square relative error (ER) of each formula for four groups of bottom slope and all cases.

Formulas	m = 0	$0 < m \le 0.07$	$0.07 < m \le 0.10$	m > 0.10	All 574
	(64 cases)	(338 cases)	(102 cases)	(70 cases)	cases
PS1 (Eq. 2.12)	13.22	9.96	12.49	11.33	10.76
PS2 (Eq. 2.16)	10.04	10.67	12.69	11.31	10.96
PS3 (Eq. 2.18)	11.64	10.87	11.83	11.77	11.17

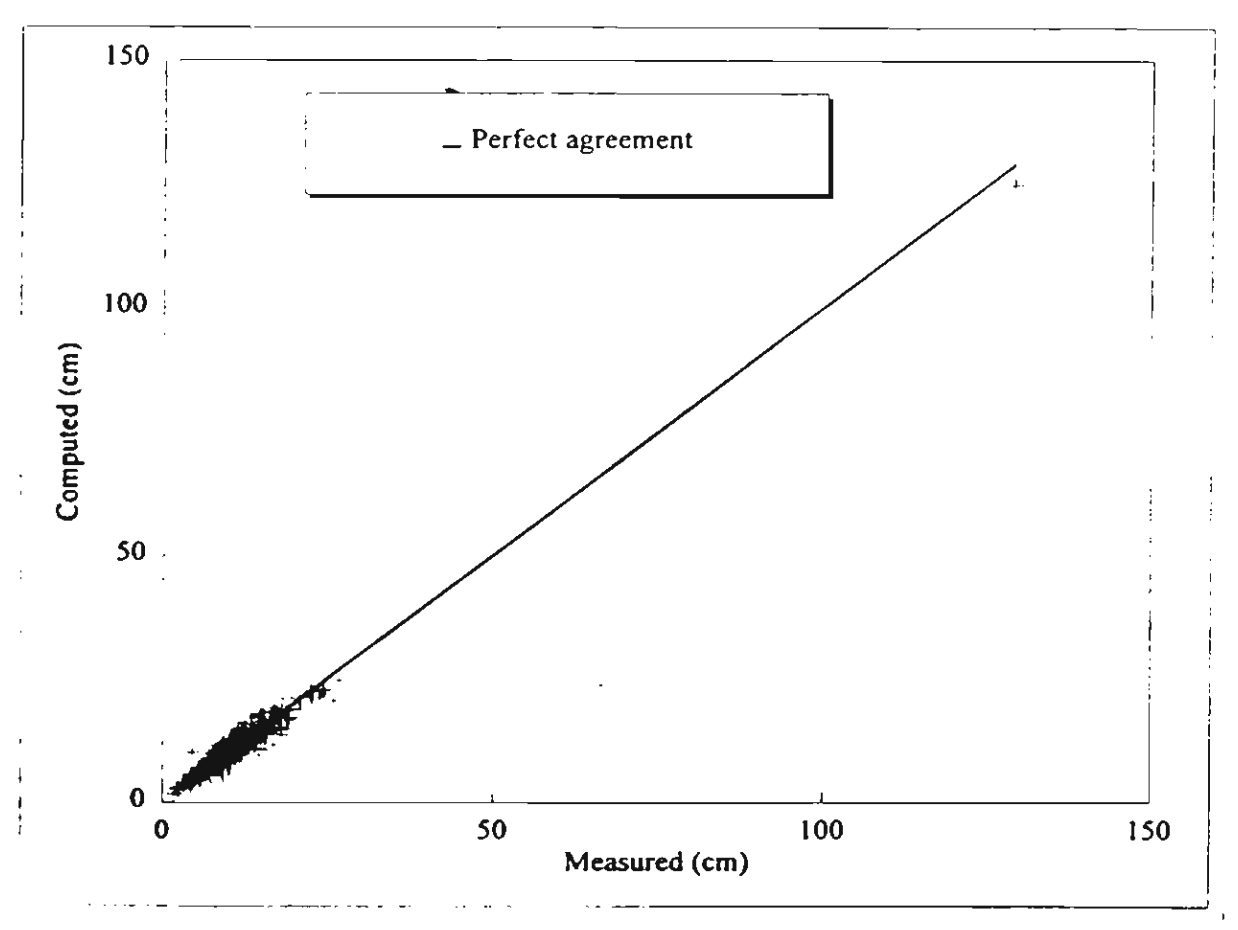


Figure 2.6: Comparison between measured and computed breaking wave heights from the PS1 formula (measured data from 24 sources shown in Table 2.1).

2.2 Regular Wave Height Transformation

The wave height transformation can be computed from the energy flux balance equation (Eq. 2.1) by substituting the formula of the energy dissipation rate, $D_{\it B}$, and numerical integrating from offshore to shoreline. The main difficulty of energy flux conservation approach is how to formulate the energy dissipation rate, $D_{\it B}$, inside the surf zone. The phenomenon of wave breaking is very complicated. At present stage of knowledge, any type of formula for computing $D_{\it B}$ has to be based on empirical formula.

During the last few decades, a number of studies and experiments have been carried out to develop the energy dissipation models. Owing to the complexity of wave breaking mechanism, any type of model for computing the rate of energy dissipation has to be based on empirical or semi-empirical formula calibrated with the experimental results. To make the empirical formula reliable, it is necessary to calibrate or verify the formula with a large amount and wide range of experimental results. It is the purpose of this study to develop the energy dissipation model based on wide range of experimental conditions.

Experimental data from 11 sources, including 490 cases, have been collected for calibration and verification of the present models. A summary of the collected experimental results is given in Table 2.3. The experiments cover wide range of wave and bottom topography conditions, including both small and large-scale laboratory. Most of the experiments were performed under fixed bed conditions, except data of Kajima et al. (1983), Kraus and Smith (1994), Shibayama and Horikawa (1985), which were performed under movable bed conditions.

The main target of the next sections is to develop an empirical formula for computing the energy dissipation rate for regular wave breaking.

2.2.1 Energy dissipation

A major problem of wave field calculation inside the surf zone is how to evaluate the rate of energy dissipation. A number of works on theoretical and experimental studies have been performed to draw a clearer picture of the energy dissipation rate, $D_{\it B}$. Various models have been proposed, by previous researchers, for computing the energy dissipation rate, $D_{\it B}$. Widely used formulas for computing energy dissipation rate are the Bore model and the model of Dally et al. (1985). A briefly reviews of these two models are described as follows.

Table 2.3: Summary of collected experimental data used to validate the present models.

Sources	No. of	Wave	Bed condition	Apparatus
	cases	condition		
Hansen and Svendsen (1984)	1	regular	plane beach	small-scale
Horikawa and Kuo (1966)	213	regular	plane and	small-scale
			stepped beach	
Kajima et al. (1983)	79	regular	sandy beach	large-scale
Kraus and Smith (1994)	57	regular	sandy beach	large-scale
Nadaoka et al. (1982)	2	regular	plane beach	small-scale
Nagayama (1983)	12	regular	plane, stepped	small-scale
			and barred	
			beach	
Okayasu et al.(1988)	10	regular	plane beach	small-scale
Sato et al. (1988)	3	regular	plane beach	smail-scale
Sato et al. (1989)	2	regular	plane beach	small-scale
Shibayama and Horikawa (1985)	10	regular	sandy beach	small-scale
Smith and Kraus (1990)	101	regular	plane and	small-scale
			barred beach	
Total	490			

a) Bore model, originally introduced by Le Mehaute (1962), is developed based on an assumption that the energy dissipation rate of a broken wave is similar to the dissipation rate of a hydraulic jump. Several researchers have proposed slightly different forms of the energy dissipation rate, e.g.,

Battjes and Janssen (1978):
$$D_B = \frac{\rho g H^2}{4T} = \frac{2}{T} E$$
 (2.20)

Thornton and Guza (1983):
$$D_B = \frac{\rho g H^3}{4Th} = \frac{2H}{Th} E$$
 (2.21)

where ρ is the density of water, g is the acceleration due to gravity, H is the wave height, T is the wave period, and h is the water depth.

b) The model of Dally et al. (1985) is based on the observation of stable wave height on the horizontal bed. They assumed that the energy dissipation rate is proportional to the difference between the local energy flux and the stable energy flux, divided by the local water depth as

$$D_{E} \propto \frac{\left[Ec_{g} - E_{s}c_{g}\right]}{h} \tag{2.22}$$

or
$$D_B = \frac{K_d c_g}{h} [E - E_s] = \frac{K_d c_n}{h} [E - E_s]$$
 (2.23)

where

$$E_{s} = \frac{1}{8} \rho g H_{s}^{2} = \frac{1}{8} \rho g (\Gamma h)^{2}$$
 (2.24)

$$n = [1 + 2kh/\sinh(2kh)]/2$$
 (2.25)

in which K_d is a constant (decay coefficient), c is the phase velocity, E_s is the stable energy density, H_s is the stable wave height and Γ is the stable wave factor.

From the model calibration with the laboratory data of Horikawa and Kuo (1966), Dally et al. (1985) found that $K_d = 0.15$ and Γ is varied case by case between 0.35-0.48. However, finally, they suggested to use $\Gamma = 0.4$ for general cases. The Dally et al.'s model has been verified extensively for a variety of wave conditions (e.g., Ebersole, 1987; Larson and Kraus, 1989). The advantage of Dally et al.'s model is that it is able to reproduce the pause (or stop breaking) in the wave breaking process at a finite wave height on a horizontal bed or in the recovery zone while the bore model gives a continuous dissipation due to wave breaking.

From the above empirical formulas (Eqs. 2.20-2.23), we see that the energy dissipation rate, $D_{\rm H}$, may be a function of the energy density, E. Moreover, the energy dissipation rate should be equal to zero for recovered wave. Therefore, in the present study, the energy dissipation rate is assumed to be proportional to the difference between the local energy density and stable energy density:

$$D_B \propto \left[E - E_s \right] \tag{2.26}$$

or
$$D_{\mathcal{B}} = \beta \left[E - E_{s} \right] \tag{2.27}$$

where β is the proportionality constant.

Rewriting Eq. (2.27) in term of wave height leads to

$$D_{B} = \beta \frac{\rho g}{8} \Big[H^{2} - (\Gamma h)^{2} \Big]$$
 (2.28)

The energy dissipation rate of Eq. (2.28) contains two parameters β and Γ which can be determined empirically from the measured wave heights. The published experimental data from small-scale and large-scale experiments performed under regular wave actions are used to determine the parameters β and Γ . Total 11 sources of published experimental results, including 490 cases, are used in this section (see Table 2.3).

2.2.1.1 Determination of parameter β

By comparison of Eq. (2.27) to Eqs. (2.20), (2.21) and (2.23), respectively, we see that there may be four possible forms of β . Therefore, there are four possible models of the energy dissipation rate, $D_{\rm H}$:

model (1):
$$D_B = K_1 \frac{2}{T} (E - E_s) = K_1 \frac{\rho g}{4T} [H^2 - (\Gamma h)^2]$$
 (2.29)

where $\beta = K_1 \frac{2}{T}$

model (2)
$$D_B = K_2 \frac{2II}{Th} (E - E_s) = K_2 \frac{\rho g II}{4Th} [H^2 - (\Gamma h)^2]$$
 (2.30)

where $\beta = K_2 \frac{2H}{Th}$.

model (3)
$$D_B = K_3 \frac{cn}{h} (E - E_1) = K_3 \frac{\rho gcn}{8h} [H^2 - (1h)^2]$$
 (2.31)

where $\beta = K_3 \frac{cn}{h}$.

model (4)
$$D_B = K_4 \frac{c}{h} (E - E_x) = K_4 \frac{\rho gc}{8h} [H^2 - (\Gamma h)^2]$$
 (2.32)

where $\beta = K_4 \frac{c}{h}$.

in which $K_1 - K_4$ are constants, which can be found from model calibrations. Model 3 (Eq. 2.31) is the same model with Dally et al. (1985).

In order to select the proper form of β or D_{θ} , the above four models (Eqs. 2.29-2.32) will be examined by using measured wave heights inside the surf zone.

By rewriting Eq. (2.1) in term of wave height, it becomes

$$\frac{\rho g}{8} \frac{\partial (H^2 c_{_{R}} \cos \theta)}{\partial x} = -D_{_{H}} \tag{2.33}$$

The wave height transformation is computed from the energy flux balance equation (Eq. 2.33) by substituting the above possible expressions of D_B and numerical integrating from breaking point to shoreline. In this subsection, Γ =0.4 is used as suggested by Dally et al. (1985) and it will be modified later in the next subsection.

In order to evaluate the accuracy of the prediction, the verification results are presented in term of rms relative error, ER, which is defined as Eq. (2.19).

A calibration for models 1-4 was conducted by varying the values of $K_1 - K_4$ until the minimum error (ER) between measured and computed wave heights is obtained. The optimum values of $K_1 - K_4$ are 0.90, 0.98, 0.15 and 0.15, respectively, which give the average rms relative error of each model equal to 20.23, 18.66, 17.84 and 17.55, respectively.

The rms relative errors (ER) of each model for all cases of collected experiments are shown in Table 2.4. From Table 2.4, among the four possible models, the model 4 (Eq. 2.32) appeared to be the best. Therefore, the proper form of the parameter β is recommended to be

$$\beta = 0.15 \frac{c}{h} \tag{2.34}$$

Therefore, the energy dissipation rate can be written as

$$D_{B} = K_{a} \frac{c}{h} [E - E_{s}] = K_{a} \frac{c\rho g}{8h} [H^{2} - (\Gamma h)^{2}]$$
 (2.35)

where $K_a = 0.15$ is the constant.

Comparing Eq. (2.35) with Dally et al.'s model (Eq. 2.23), we see that Eq. (2.35) is similar to the Dally et al.'s model (Eq. 2.23) except the factor n.

It should be noted that we could get the same form as Eq. (2.35), if we assume that the energy dissipation rate is proportional to the difference between the energy per unit width (EL) and the stable energy per unit width (E_sL) , divided by the local water depth and wave period as

$$D_{B} \propto \frac{\left[EL - E_{s}L\right]}{hT} \tag{2.36}$$

or
$$D_B = K_a \frac{L}{hT} [E - E_s] = K_a \frac{c}{h} [E - E_s]$$
 (2.37)

where K_a is the proportional constant. Rewriting Eq. (2.37) in terms of wave height yields

$$D_{B} = K_{a} \frac{c\rho g}{8h} \Big[H^{2} - (\Gamma h)^{2} \Big]$$
 (2 38)

which is the same as Eq. (2.35).

Table 2.4: Root mean square relative error (ER) of the four possible forms of $D_{\it B}$.

No	Sources	Total	$D_{\scriptscriptstyle B}$ from	$D_{\scriptscriptstyle B}$ from	D_{B} from	$D_{\it E}$ from
		No of	Eq. 2.29	Eq. 2.30	Eq. 2.31	Eq. 2.32
		cases	K ₁ =0.90	K ₂ =0.98	K ₃ =0.15	K₄=0.15
1	Hansen and Svendsen (1984)	1	5.14	4.82	13.83	16.15
2	Horikawa and Kuo (1966),	101	11.98	14.21	13.87	13.30
	slope=0					
	Horikawa and Kuo (1966),	112	29.44	22.99	17.86	20.64
	slope=1/80-1/20					
3	Kajima et al. (1983)	79	26.03	19.29	20.06	18.36
4	Kraus and Smith (1994)	- 57	21.58	26.25	21.87	20.86
5	Nadaoka et al. (1982)	2	21.70	15.44	8.38	11.97
6	Nagayama (1983)	12	10.00	9.69	9.55	9.19
7	Okayasu et al. (1988)	10	17.39	16.06	13.57	14.18
8	Sato et al. (1988)	3	15.20	12.43	8.11	11.35
9	Sato et al. (1989)	2	25.39	17.75	24.76	31.83
10	Shibayama and Horikawa	10	19.25	17.68	17.15	16.23
	(1986)					
11	Smith and Kraus (1990)	101	24.73	25.11	21.98	19.44
	Total	490	20.23	18.66	17.84	17.55

2.2.1.2 Determination of the parameter Γ

Since the parameter Γ changes between 0.35-0.48 (Dally et al., 1985), the objective of this subsection is to determine the empirical formula of the parameter Γ .

After substituting Eq. (2.35) into Eq. (2.1), the equation of energy flux balance can be written as

$$\frac{\partial \left(Ec_{g}\cos\theta\right)}{\partial x} = K_{\sigma}\frac{c\rho\,g}{8h}\Big[H^{2} - (\Gamma h)^{2}\Big] \tag{2.39}$$

Considering Eq. (2.39), the measured Γ can be determined from the measured wave height, period and water depth by using the following formula (rewriting Eq. 2.39).

$$\Gamma = \frac{1}{h} \sqrt{H^2 - \frac{\partial (Ec_g \cos \theta)}{\partial x} \frac{8h}{0.15c\rho g}}$$
 (2.40)

Using the measured wave heights, periods, and water depths from the experimental data of Kajima et al., (1983), the measured Γ can be determined from Eq. (2.40). An attempt is

made to correlate the parameter Γ with the wave parameters. Among the various possibilities, the correlation between Γ and h/\sqrt{LH} appeared to be the best (see Fig. 2.7). A formula for the stable wave factor Γ , from Fig. 2.7, can be expressed as

$$\Gamma = \exp\left[-0.36 - 1.25 \frac{h}{\sqrt{LH}}\right] \tag{2.41}$$

Substituting Γ from Eq. (2.41) into Eq. (2.35), finally, the energy dissipation rate $D_{\it B}$ of the present study can be expressed as

$$D_B = \frac{0.15c\rho g}{8h} \left[H^2 - \left(h \exp(-0.36 - 1.25 \frac{h}{\sqrt{I.H}}) \right)^2 \right]$$
 (2.42)

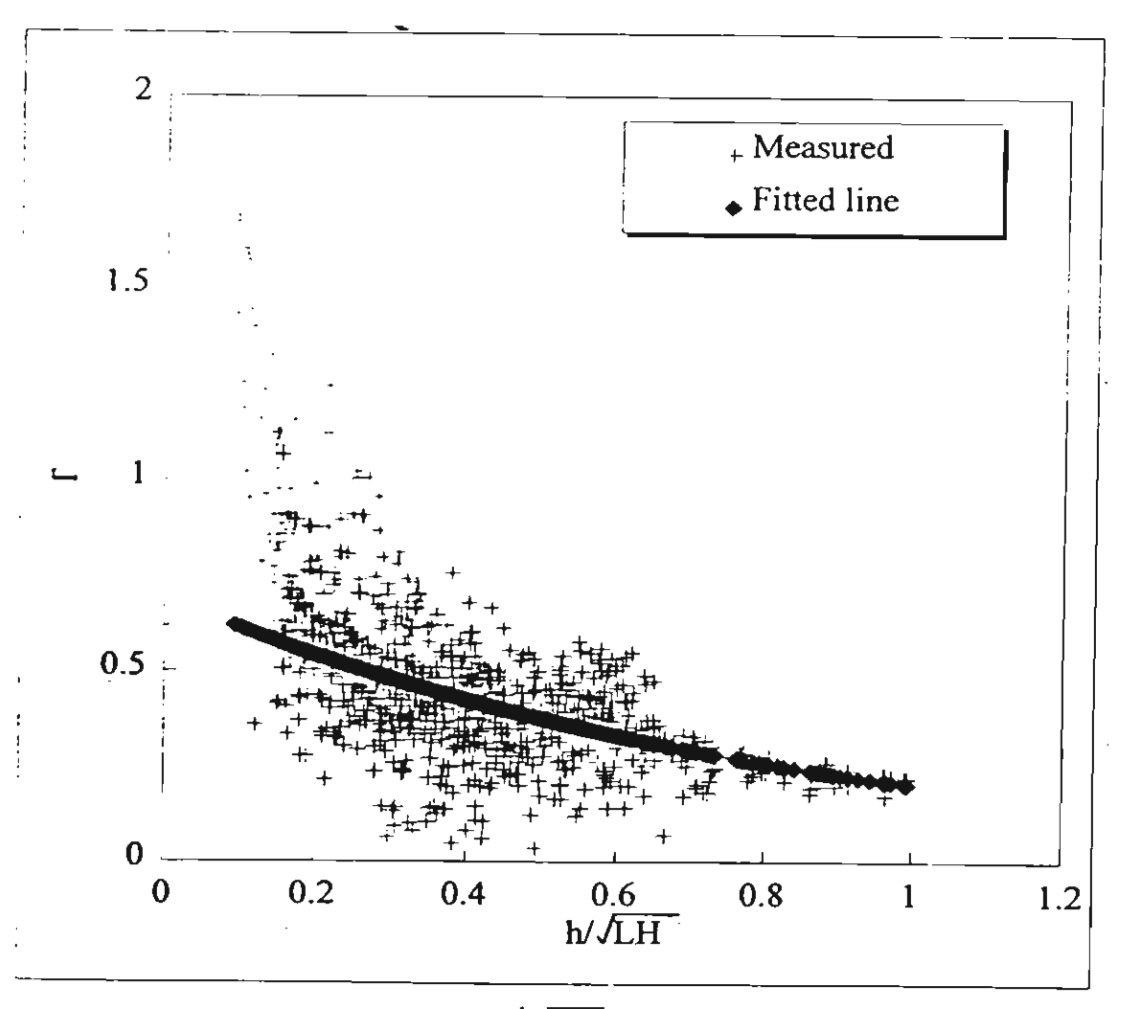


Figure 2.7: Relationship between Γ and h/\sqrt{LH} (laboratory data from Kajima et al., 1983).

2.2.1.3 Model verification

Comparisons between measured and computed wave heights inside the surf zone are used to verify the model. The verification is performed for 490 cases of 11 sources of collected laboratory data. The verification by using these independent data sources and wide range of experiment conditions are expected to clearly demonstrate the accuracy of the present model.

The wave height transformation is computed from the energy flux balance equation (Eq. 2.33) by substituting $D_{\rm H}$ from Eq. (2.42) and numerical integration, using backward finite difference scheme, from breaking point to shoreline. All coefficients in the model are kept to be constant for all cases in the verification. Comparison between measured and computed wave heights for all 490 cases are shown in Fig. 2.8. Columns 4 and 5 of Table 2.5 show the rms relative error, ER, of the Dally et al.'s model (Eq. 2.23) and the present model (Eq. 2.42), respectively. From Table 2.5 we see that the results of computed wave height of present model are better than those of Dally et al.'s model, for most cases. The average rms relative error, for all 490 cases, by the present model is 15.8 % while that by Dally et al.'s model is 17.8 %.

Table 2.5: Root mean square relative error (ER) of Dally's model and present model.

Sources	Total No.	Dally	Present
	of cases	model,	study,
		(Eq.2.23)	(Eq.2.42)
Hansen and Svendsen (1984)	1	13.83	7.00
Horikawa and Kuo (1966), slope=0	101	13.87	11.66
Horikawa and Kuo (1966), slope=1/80-1/20	112	17.86	17.68
Kajima et al. (1983)	79	20.06	16.37
Kraus and Smith (1994)	57	21.87	19.16
Nadaoka et al. (1982)	2	8.38	10.81
Nagayama (1983)	12	9.55	8.61
Okayasu et al. (1988)	10	13.57	11.30
Sato et al. (1988)	3	8.11	7.74
Sato et al. (1989)	2	24.76	19.78
Shibayama and Horikawa (1986)	10	17.15	17.69
Smith and Kraus (1990)	101	21.98	20.44
Total	490	17.84	15.75
	Hansen and Svendsen (1984) Horikawa and Kuo (1966), slope=0 Horikawa and Kuo (1966), slope=1/80-1/20 Kajima et al. (1983) Kraus and Smith (1994) Nadaoka et al. (1982) Nagayama (1983) Okayasu et al. (1988) Sato et al. (1988) Sato et al. (1989) Shibayama and Horikawa (1986) Smith and Kraus (1990)	Hansen and Svendsen (1984) Horikawa and Kuo (1966), slope=0 Horikawa and Kuo (1966), slope=1/80-1/20 Kajima et al. (1983) Kraus and Smith (1994) Nadaoka et al. (1982) Nagayama (1983) Okayasu et al. (1988) Sato et al. (1988) Sato et al. (1989) Shibayama and Horikawa (1986) Smith and Kraus (1990)	of cases model, (Eq.2:23) Hansen and Svendsen (1984) 1 13.83 Horikawa and Kuo (1966), slope=0 101 13.87 Horikawa and Kuo (1966), slope=1/80-1/20 112 17.86 Kajima et al. (1983) 79 20.06 Kraus and Smith (1994) 57 21.87 Nadaoka et al. (1982) 2 8.38 Nagayama (1983) 12 9.55 Okayasu et al. (1988) 10 13.57 Sato et al. (1988) 3 8.11 Sato et al. (1989) 2 24.76 Shibayama and Horikawa (1986) 10 17.15 Smith and Kraus (1990) 101 21.98

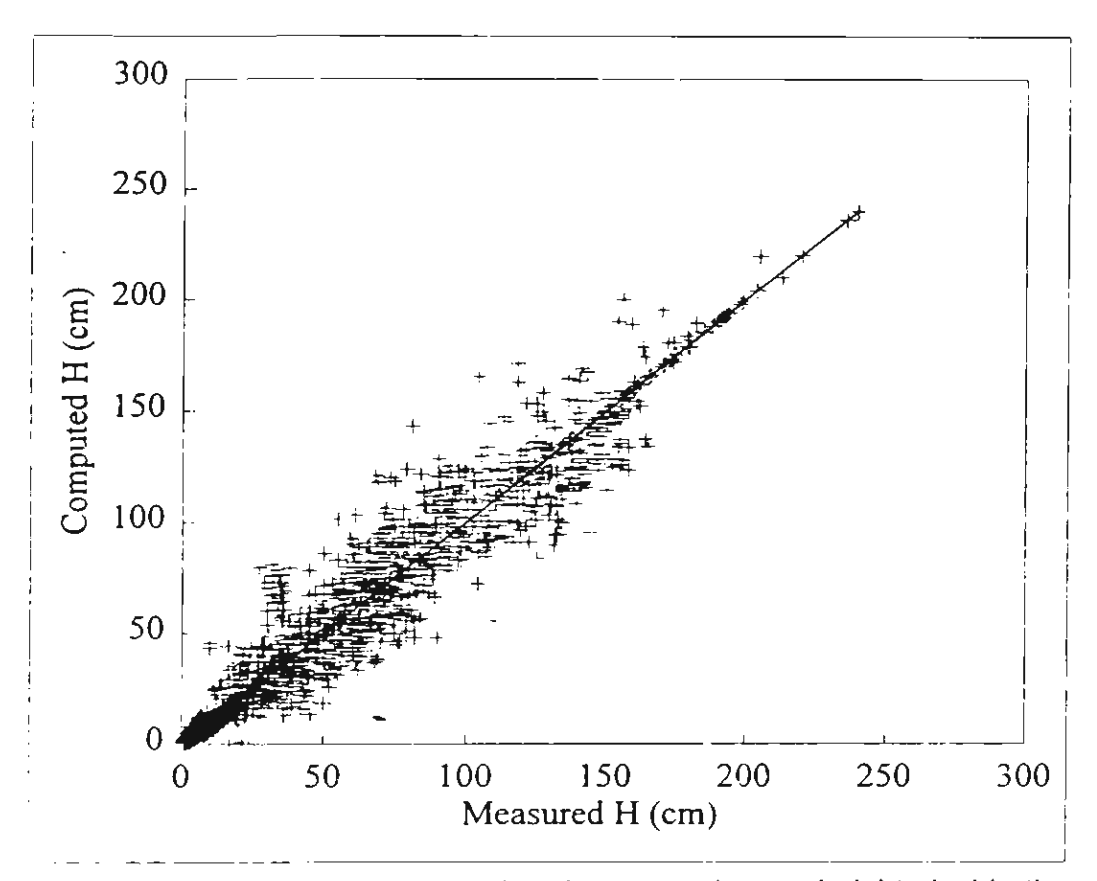


Figure 2.8: Comparison between computed and measured wave heights inside the surf zone (measured data from Table 2.3).

2.2.2 Breaking location

When waves propagate to the nearshore zone, wave profiles are steepen and eventually waves break and it will induce strong turbulence. At the present stage, the knowledge of breaking wave is not enough to describe details of breaking process. Empirical method must be used to predict the breaking location.

Considering wide range of data, the author (see section 2.1) proposed an empirical formula for computing the initiation of breaking wave height. However if this formula is used together with linear wave theory, the predicted breaking point, in some cases, will shift on shoreward of the real one. In those cases, linear wave theory gives under estimation of wave height just before the breaking point. To avoid this problem, Watanabe et al. (1984) used linear wave theory to covert breaking depth diagram of Goda (1970) to be the diagram of particle velocity-celerity ratio (\hat{u}/c) and used it to determine the breaking point (Isobe, 1987). For the convenience of numerical calculation, the diagram of Watanabe et al. (1984) was approximated by Isobe (1987) as

$$\left(\frac{\hat{u}}{c}\right)_{b} = 0.53 - 0.3 \exp\left[-3\sqrt{\frac{h_{b}}{L_{o}}}\right] + 5m_{b}^{3/2} \exp\left[-45\left(\sqrt{\frac{h_{b}}{L_{o}}} - 0.1\right)^{2}\right]$$
(2.43)

where \hat{u} is the amplitude of horizontal water particle velocity at the mean water level, L_o is the deep-water wavelength, m_b is the bottom slope and subscript b denote the quantity at breaking point. The variables \hat{u} and c are calculated based on linear wave theory.

Since wave height is the convenient variable in this study, Eq. (2.43) is transformed in term of breaking wave height, by using linear wave theory.

$$H_{b} = \frac{L_{o}}{\pi \coth^{2}(k_{b}h_{b})} \left\{ 0.53 - 0.3 \exp\left[-3\sqrt{\frac{h_{b}}{L_{o}}}\right] + 5m_{b}^{3/2} \exp\left[-45\left(\sqrt{\frac{h_{b}}{L_{o}}} - 0.1\right)^{2}\right] \right\}$$
(2.44)

Eq. (2.44) will be used to compute the location of wave breaking. Since Eq. (2.44) is originated from Goda breaking depth diagram, Eq. (2.44) will be call as Goda breaking index.

2.2.3 Wave model structure and results

The numerical model is based on the energy flux conservation (Eq. 2.1). Backward finite difference scheme is used to compute wave height transformation from energy flux conservation equation. The finite difference method replaces the partial differential operator in Eq. (2.1) with algebraic operations at the grid points as ($\theta = 0$ for cross-shore propagation)

$$\frac{1}{8} \rho g \frac{\left(H_i^2 c_{gi} - H_{i-1}^2 c_{gi-1}\right)}{\Delta x} = -D_{Bi-1}$$
 (2.45)

or
$$H_{i} = \sqrt{\left(H_{i-1}^{2} c_{gi-1} - \frac{8\Delta x}{\rho g} D_{Bi-1}\right) / c_{gi}}$$
 (2.46)

where subscript i denote the quantity at the grid number i.

Eq. (2.46) enables the grid-by-grid explicit computation of the value H_i . The numerical procedure for computing wave height transformation from offshore to shoreline can be summarized as the followings.

- 1. Input the initial water depth (h) at each grid, wave period (T) and grid distance (Δx) .
- 2. Input incident wave height at the first grid.
- 3. Compute group velocity (c_x) for each grid (using linear wave theory).
- 4. Compute the breaking wave height (H_{hi-1}) from Goda breaking index (Eq. 2.44).
- 5. If $H_{i-1} < H_{bi-1}$, the wave is in the offshore zone. The wave height can be computed from Eq. (2.46) by using $D_{Ri-1} = 0$.
- 6. If $H_{i-1} \ge H_{bi-1}$, the wave is in the surf zone. The wave height can be computed from Eq. (2.46) by using D_{bi-1} from Eq. (2.42).
- 7. The wave model allows wave reformation to take place when the local wave height reaches the stable wave height in which energy dissipation is equal to zero. In the

reformation zone, wave propagates in the same manner as in offshore zone and steps 4-6 will be repeated.

- 8. The steps 1-7 are repeated until the wave height for all grids have been computed.
- 9. Mean water level (wave set-up or set-down). $\bar{\varsigma}$, is computed from the momentum conservation equation as

$$\frac{\partial \,\overline{\varsigma}}{\partial \,x} = -\frac{1}{\rho \,gh} \frac{\partial \,S_{xx}}{\partial \,x} \tag{2.47}$$

where $S_{xx} = \left(\frac{1}{2} + \frac{2kh}{\sinh 2kh}\right)E$ is the normal radiation stress in x-direction. Backward finite difference scheme is used to solve Eq. (2.47). The finite difference form of Eq. (2.47) is expressed as

$$\frac{\left(\overline{\varsigma}_{i} - \overline{\varsigma}_{i-1}\right)}{\Delta x} = -\frac{1}{\rho gh} \frac{\left(S_{xxi} - S_{xxi-1}\right)}{\Delta x} \tag{2.48}$$

At the offshore boundary, the mean water level is set to be equal to zero. The mean water level, $\bar{\zeta}$, for all grids can be computed from Eq. (2.48).

10. The steps 1-9 are repeated until the values of mean water level reach a steady solution. About 2 or 3 iterations are enough to get a steady solution.

Comparison between measured and computed wave height for all cases of Kajima et al. (1983) are shown in Fig. 2.9. Figs. 2.10 and 2.11 show the typical examples of computed and measured wave height transformation. The results of the present wave model can be summarized as follows.

- a) In the offshore zone: the computed results show that linear wave theory gives an under estimation of wave height at the location of high Ursell number (near breaking point of case 2.2 in Fig. 2.10).
- b) At the breaking point: case 2.2 of Fig. 2.10 clearly shows the under estimation of wave height but breaking location, computed from Eq. (2.44), is quite well. Wave breaking always occurs at the shoreward slope of bar. In some cases, the predicted breaking location shifts seaward of the measured one (e.g., cases 2.1 and 6.1) and some cases are shift shoreward (e.g., case 2.3). However, Eq. (2.44) has a trend to give good prediction in general cases.
- c) In the surf zone: as seen in Figs. 2.10 and 2.11, the energy dissipation model gives good prediction compared with the measured wave height. However, wave reformation in cases 4.2 and 4.3 can not be predicted. Even if we use the value Γ = 0.4, it still can not predict the wave reformation. This problem is also found by Larson and Kraus (1989).
- d) In general, we can say that the model gives reasonably well estimation. The main merit of this model is that it requires only a few seconds to get the solution.

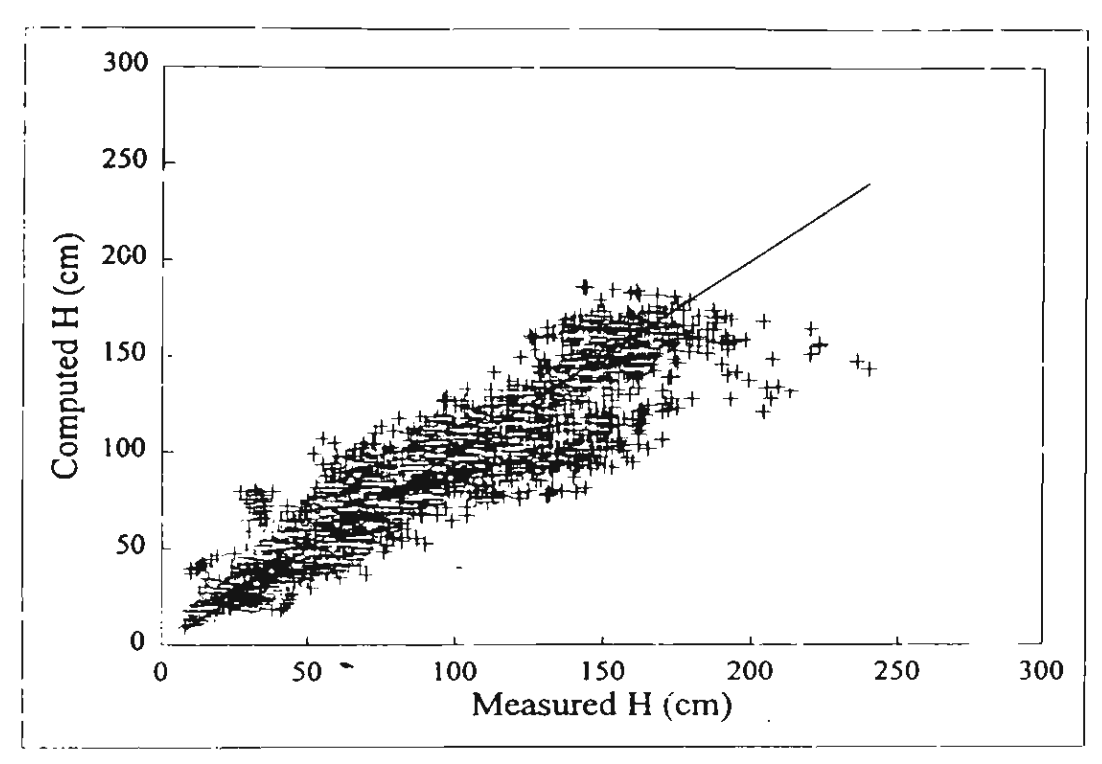


Figure 2.9: Comparison between computed and measured wave heights (measured data from Kajima et al., 1983).

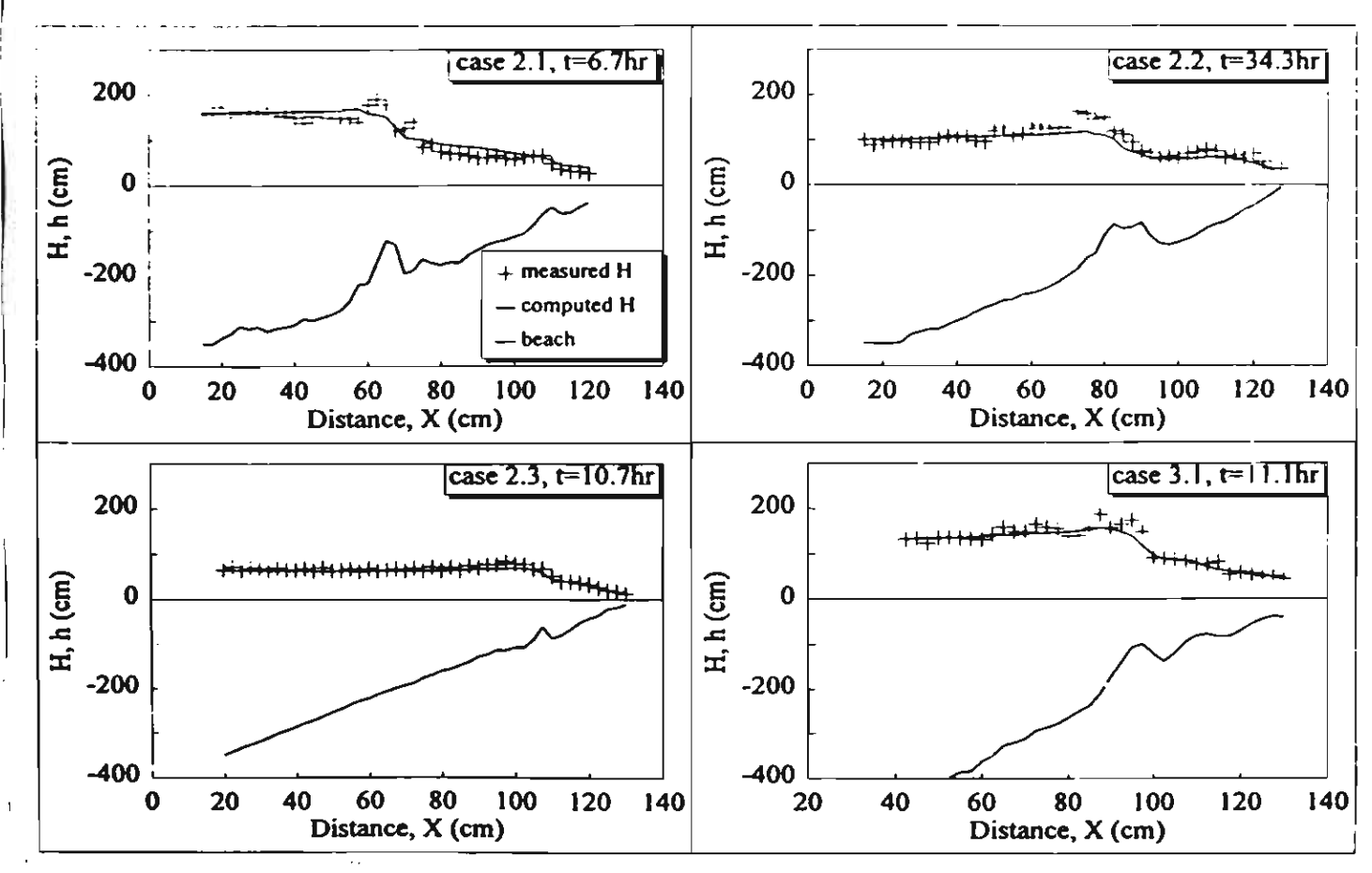


Figure 2.10: Examples of computed and measured wave height transformations (measured data from Kajima et al., 1983, cases 2.1, 2.2, 2.3, and 3.1)

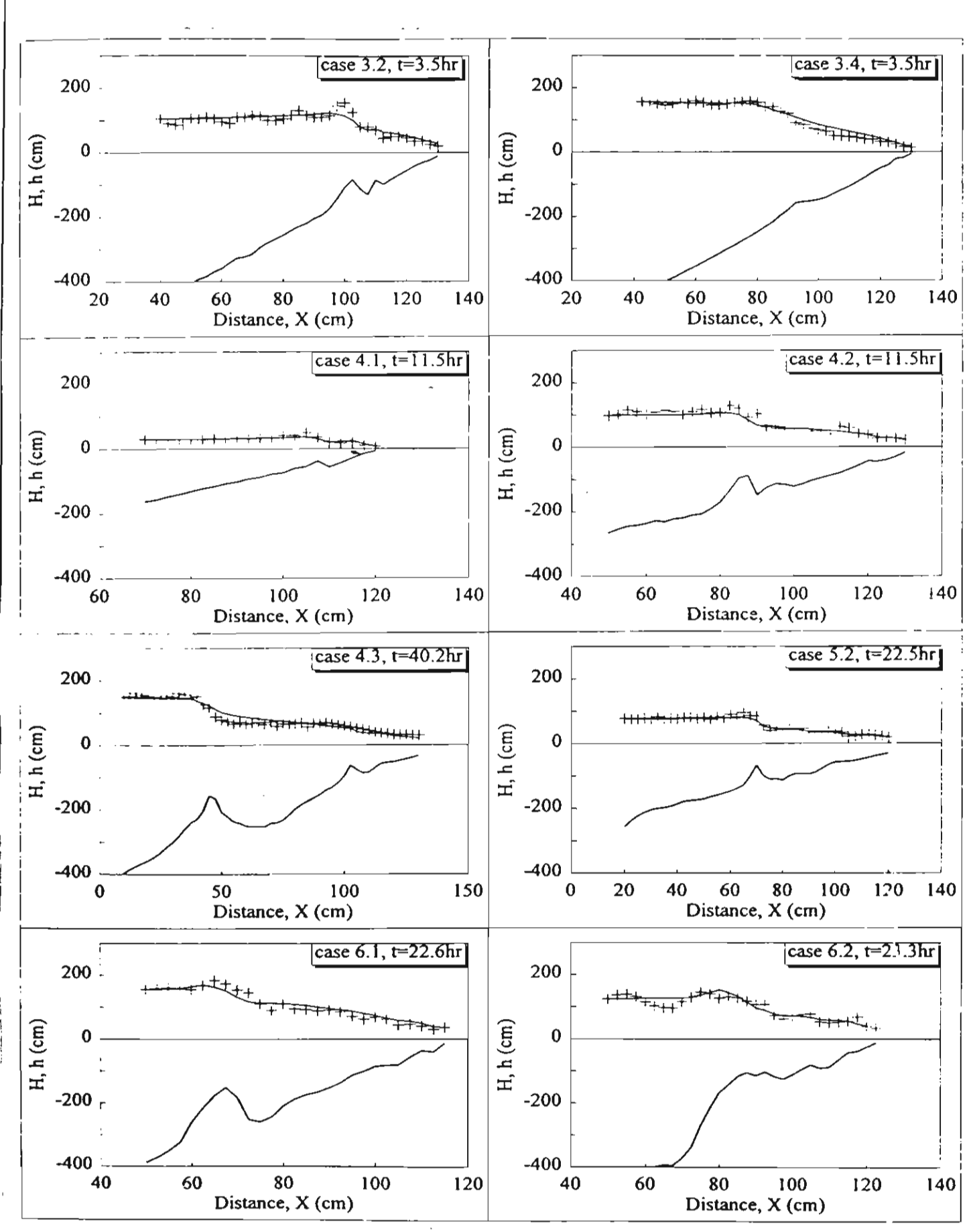


Figure 2.11: Examples of computed and measured wave height transformations (measured data from Kajima et al., 1983, cases 3.2, 3.4, 4.1, 4.2, 4.3, 5.2, 6.1, and 6.2).

2.3 Irregular Wave Height Transformation

Irregular wave breaking is more complex than regular wave breaking. In contrast to regular waves there is no well-defined breaking point for irregular waves. The highest waves tend to break at greatest distances from the shore. Thus, the energy dissipation of irregular waves occurs over a considerably greater area than that of regular waves. The experimental results from laboratory and field experiments have been collected for calibration and verification of the model. A summary of the collected experimental results is given in Table 2.6.

Table 2.6: Summary of collected experimental data used to validate the present models.

Sources	No. of	Wave	Bed condition	Apparatus
	cases	condition		
Kraus and Smith (1994)	_ 128	irregular	sandy beach	large-scale
Smith et al. (1993)	4	irregular	sandy beach	field
Smith and Kraus (1990)	12	irregular	plane and	small-scale
			barred beach	
Thornton and Guza (1986)	4	irregular	sandy beach	field
Total	148			

2.3.1 Model development

Dally (1992) used regular wave model of Dally et al. (1985) to simulate transformation of irregular wave by using wave-by-wave approach. This means that Dally assumed that $D_{\mathcal{B}}$ is proportional to the difference between <u>local energy flux of a breaking wave</u> and stable energy flux. Also wave-by-wave approach requires much computation time. Therefore it may not suitable to use in a beach deformation model.

However, the model becomes simple if we set an assumption, similar to that of present regular wave model, that the average rate of energy dissipation in breaking waves is proportional to the difference between <u>local mean energy density</u> and stable energy density. After incorporating the fraction of breaking, the average rate of energy dissipation in irregular wave breaking, \overline{D}_B , can be expressed as

$$\overline{D}_B = \frac{K_5 Q_b c_p}{h} \left[E_m - E_s \right] \tag{2.49}$$

where

$$E_m = \frac{1}{8} \rho \, g H_{rm}^2 \tag{2.50}$$

$$E_{\tau} = \frac{1}{8} \rho g H_{\tau}^{2} = \frac{1}{8} \rho g (\Gamma_{r} h)^{2}$$
 (2.51)

in which all variables are computed based on the linear wave theory, K_5 is the proportional constant, Q_b is the fraction of breaking waves, c_p is the phase velocity related to the peak spectral wave period T_p , h is the water depth, E_m is the local mean energy density, E_s is the stable energy density, H_{rms} is the root mean square wave height, H_s is the stable wave height and Γ_s is the stable wave factor of irregular wave.

Rewriting Eq. (2.49) in term of wave height yields

$$\overline{D}_B = \frac{K_5 Q_b c_p \rho g}{8h} \left[H_{rms}^2 - (\Gamma_i h)^2 \right]$$
 (2.52)

The stable wave factor, Γ_i , is determined by applying Eq. (2.41) as

$$\Gamma_{r} = \exp \left[K_{6} \left(-0.36 - 1.25 \frac{h}{\sqrt{L_{p} H_{rms}}} \right) \right]$$
 (2.53)

where K_6 is the coefficient, L_p is the wavelength related to the peak spectral wave period. Substituting Eq. (2.53) into Eq. (2.52) yields

$$\overline{D}_{B} = \frac{K_{5}Q_{h}c_{p}\rho g}{8h} \left[H_{mi}^{2} - \left(h \exp(-0.36K_{e} - 1.25K_{6} \frac{h}{\sqrt{L_{r}H_{min}}}) \right)^{2} \right]$$
 (2.54)

The local fraction of breaking waves, Q_h , is determined from the derivation of Battjes and Janssen (1978) based on the assumption of truncated Rayleigh distribution at the maximum wave height:

$$\frac{1 - Q_b}{-\ln Q_b} = \left(\frac{H_{min}}{H_b}\right)^2 \tag{2.55}$$

where H_b is the breaking wave height that can be computed by using the breaking criteria of Goda (1970):

$$H_{b} = K_{2}L_{o} \left\{ 1 - \exp \left[-1.5 \frac{\pi h}{L_{o}} \left(1 + 15 m_{u}^{4-1} \right) \right] \right\}$$
 (2.56)

where K_7 is the coefficient, L_o is the deep-water wavelength related to the peak spectral wave period, and m_o is the average bottom slope.

Since Eq. (2.55) is an implicit equation, the iteration process is necessary to compute the fraction of breaking waves, Q_h . It will be more convenient if we can compute Q_h from the explicit form of Eq. (2.55). From the multi-regression analysis, the explicit form of Q_h can be expressed as the following (with R^2 =0.999):

$$Q_{b} = \begin{cases} 0 & for \frac{H_{mix}}{H_{b}} \le 0.43 \\ -0.738 \left(\frac{H_{mix}}{H_{b}}\right) - 0.280 \left(\frac{H_{mix}}{H_{b}}\right)^{2} + 1.785 \left(\frac{H_{mix}}{H_{b}}\right)^{3} + 0.235 & for \frac{H_{mix}}{H_{b}} > 0.43 \end{cases}$$
(2.57)

The energy dissipation model (Eqs. 2.54, 2.56 and 2.57) contains 3 coefficients, $K_5 - K_7$, that can be found from model calibration.

2.3.2 Model calibration

The model is calibrated for determining the optimal values of the coefficients $K_s - K_7$ in Eqs. (2.54) and (2.56). The calibration is carried out with the large-scale experimental data from the SUPERTANK Laboratory Data Collection Project (Kraus and Smith, 1994). The SUPERTANK project was conducted to investigate cross-shore hydrodynamic and sediment transport processes, during the period August 5 to September 13, 1992, at Oregon State University, Corvallis, Oregon, USA. A 76-m-long sandy beach was constructed in a large wave tank of 104 m long, 3.7 m wide, and 4.6 m deep. Wave conditions involved regular and irregular waves. The 20 major tests were performed and each major test consisted of several cases (see Table 2.7). Most of the major tests were performed under the irregular wave actions, except the test No. STBO, STEO, STFO, STGO, STHO, and STIO. The collected experiments for irregular waves include 128 cases of rms wave height profiles, covering incident rms wave heights from 13.9 cm to 60.1 cm, peak wave periods from 2.8 sec to 9.8 sec.

The *rms* wave height transformation is computed by the numerical integration of energy flux balance equation (Eq. 2.1) with the energy dissipation rate \overline{D}_R of Eq. (2.54):

$$\frac{\partial \left(H_{\text{rms}}^2 c_{\text{gp}} \cos \theta\right)}{\partial x} = -\frac{K_5 Q_b c_p}{h} \left[H_{\text{rms}}^2 - \left(h \exp(-0.36K_6 - 1.25K_6 \frac{h}{\sqrt{L_p H_{\text{rms}}}})\right)^2\right]$$
(2.58)

where Q_k is computed from Eq. (2.57), and H_k is computed from Eq. (2.56).

Eq. (2.58) is solved by backward finite difference scheme. Trial simulations indicated that $K_5=0.10$, $K_6=1.60$, and $K_7=0.10$ give good agreement between measured and computed rms wave heights. Finally, the energy dissipation rate of irregular wave breaking can be written as

$$\overline{D}_{B} = \frac{0.1 Q_{b} c_{p} \rho g}{8h} \left[H_{max}^{2} - \left(h \exp(-0.58 - 2.00 \frac{h}{\sqrt{L_{p} H_{max}}}) \right)^{2} \right]$$
 (2.59)

Comparison between measured and computed *rms* wave heights for all 128 cases are shown in Fig. 2.12. Table 2.7 shows the *rms* relative error, *ER*, of the present model for each major tests. The average *rms* relative error, *ER*, for all 128 cases is 9.8 % which indicates good prediction. Typical examples of computed *rms* wave height transformation for each major test are shown in Figs. 2.13 and 2.14. From Table 2.7 and Figs. 2.13-2.14, it can be seen that the model results generally show good prediction, except the test no. STKO (broad-crested offshore mound). Furthermore, for some cases, the model tends to underpredict the wave heights very close to the shore.

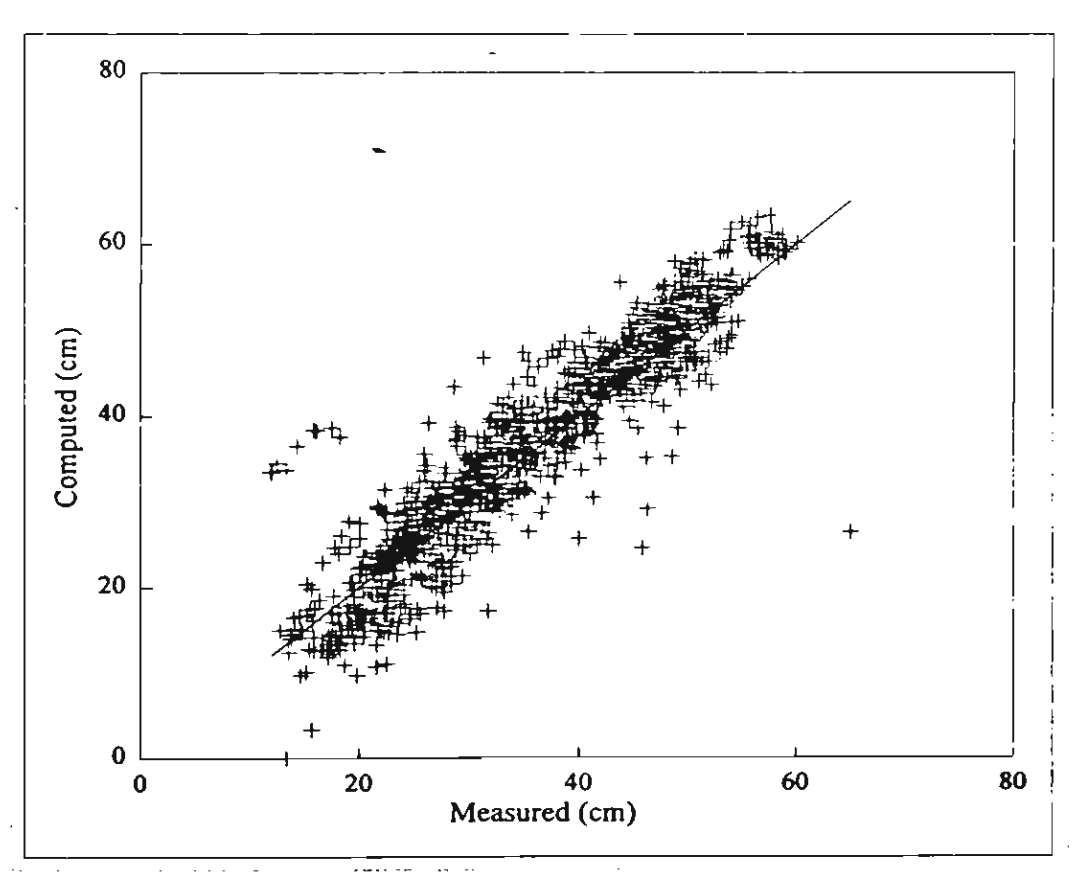


Figure 2.12: Comparison between computed and measured *rms* wave height for 128 cases of large-scale experiments (measured data from Kraus and Smith, 1994).

Table 2.7: Root mean square relative error ($\it ER$) of the present model comparing with irregular wave data of Kraus and Smith (1994).

	<u> </u>	-, -	
Test No.	Description	Total No.	ER of
		of cases	Present
			study
ST10	Erosion toward equilibrium, irregular waves	26	5.77
ST20	Acoustic profiler tests, regular and irregular waves	8	6.86
ST30	Accretion toward equilibrium, irregular waves	19	10.01
ST40	Dedicated hydrodynamics, irregular waves	12	10.37
ST50	Dune erosion, Test 1 of 2, irregular waves	8	12.11
ST60	Dune erosion, Test 2 of 2, irregular waves	9	9.72
ST70	Seawall, Test 1 of 3, irregular waves	9	7.87
ST80	Seawall, Test 2 of 3, irregular waves	3	10.98
ST90	Berm flooding, Test 1 of 2, irregular waves	3	4.32
STAO	Foredune erosion, irregular waves	1	4.94
STBO	Dedicated suspended sediment, regular waves	0	-
STCO	Seawall, Test 3 of 3, irregular waves	8	10.88
STDO	Berm flooding, Test 2 of 2, irregular waves	3	12 39
STEO	Laser Doppler velocimeter, Test 1 of 2, regular waves	0	-
STFO	Laser Doppler velocimeter, Test 2 of 2, regular waves	0	•
STGO	Erosion toward equilibrium, regular waves	0	-
STHO	Erosion, transition toward accretion, regular waves	0	-
STIO	Accretion toward equilibrium, regular waves	0	
STJO	Narrow-crested offshore mound, reg. and irreg. waves	10	10.12
STKO	Broad-crested offshore mound, reg. and irreg. waves	9	22.18
	Diodu-created charlote fround, reg. and irreg. waves		4

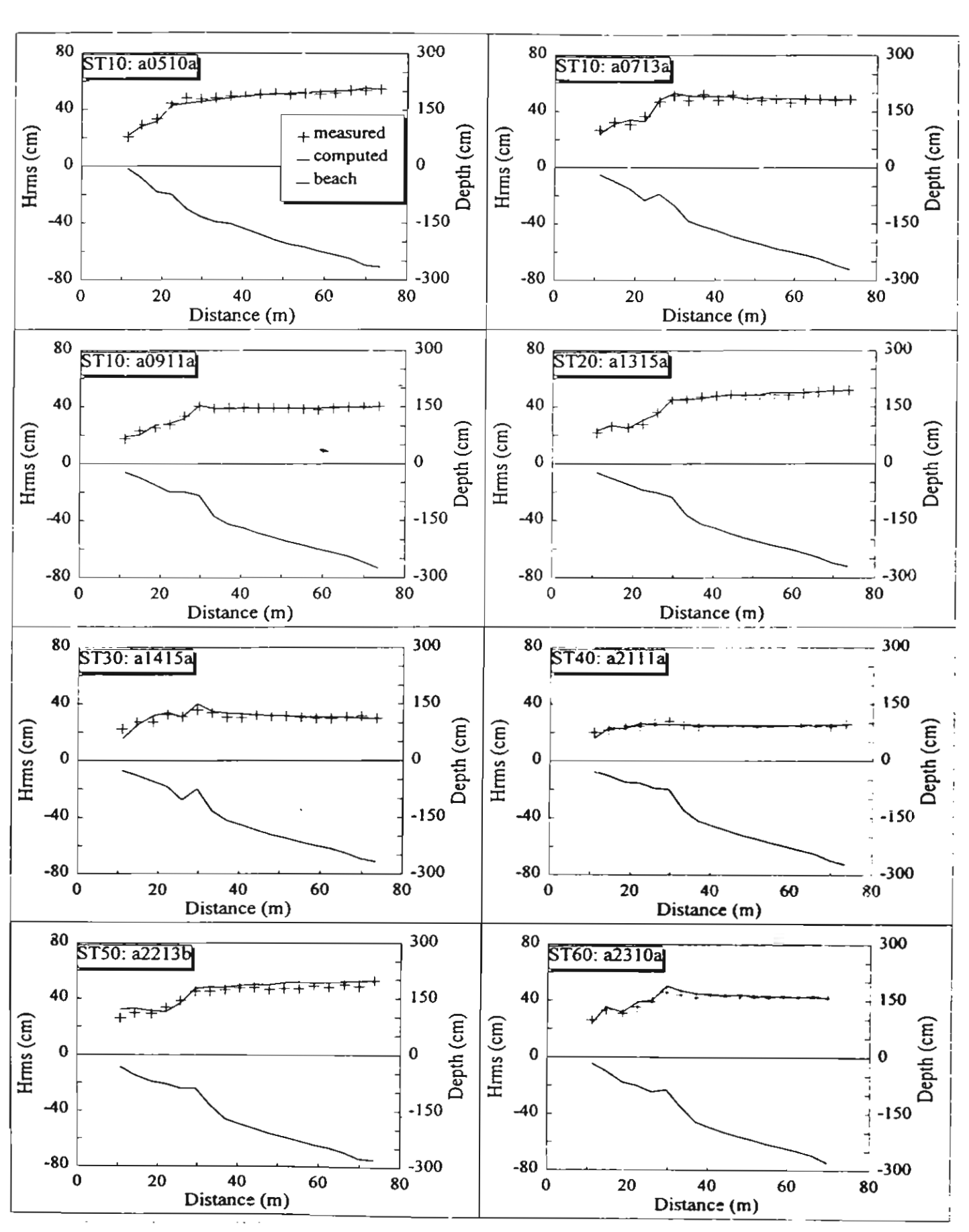


Figure 2.13: Examples of computed and measured *rms* wave height transformation for Test No. ST10-ST60 (measured data from Kraus and Smith, 1994).

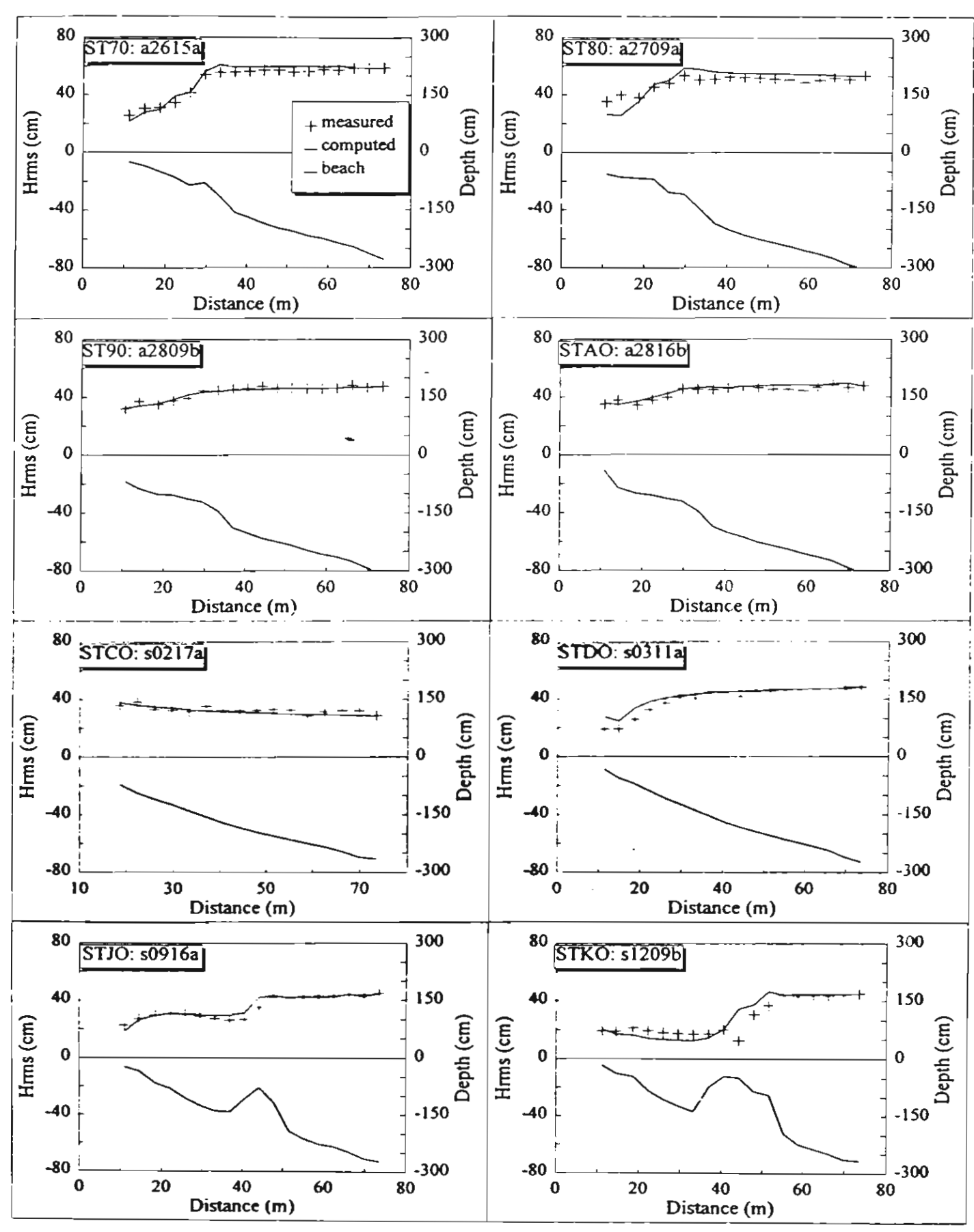


Figure 2.14: Examples of computed and measured *rms* wave height transformation for Test No. ST70-STKO (measured data from Kraus and Smith, 1994).

2.3.3 Model verification

Since the present model is calibrated with only the data from the large-scale experiments, there is still a need of data from small-scale and field experiments for confirming ability of the present model. Three sources of experimental results are collected to verify the model, i.e., small-scale experimental data of Smith and Kraus (1990), field data from the DELILAH project (Smith et al., 1993) and field data of Thornton and Guza (1986).

The wave height transformation is computed from the energy flux balance equation (Eq. 2.58) by using backward finite difference scheme, from offshore boundary to shoreline. All coefficients in the model are kept to be constant for all cases in the verification.

2.3.3.1 Comparison with small-scale laboratory data

The small-scale laboratory data of Smith and Kraus (1990) is used in this subsection. The experiment was conducted to investigate the macro-features of wave breaking over bars and artificial reefs using small wave tank of 45.70-m-long, 0.46-m-wide, and 0.91-m-deep. Both regular and irregular waves were employed in this experiment. Total 12 cases were performed for irregular wave tests. Three irregular wave conditions were generated for three bar configurations as well as for a plane beach.

Comparison between measured and computed *rms* wave heights for all cases are shown in Fig. 2.15. The average *rms* relative error, *ER*, for all cases is 11.9 % which indicates a good prediction of the model. Fig. 2.16 shows the typical examples of computed *rms* wave height transformation for incident *rms* wave height of 10 cm, peak period of 1.75s and four bottom conditions. The model results generally show good agreement with the measured data. However, the model could not predict the rapid increase and decrease in wave heights near the narrow-crested bar. Also, the model gives under prediction for the wave heights close to the shore.

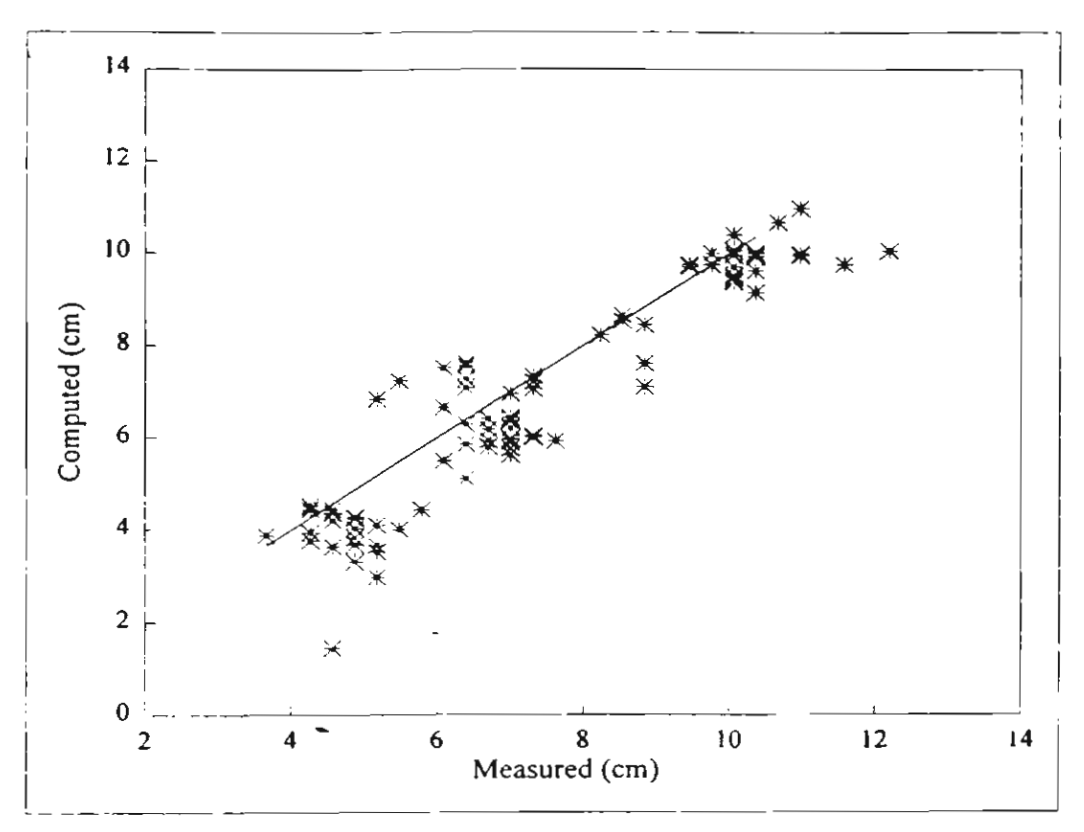


Figure 2.15: Comparison between computed and measured *rms* wave height for 12 cases of small-scale experiments (measured data from Smith and Kraus, 1990).

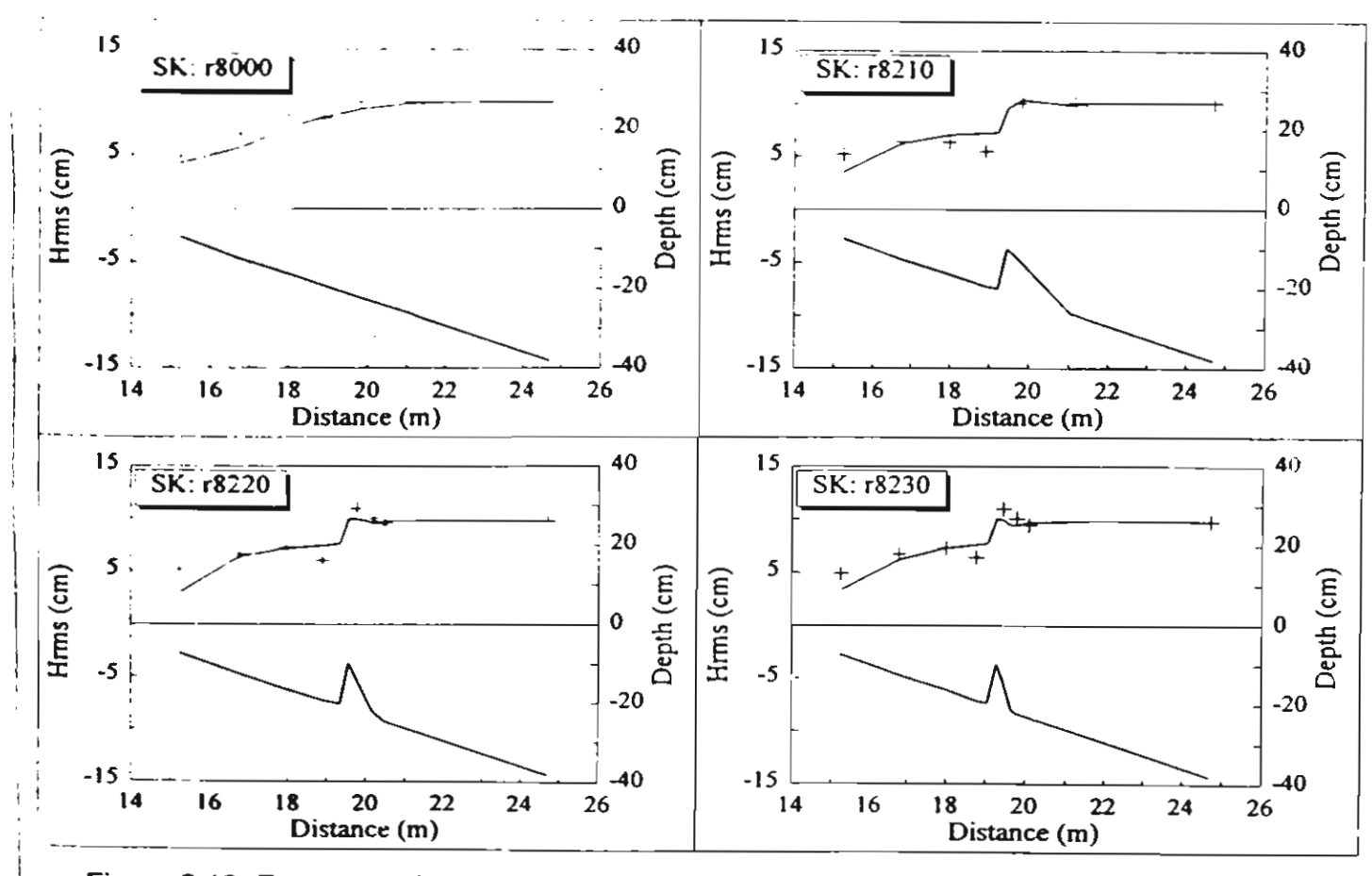


Figure 2.16: Examples of computed and measured H_{rms} for incident H_{rms} = 10 cm, T_p = 1.75s, and four bottom conditions (measured data from Smith and Kraus, 1990).

2.3.3.2 Comparison with field data

Two field data from the DELILAH project (Smith et al., 1993) and Thornton and Guza (1986) are used in this subsection. DELILAH (Duck Experiment on Low-frequency and Incident-band Longshore and Across-shore Hydrodynamics) project was conducted on the barred beach in Duck, North Carolina, USA, to measure currents waves, wind, tide, and beach profiles, during the period October 1-19, 1990.

Thornton and Guza's (1986) experiment was conducted on a beach with nearly straight and parallel depth contours at Leadbetter Beach, Santa Barbara, California, USA, to measure longshore currents, waves, and beach profiles, during the period January 30 to February 23, 1980.

Comparison between computed and measured *rms* wave heights for all cases are shown in Fig. 2.17. Fig. 2.18 shows the typical examples of computed and measured *rms* wave height transformation for the cases of DELILAH project. The model results generally show good agreement with the measured data. However, the predicted wave heights are consistently smaller than the measured wave heights shoreward the bar. Fig. 2.19 shows the typical examples of computed and measured *rms* wave height transformation for the cases of Thornton and Guza (1986). The model results also generally show good agreement with the measured data. However, the model gives slightly over estimation in the offshore region.

2.3.3.3 Summary

The result of verification for each data source is summarized in Table 2.8. It can be seen that the model is capable of simulating the increase in *rms* wave height due to shoaling and subsequent decrease due to wave breaking over wide range of wave conditions and various shapes of beach profiles. The validity of model was confirmed by small and large scale laboratory and field data. The average *rms* relative error, *ER*, of the model is 10.1 %.

Table 2.8: Root mean square relative error (ER) of the present model.

No.	Sources	No. of data set	Apparatus	ER
1	Kraus and Smith (1994)	128	large-scale	9.75
2	Smith and Kraus (1990)	12	small-scale	11.90
3	Smith et al. (1993)	4	field	14.54
4	Thornton and Guza (1986)	4	field	14.41
	Total	148		10.08

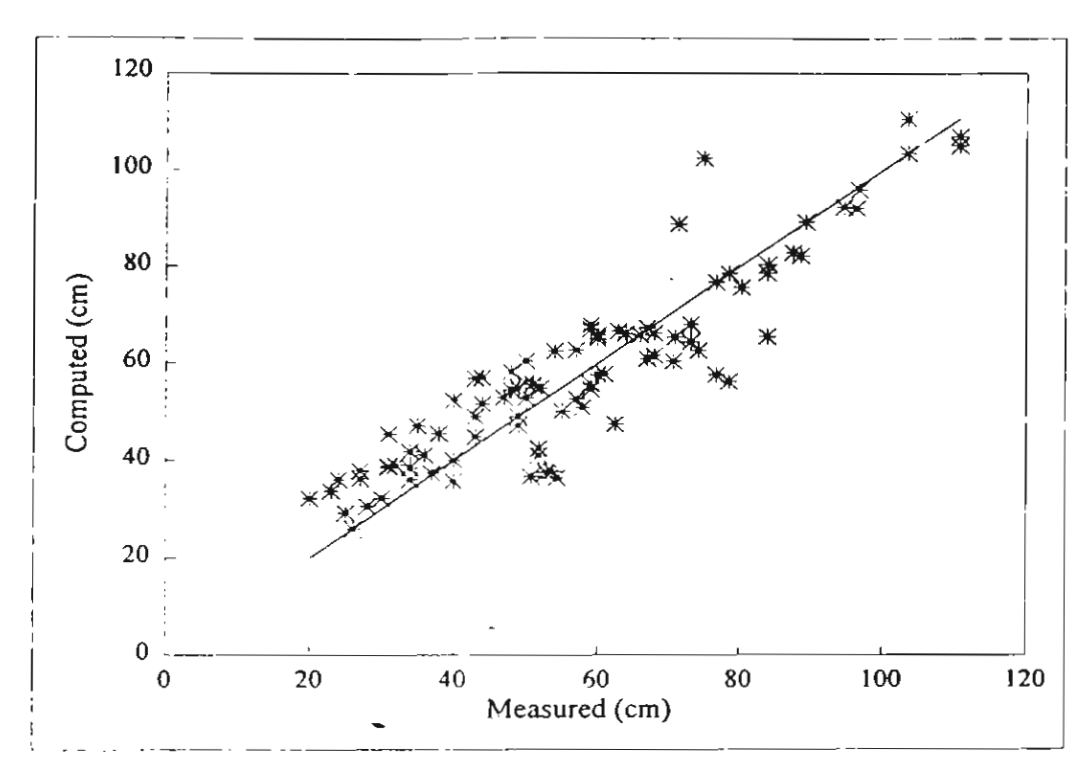


Figure 2.17: Comparison between computed and measured *rms* wave height for 8 cases of field experiments (measured data from Smith et al., 1993, and Thornton and Guza, 1986).

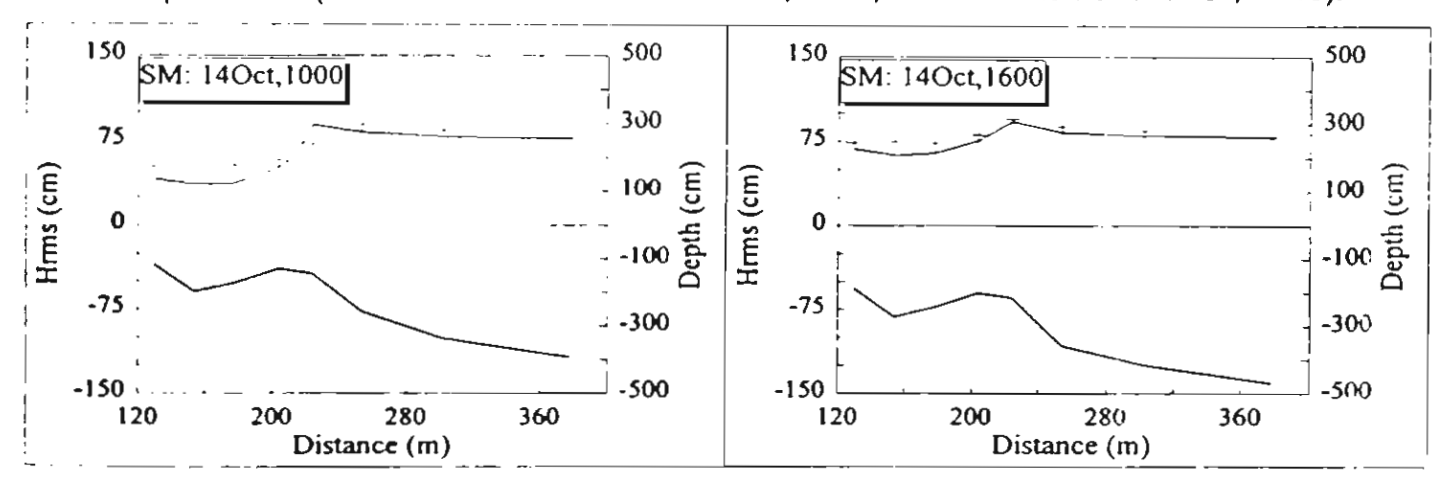


Figure 2.18: Examples of computed and measured *rms* wave height transformation for cases 1000 and 1600 (measured data from Smith et al., 1993).

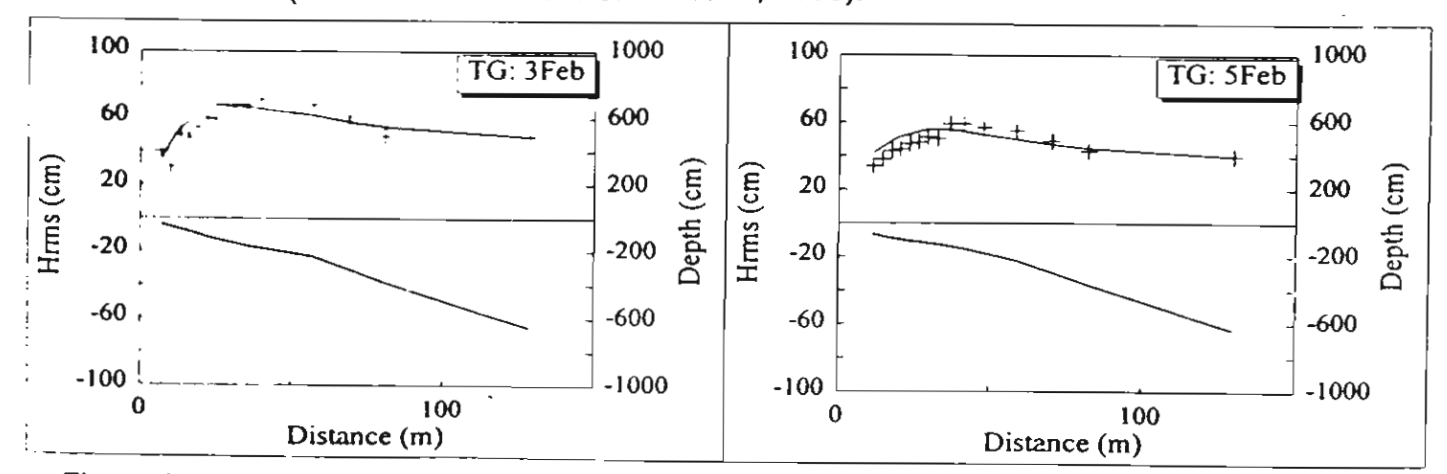


Figure 2.19: Examples of computed and measured *rms* wave height transformation for cases 3Feb and 5Feb (measured data from Thornton and Guza, 1986).

Chapter 3: UNDERTOW VELOCITY

In order to predict the on-offshore suspended sediment transport rate, it is necessary to predict the vertical distribution of sediment concentration and velocity profile accurately. This chapter concentrates on the derivation of formulas for predicting the time-averaged velocity profile under monochromatic wave actions.

From laboratory and field observations, it is well known that, water waves induce a steady drift of fluid particles (mass transport velocity) in additional to an oscillatory motion both for non-breaking and breaking waves. Because of the additional mass flux caused by surface roller, the mass transport velocity induced by breaking waves, commonly referred to as undertow, is larger than that induced by non-breaking waves (Hansen and Svendsen, 1984).

Although, the magnitudes of these time-averaged flow components are generally smaller than those of oscillatory components, it has a significant effect on the sediment transport, especially, in on-offshore direction. From the previous works, many models have been established and give satisfactory results of time-averaged velocity (compared with the limited number of the experimental results). The purposed of this study is to find a proper explicit formula, which can be computed from the flow parameters that emerge as output from the wave model, based on wide range of experimental results.

This chapter concentrates on the derivation of a simple formula for predicting the profile of undertow induced by regular waves (sec. 3.1). After that the formula is applied to compute the undertow profile induced by irregular waves (sec. 3.2).

3.1 Undertow Velocity Induced by Regular Waves

From the previous research works, a number of models have been established for computing undertow profiles. Since the formulas or assumptions in each model are different, the computed results from various models must differ from each other and (may be) from the measured data. We cannot see clearly which model is better than the others, because every model usually shows that it gives a good prediction being compared with a limited range of the experimental conditions. In order to confirm the underlying assumptions in the model, wide range of experimental conditions should be used in the calibration or verification of the model. Unlike many other existing models, wide range of experimental conditions is used to develop and verify the present model.

Laboratory data of undertow profiles from 6 sources, including 379 undertow profiles, have been collected for calibration and verification of the present model. These include small-scale and large-scale laboratory data obtained from a variety of wave and bottom conditions. A summary of the collected laboratory data is given in Table 3.1. Case number in Table 3.1 is kept to be the same as the originals. The experiments of Nadaoka et al. (1982), Hansen and Svendsen (1984) and Okayasu et al. (1988) were performed over the smooth bed conditions, while the experiments of CRIEPI (Kajima et al., 1983), SUPERTANK (Kraus and Smith, 1994) and Cox et al. (1994) were performed over the rough bed conditions. The experiments of CRIEPI (Kajima et al., 1983) and SUPERTANK (Kraus and Smith, 1994) were performed in large-scale wave flume and other experiments were performed in small-scale wave flume.

Due to the limited of measuring points in the large-scale experiments of CRIEPI (Kajima et al., 1983) and SUPERTANK (Kraus and Smith, 1994), the measured data may difficult to be used in the model calibration. Only the measured undertow inside the surf zone of Nadaoka et al. (1982), Hansen and Svendsen (1984), Okayasu et al. (1988) and Cox et al. (1994) are used to calibrate the present model. However, all of the collected data are used to verify the present model.

3.1.1 Governing equation

For computing the beach deformation, the undertow model should be kept as simple as possible because of the frequent changing of wave and bottom profiles. Therefore the present undertow profile is calculated based on the assumption of eddy viscosity model. By considering time-averaged values, the eddy viscosity model can be expressed as

$$\tau = \rho v_{i} \frac{\partial U}{\partial \tau} \tag{3.1}$$

where τ is the time-averaged shear stress, ρ is fluid density, ν_i is the time-averaged eddy viscosity coefficient, U is the time-averaged velocity or undertow, and z is the upward vertical coordinate from the bed.

To solve the eddy viscosity model [Eq. (3.1)], the expression of τ/v_r , should be known and one boundary condition of velocity should be also given. The mean velocity (vertically averaged from bed to wave trough), U_m , is used as the boundary condition of Eq. (3.1).

Table 3.1: Summary of collected laboratory data used to validate the present model.

Sources	Case No.	Total No.	Bed conditions	Apparatus
		of profiles		
Nadaoka et al. (1982)	1	7	plane, smooth	small-scale
	5	7		
Hansen and Svendsen (1984)	1	4	plane, smooth	small-scale
Okayasu et al. (1988)	1	6	plane, smooth	small-scale
	2	6		
	3	6		
	4	6		
	⁻ 6	7		
	7	6		
	8	7		
	9	6		
	10	6		
Cox et al. (1994)	1	6	plane, rough	small-scale
CRIEPI (1983)	2.1	13	sandy beach	large-scale
	2.3	10		
	3.3	16		
	3.4	13		
	4.1	10		
	4.2	22		
	4.3	48		
	5.2	57	-	
	6.1	21		
	6.2	19		
SUPERTANK (1994)	STEO	8	sandy beach	large-scale
	STFO	4		
	STGO	10		
	STHO	10		
	STIO	38		
Total		379		

3.1.2 Shear stress and eddy viscosity coefficient

In the eddy viscosity model, vertical distribution of shear stress, τ , and eddy viscosity coefficient, ν_i , are important for the analysis of vertical distribution of the undertow. Okayasu et al. (1988) showed through experiments that the vertical distribution of the shear stress and eddy viscosity coefficient, from bed to wave trough, are linear functions of the vertical elevation. Since the turbulence in the surf zone is mainly caused by broken waves, the shear stress and eddy viscosity coefficient may depend on the rate of energy dissipation due to wave breaking. Thus the formula of shear stress, τ , is assumed to be

$$\tau = \rho^{1/3} D_R^{2/3} \left[k_1 \frac{z}{d} + k_2 \right]$$
 (3.2)

where D_k is the energy dissipation rate of a broken wave, d is the water depth at wave trough, k_1 and k_2 are the coefficients.

The eddy viscosity coefficient, v_i , is calculated by

$$v_{i} = k_{3} \left(\frac{D_{R}}{\rho}\right)^{1/3} z \tag{3.3}$$

where k_3 is also a coefficient.

So, τ/v , can be expressed as

$$\frac{\tau}{v_{\star}} = \rho^{2/3} D_{h}^{1/3} \left[\frac{k_{4}}{d} + \frac{k_{5}}{z} \right] \tag{3.4}$$

where $k_4 = k_1/k_3$, and $k_5 = k_2/k_3$.

The main attention in this section is to find out the appropriate values of the coefficients k_4 and k_5 in Eq. (3.4). It should be noted that, the ratio of turbulent shear stress and eddy viscosity coefficient in Eq. (3.4) depends only on energy dissipation of the breaking waves. The turbulence caused by bed roughness is not included in this equation. This means that Eq. (3.4) may be invalid at the region closed to the bed (inside the bottom boundary layer). For the rough bed experiments, only the laboratory data outside the boundary layer is used in the model calibration.

The experiments of Nadaoka et al. (1982), Hansen and Svendsen (1984), Okayasu et al. (1988) and Cox et al. (1994) are used to examine the ability of Eq. (3.4). Since the measured values of τ and ν , are not available, we have to examine Eq. (3.4) in terms of velocity. Substituting Eq. (3.4) into Eq. (3.1), then take an integration, the time-averaged velocity or undertow profile can be expressed as

$$U = \int \left(\frac{D_h}{\rho}\right)^{1/3} \left[\frac{k_4}{d} + \frac{k_5}{z}\right] dz \tag{3.5}$$

Then

$$U = \left(\frac{D_B}{\rho}\right)^{1/3} \left[\frac{k_4 z}{d} + k_5 \ln z\right] + U_\sigma \tag{3.6}$$

where U_a is an integral constant.

The mean velocity, $U_{\mathbf{m}}$, is defined as

$$U_m = \frac{1}{d} \int_{z_0}^{d} U dz \tag{3.7}$$

where z_n is the height of bottom roughness.

Substituting Eq. (3.6) into Eq. (3.7) then taking an integration and assuming z_{σ} is very small comparing with the water depth of wave trough (d), the integral constant U_{σ} is expressed as

$$U_{a} = U_{m} - \left(\frac{D_{B}}{\rho}\right)^{1/3} \left[\frac{k_{4}}{2} + k_{5} (\ln d - 1)\right]$$
 (3.8)

Substitution of Eq. (3.8) into Eq. (3.6) yields

$$U = \left(\frac{D_B}{\rho}\right)^{1/3} \left[k_4 \left(\frac{z}{d} - \frac{1}{2}\right) + k_5 \left(\ln \frac{z}{d} + 1\right) \right] + U_m \tag{3.9}$$

According to the difference of observed breaking wave shape, Svendsen et al. (1978) suggested to divide the surf zone into transition zone and inner zone. The behavior of the variation of wave height and mean water level inside the transition zone is quite different from the inner surf zone. In the transition zone, wave height decays rapidly and mean water level is relatively constant then abrupt change in slope at the transition point (Svendsen, 1984a; and Basco and Yamashita, 1986). Okayasu (1989) defined the transition point as the point where fully developed bore-like wave is formed. It is interesting to note that from the experimental results of Nadaoka et al. (1982), Okayasu et al. (1988) and Cox et al. (1994), the maximum of mean velocity occurs at the transition point. In summary, we may use four criterions to define the transition point, i.e., mean water level, wave height, mean velocity and bore formation.

The experimental results of Okayasu (1989, pp. 33 and 36-38) show that the turbulence, induced by breaking waves, in the transition zone is different from the inner zone. Since the mechanisms of turbulence induced by breaking wave (or surface roller) in these two zones are different, the different treatment is necessary. To incorporate this process, for the sake of simplicity, Eq. (3.9) may be written as follows.

$$U = k_6 \left(\frac{D_B}{\rho}\right)^{1/3} \left[k_4 \left(\frac{z}{d} - \frac{1}{2}\right) + k_5 \left(\ln \frac{z}{d} + 1\right) \right] + U_m$$
 (3.10)

where k_6 is the coefficient introduced herein to account for the growing of surface roller in the transition zone.

In order to investigate the validity of the model, the validation data should be compatible with the assumption on which the model itself is based. As mention before, the proposed model is not valid inside the bottom boundary layer. Therefore the data that used to calibrate the present model should be between the upper edge of bottom boundary layer and the wave trough. Since the experiments of Nadaoka et al. (1982), Hansen and Svendsen (1984) and Okayasu et al. (1988) were performed under the smooth bed conditions, all measured velocities below the wave trough are used in the present study. However, the experiment of Cox et al. (1994) was perform under the rough bed condition. Therefore only the measured velocities between the upper edge of bottom boundary layer and the wave trough are used.

The multi-regression analysis between measured U vs. $\left(\frac{z}{d} - \frac{1}{2}\right)$ and $\left(\ln\frac{z}{d} + 1\right)$ is performed to determine the measured U_m and to justify the use of Eq. (3.10). Totally 76 measured undertow profiles inside the surf zone of Nadaoka et al. (1982), Hansen and Svendsen (1984), Okayasu et al. (1988) and Cox et al. (1994) are analyzed. The averaged regression coefficient (R^2), of 76 undertow profiles, is 0.86. This means that the Eq. (3.10), or Eq. (3.4), is fitted well with the measured undertow profiles inside the surf zone.

From the bore model (Thornton and Guza, 1983), $D_{\rm R}$ can be expressed as

$$D_B = \frac{\rho g H^3}{4Th} \tag{3.11}$$

where g is the acceleration of the gravity, H is the wave height, T is the wave period, and h is the mean water depth.

Substituting Eq. (3.11) into Eq. (3.10), the formula of U becomes

$$U = k_6 \left(\frac{gH^3}{4Th}\right)^{1/3} \left[k_4 \left(\frac{z}{d} - \frac{1}{2}\right) + k_5 \left(\ln\frac{z}{d} + 1\right)\right] + U_m \tag{3.12}$$

Eq. (3.12) shows that the derived undertow profile consists of two parts, i.e., linear part and logarithmic part, and contains 3 coefficients, $k_4 - k_6$.

In order to evaluate the accuracy of the prediction, the verification results are presented in term of root mean square relative error (ER), which expressed as:

$$ER = 100 \sqrt{\frac{\sum_{i=1}^{m} (U_{ci} - U_{oi})^{2}}{\sum_{i=1}^{m} U_{oi}^{2}}}$$
(3.13)

where i is the velocity number, U_{ci} is the computed velocity of number i, U_{ci} is the measured velocity of number i, tn is the total number of measured velocity.

According to Rattanapitikon and Shibayama (1993), the coefficient k_6 is taken to be 0.3 at the breaking point and to be 1 at the inner surf zone. Since the measured undertow profiles

of Nadaoka et al. (1982) and Okayasu et al. (1988) show logarithmic profile at the breaking point (see Figs. 3.2a, 3.2d, 3.3a, 3.3d, 3.3g and 3.3j). The coefficient k_4 (of the linear part of Eq. 3.12) may be caused by the surface roller which is zero at the breaking point and gradually increase in transition zone until fully developed at the transition point and inner surf zone. Therefore the coefficient k_4 is taken to be 0 at the breaking point and to be 1 at the inner surf zone (including transition point). The optimal values of k_5 at the breaking point and inner surf zone are determined by trial and error. The minimum error, ER, between measured and computed undertow profile is obtained when $k_5 = -0.21$, at both of the breaking point and inner surf zone. The coefficients $k_4 - k_6$ at the breaking point and inner surf zone are summarized as follow.

Coefficients	Breaking point	Inner surf zone
k_{4}^{-}	0.00	1.00
<i>k</i> ₅	-0.21	-0.21
k ₆	0.30	1.00

In the transition zone, the coefficients k_4 and k_6 are assumed to increase linearly with distance from breaking point to the transition point. The coefficient k_5 is assumed to be -0.21 throughout the transition zone. The formula for undertow profile, therefore, can be written as

$$U = b_1 \left(\frac{gH^3}{4Th}\right)^{1/3} \left[b_2 \left(\frac{z}{d} - \frac{1}{2}\right) - 0.21 \left(\ln \frac{z}{d} + 1\right)\right] + U_m \tag{3.14}$$

where $b_{\rm 1}$ and $b_{\rm 2}$ are the coefficients and expressed as

$$b_{1} = \begin{cases} 0.3 + 0.7 \frac{x_{h} - x}{x_{h} - x_{i}} & transition zone, \\ 1 & inner zone \end{cases}$$

$$b_{2} = \begin{cases} \frac{x_{h} - x}{x_{h} - x_{i}} & transition zone, \\ 1 & inner zone. \end{cases}$$

where x is the position in cross-shore direction, x_b is the position at the breaking point, and x_b is the position at the transition point.

Unlike some existing models (e.g., the model of Cox and Kobayashi, 1997), calibration or adjustment of free parameters is not required for each case. All coefficients in the present model are kept to be constant for all cases of the computation. Fig. 3.1 shows the comparison between measured U and computed U from Eq. (3.14) in which the measured $U_{\rm m}$ is the input data. Figs. 3.2 and 3.3 show the examples of measured and computed

undertow profiles in which the measured U_m is the input data. Table 3.2 shows the rms relative error, ER, of the present model for each case. The rms relative error, ER, for all 76 data sets is 15%. From Figs. 3.1-3.3 and Table 3.2, we can judge that the Eq. (3.14) is accurate enough to be used for computing the profile (or shape) of undertows in the surf zone.

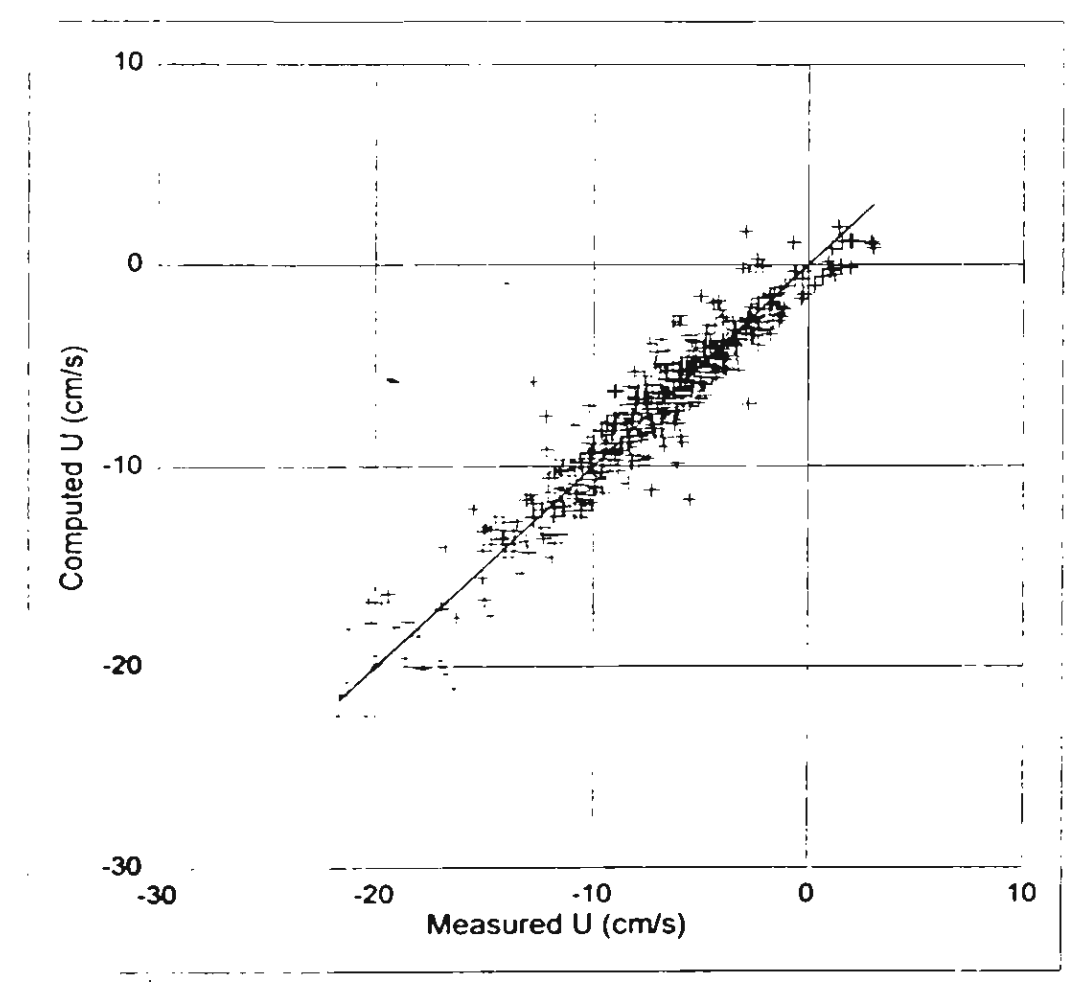


Figure 3.1: Comparison between measured and computed undertow U inside the surf zone; the mean velocity U_{\perp} is given data (measured data from 4 sources as shown in Table 3.2).

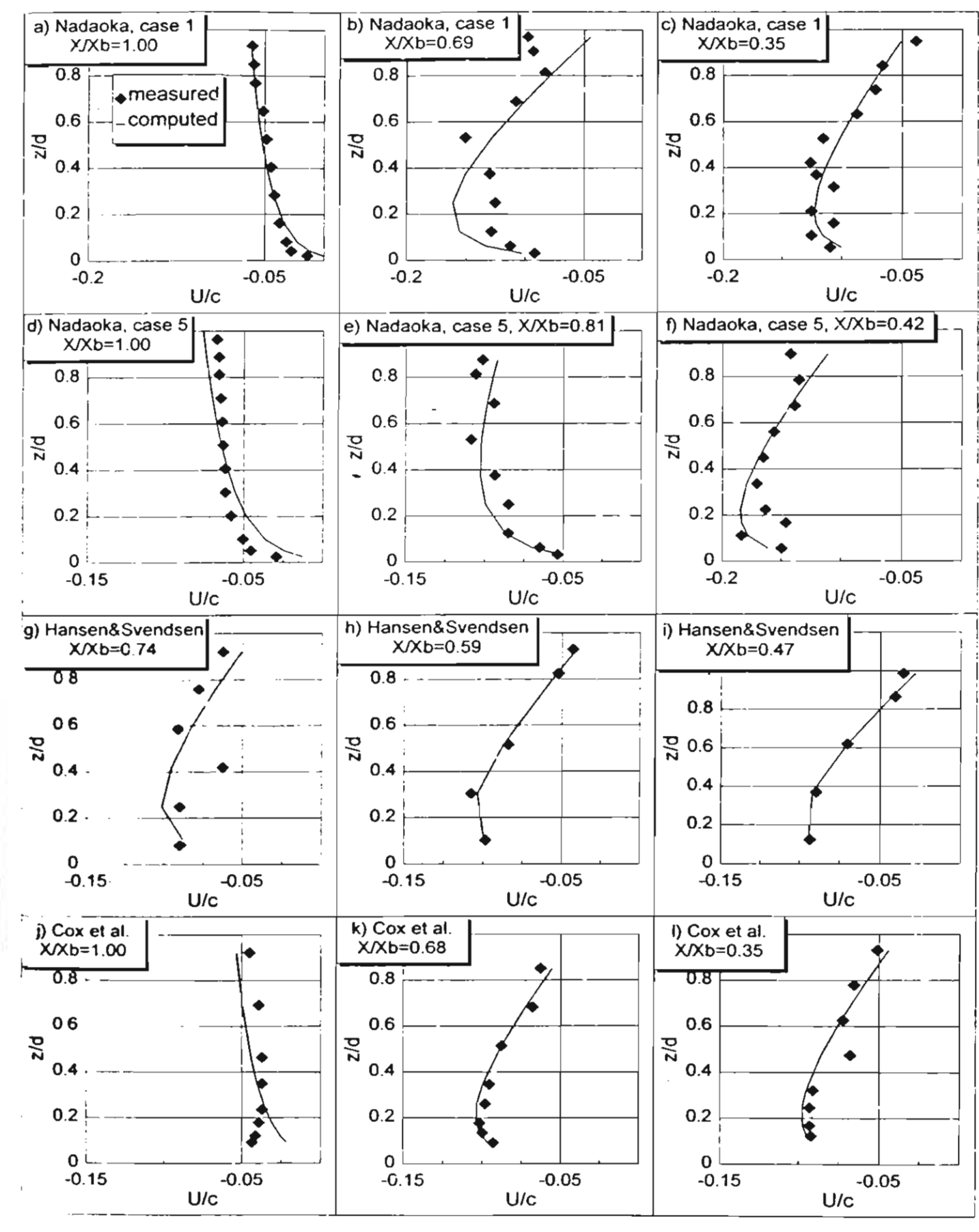


Figure 3.2: Examples of measured and computed undertow profiles in which the mean velocity $U_{\it m}$ is given data (measured data from Nadaoka et al., 1982; Hansen and Svendsen, 1984; and Cox et al., 1994).

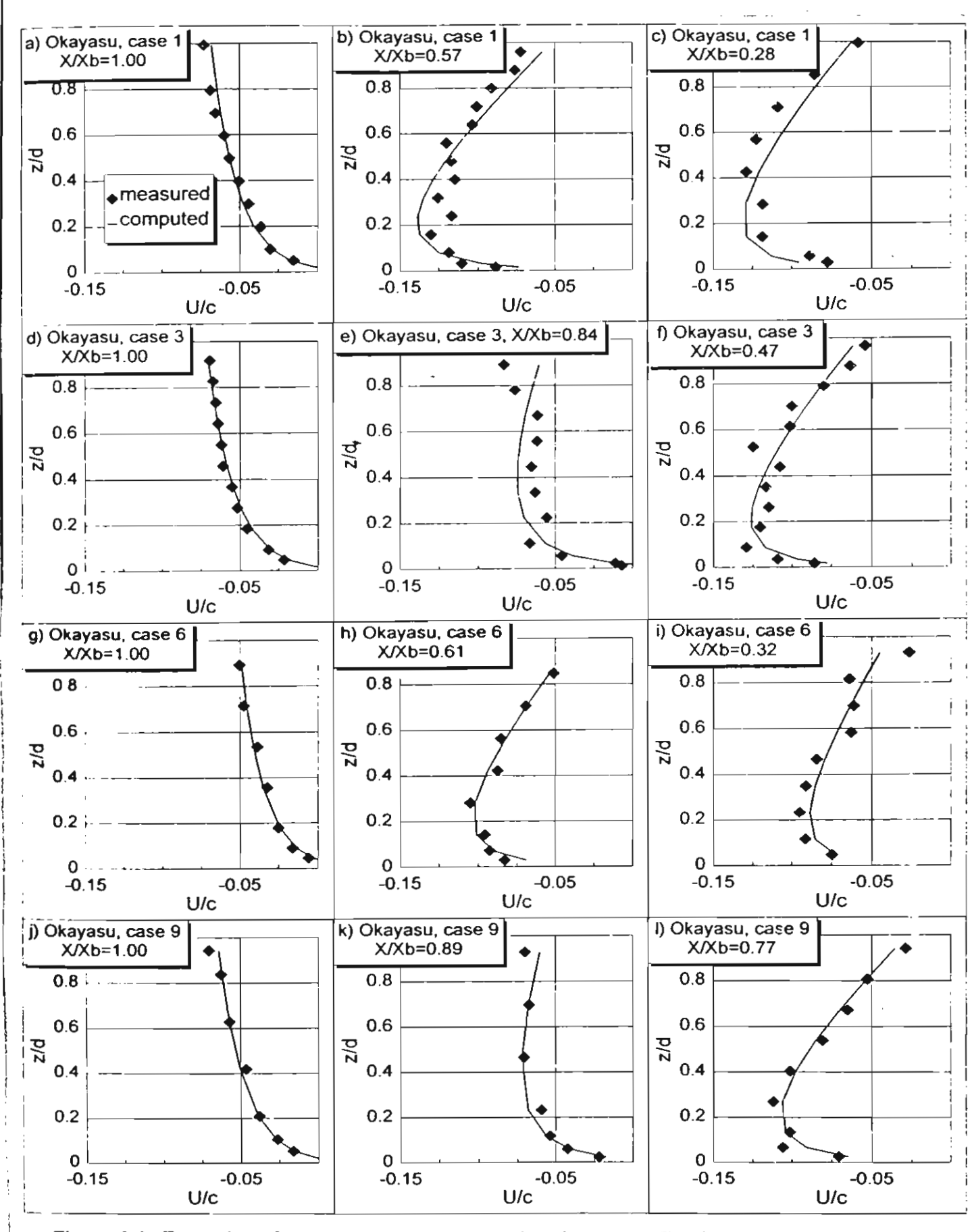


Figure 3.3: Examples of measured and computed undertow profiles in which the mean velocity $U_{\it m}$ is given data (measured data from Okayasu et al., 1988).

Table 3.2: Root mean square relative error (ER) of computed undertow from Eq. (3.14) in which measured $U_{\it m}$ is the given data.

Sources	Case	Total No.	Total No. of	ER of
	No.	of profiles	data points	Eq. (3.14)
Nadaoka et al. (1982)	1	6	65	19.76
	5	5	51	11.88
Hansen and Svendsen (1984)	1	4	22	13.68
Okayasu et al. (1988)	1	6	62	13.91
	2	6	53	16.09
	- 3	6	62	16.03
	4	6	54	13.99
	6	7	51	14.35
	7	6	40	16.43
	8	7	54	10.83
	9	6	46	13.40
	10	6	43	20.20
Cox et al. (1994)	1	5	43	13.08
Total		76	64 6	15.06

3.1.3 Mean undertow velocity

The mean velocity, U_m , is assumed to consist of two components, one is due to the wave motion and the other one due to the surface roller (Svendsen, 1984b).

$$U_m = U_w + U_r \tag{3.15}$$

where $U_{\mathbf{x}}$ is the mean velocity due to wave motion, and $U_{\mathbf{r}}$ is the mean velocity due to surface roller

Various formulas for computing $U_{\star \star}$ and U_{r} have been suggested by the previous researchers. However, no direct literature has been published to describe clearly the applicability and accuracy of each formula. Therefore, the objectives of this section are to investigate the performance of each formula and to develop the appropriate one comparing with the collected experimental results. The mean velocity due to wave motion and due to surface roller are presented in sections 3.1.3.1 and 3.1.3.2, respectively.

3.1.3.1 Mean velocity due to wave motion

From the previous studies, the following explicit formulas have been suggested to compute the mean velocity due to wave motion.

a) Svendsen (1984b) proposed to compute the mean velocity due to wave motion as

$$U_{\bullet} = -B_o c \left(\frac{H}{h}\right)^2 \tag{3.16}$$

where $B_o = \frac{1}{T} \int_0^T (\eta/H)^2 dt$ is the wave shape parameter, which equals 1/8 for sinusoidal waves, c is the phase velocity, η is the water surface elevation measured from mean water level, and t is time.

Svendsen (1984b) suggested to use $B_{\sigma}=0.08$, while Hansen and Svendsen (1987) suggested to use $B_{\sigma}=0.09$. However, from the experimental results of Hansen and Svendsen (1984) and Okayasu et al. (1988), B_{σ} varies with a quite wide range of varieties from 0.05 to 0.11. Therefore it may not suitable to use B_{σ} as a constant value. Using the measured B_{σ} of Hansen and Svendsen (1984) and Okayasu et al. (1988), the following formula is fitted well with the measured B_{σ} in the surf zone ($R^2=0.81$, see Fig. 3.4):

$$B_o = 0.125 + 0.6m_a - 0.089 \frac{H}{h} \tag{3.17}$$

where m_a is the average bottom slope.

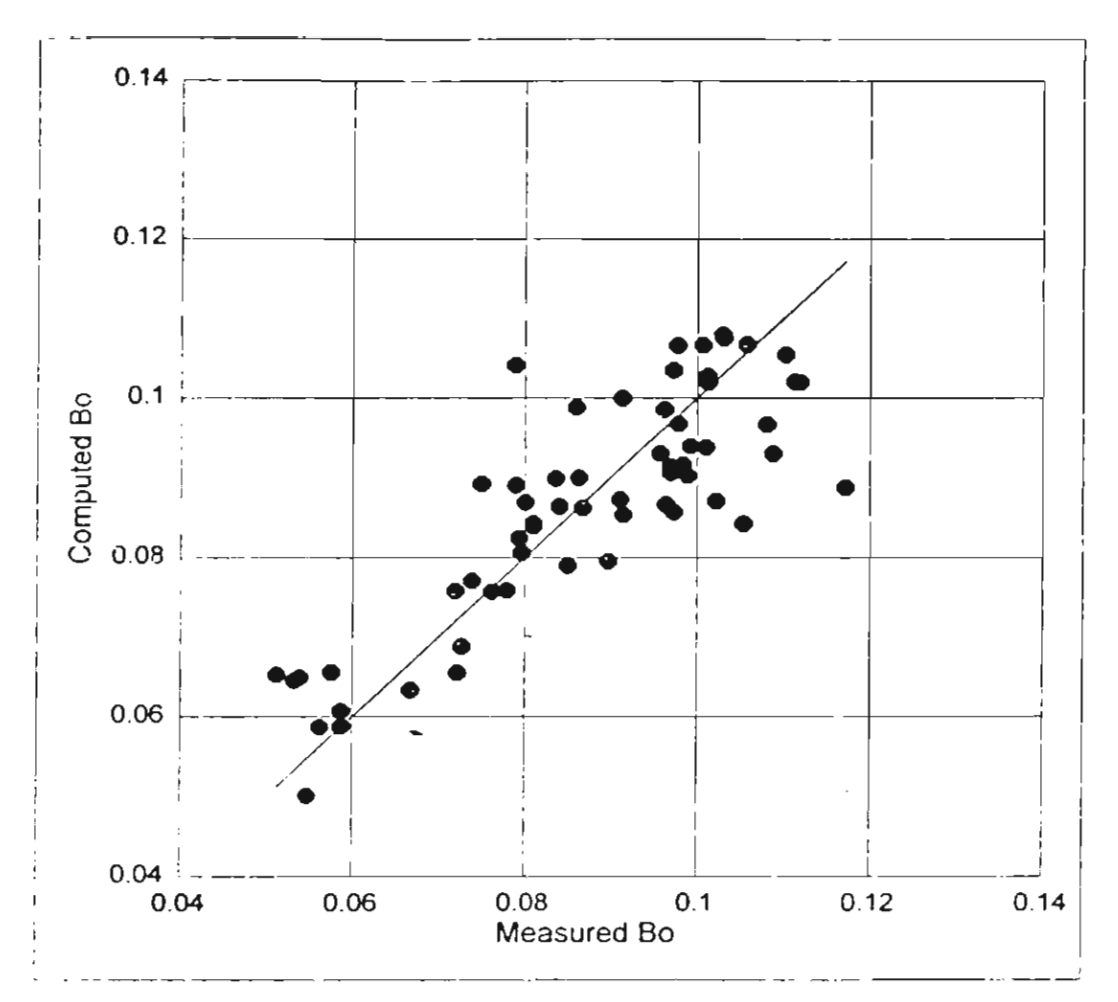


Figure 3.4: Comparison between measured and computed wave shape parameter B_o (measured data from Hansen and Svendsen, 1984; and Okayasu et al., 1988).

b) Hansen and Svendsen (1987) found that the oscillatory particle velocities are significantly smaller than predicted by linear wave theory. Therefore, equation for computing U_{w} of Svendsen (1984b) is modified to be

$$U_{w} = -k_{7} B_{o} c \left(\frac{H}{h}\right)^{2} \tag{3.18}$$

where k_7 is the coefficient and $k_7=0.7$ is recommended by Hansen and Svendsen (1987).

c) Stive and Wind (1986) proposed an empirical formula for computing the mean velocity for entire surf zone as

$$U_m = -0.1H\sqrt{\frac{g}{h}} \tag{3.19}$$

The coefficient 0.1 is from the best fit with the laboratory data. However, Stive and Battjes (1984) suggested using this coefficient as 0.125.

Eq. (3.19) may be written in the form of $U_w + U_r$ as

$$U_m = -k_8 H \sqrt{\frac{g}{h}} - k_9 H \sqrt{\frac{g}{h}}$$
 (3.20)

where k_8 and k_9 are the coefficients.

Therefore the mean velocity due to wave motion, $U_{\mbox{\tiny ω}}$, of Stive and Wind (1986) can be expressed as

$$U_{w} = -k_{g}H\sqrt{\frac{g}{h}} \tag{3.21}$$

d) Sato et al. (1988) proposed to use Eulerian mass transport velocity as

$$U_{w} = -\frac{1}{8} \frac{\sigma H^2 \coth(kh)}{h} \tag{3.22}$$

where σ is the angular frequency, and k is the wave number.

Using dispersion equation, the Eq. (3.22) can be rewritten as

$$U_{w} = -\frac{1}{8} \frac{gH^{2}}{ch} \tag{3.23}$$

As found by Hansen and Svendsen (1987) and Okayasu (1989, page 61) that linear wave theory give an overestimation of U_{ω} , The Eq. (3.23) may be written as

$$U_{w} = -k_{10} \frac{gH^{2}}{ch} \tag{3.24}$$

where k_{10} is the coefficient and expected to be less than 1/8.

If the wave is not sinusoidal, the Eq. (3.24) may also be written as

$$U_{w} = -k_{11} \frac{B_{o}gH^{2}}{ch}$$
 (3.25)

where k_{11} is the coefficient and expected to be less than 1. It should be noted that the form of Eq. (3.25) will be the same as that of Eq. (3.18) for linear shallow water wave.

Based on the above previous studies (with some modifications) from a) to d), we see that there are four possible forms for computing U_{w} , i.e., Eqs. (3.18), (3.21), (3.24) and (3.25). The best-fit value of k_{π} for each equation can be determined by using regression analysis between measured U_{w} vs. each possible formula of U_{w} .

At the breaking point: the effect of surface roller is very small and is negligible, gives $U_r = 0$ and $U_m = U_w$ (e.g., Basco and Yamashita, 1986; and Okayasu et al., 1986). Therefore, the regression analysis between measured U_m (at the breaking point) vs. each possible formula of U_w is used to determine the best-fit value of k_n in each possible formula. The results of regression analysis (the best-fit value of k_n and regression coefficient R^2) are shown in the second and third column of Table 3.3.

The computed results of U_{π} from the four possible formulas, using the best-fit value of k_n , are quantified in terms of rms relative error, ER. Using the best-fit value of k_n , the rms relative error, ER, of each possible formula (comparing with the measured data at the breaking point) is shown in the fourth column of Table 3.3. Through Table 3.3, among the

four possible forms, the form of Eq. (3.25) appears to be the best. Therefore, the formula for computing U_{π} in the present study is

$$U_{w} = -0.76 \frac{B_{o}gH^{2}}{ch} \tag{3.26}$$

Table 3.3: Results of regression analysis of U_{w} and rms relative error (ER) of the four possible forms of U_{w} (using measured data at the breaking point).

Formulas	Best-fit k,	R²	ER (%)
Eq. (3.18): $U_{w} = -k_{7} B_{o} c \left(\frac{H}{h}\right)^{2}$	$k_{\gamma} = 0.83$	0.70	15.48
Eq. (3.21): $U_{w} = -k_{8}H\sqrt{\frac{g}{h}}$	$k_8 = 0.05$	0.71	15.28
Eq. (3.24): $U_{w} = -k_{10} \frac{gH^{2}}{ch}$	$k_{10} = 0.05$	0.49	20.28
Eq. (3.25): $U_{w} = -k_{11} \frac{B_{o}gH^{2}}{ch}$	$k_{11} = 0.76$	0.83	11.68

The form of Eq. (3.25) may also be derived (in the similar manner as Dean and Dalrymple, 1984, page 286) as follows;

Mass flux above the mean water level is defined as

$$M = \frac{1}{T} \int_{0}^{T} \int_{h}^{\eta + h} \rho u dz dt \tag{3.27}$$

where u is the horizontal orbital velocity above the mean water level (MWL).

Assuming u is proportional to horizontal orbital velocity at z = h;

$$u \propto \frac{gH}{2c}\cos(\sigma t) \tag{3.28}$$

or

$$u = k_{11} \frac{gH}{2c} \cos(\sigma t) \tag{3.29}$$

where k_{11} is the coefficient.

Substituting Eq. (3.29) into Eq. (3.27), then taking an integration;

$$M = \frac{1}{T} \int_{0}^{T} \int_{h}^{\eta + h} \rho k_{11} \frac{gH}{2c} \cos(\sigma t) dz dt = \frac{1}{T} \int_{0}^{T} \eta \frac{H}{2} \cos(\sigma t) \rho k_{11} \frac{g}{c} dt = k_{11} \frac{\rho gH^{2}}{c} \frac{1}{T} \int_{0}^{T} \frac{\eta^{2}}{H^{2}} dt$$
(3.30)

Since $B_o = \frac{1}{T} \int_0^T (\eta/H)^2 dt$, thus

$$M = k_{11} \frac{B_o \rho g H^2}{c} \tag{3.31}$$

Since total mass transport in any section is equal to zero, net mass flux below the mean water level (MWL) balances that above MWL. This means that the mean velocity, due to mass transport, is

$$U_{w} = -\frac{M}{\rho h} = -k_{11} \frac{B_{o}gH^{2}}{ch}$$
 (3.32)

which is the same form as Eq. (3.25).

The volume flux below or above the trough level (Q_t) may be written as

$$Q_{s} = U_{w}d = k_{11} \frac{B_{o}gH^{2}}{ch}d$$
(3.33)

It should be note that the form of Eq. (3.33) is the same as that of Svendsen (1984b) for linear shallow water wave. Therefore Eq. (3.26) can be considered as a refinement of Svendsen (1984b)'s model.

3.1.3.2 Mean velocity due to surface roller

From the previous studies, the following explicit formulas have been suggested to compute the mean velocity due to surface roller.

a) Svendsen (1984b) proposed to compute the mean velocity due to surface roller as

$$U_r = -\frac{A}{Th} \tag{3.34}$$

where A is the cross-sectional area of the roller.

Based on the experiment of Duncan (1981), Svendsen (1984b) proposed an empirical relation for computing cross-sectional area of surface roller as

$$A = k_{12}H^2 ag{3.35}$$

where k_{12} is the coefficient and determined at 0.9 on the basis of the measurement of Dancan (1981). However, Sato et al. (1988) suggested using $k_{12} = 5.6$ on the basis of the best fit with the measured undertows of Okayasu et al. (1986) and Shimada (1982).

Substituting Eq. (3.35) into Eq. (3.34), U_r can be expressed as

$$U_r = -k_{12} \frac{H^2}{Th} ag{3.36}$$

b) Stive and Wind (1986) proposed the formula for computing $U_{\rm m}$ for the entire surf zone as shown in Eqs. (3.19) and (3.20). From Eq. (3.20), $U_{\rm r}$ can be expressed as follow

$$U_r = -k_9 H \sqrt{\frac{g}{h}} \tag{3.37}$$

c) Okayasu et al. (1986) proposed to compute U_r as

$$U_r = -k_{13} \frac{cH}{d} \tag{3.38}$$

where k_{13} is the coefficient and determined at 0.06 on the basis of their measurements.

d) Okayasu et al. (1986) and Hansen and Svendsen (1987) proposed an empirical formula for computing the cross-sectional area A as

$$A = k_{14}HL \tag{3.39}$$

where L is the wave length, and k_{14} is the coefficient. On the basis of the measurements the coefficient k_{14} is determined at 0.06 for Okayasu et al. (1986) and determined at 0.07 for Hansen and Svendsen (1987).

Substituting Eq. (3.39) into Eq. (3.34), U_r can be written as

$$U_r = -k_{14} \frac{cH}{h} {(3.40)}$$

e) Okayasu et al. (1988) obtained U_{τ} by dividing the onshore mass flux by the trough level and proposed as

$$U_r = -k_{15} \frac{H^2}{dT} {(3.41)}$$

where k_{15} is the coefficient and determined to be 2.3 on the basis of their measurements.

f) Based on a hydraulic jump model of Engelund (1981), Deigaard and Fredsoe (1991) assumed the front of a broken wave is similar to that of a bore or a hydraulic jump. The cross-sectional area of the roller is approximated from the model of Engelund (1981) as

$$A = k_{16} \frac{H^3}{h} \tag{3.42}$$

where k_{16} is the coefficient and determined to be 1.42.

Substituting Eq. (3.42) into Eq. (3.34), U_r can be expressed as

$$U_{r} = -k_{16} \frac{H^{3}}{Th^{2}} \tag{3.43}$$

g) It is also interesting to assume that $U_r \propto U_w$; the equation of U_r therefore can be expressed as

$$U_r = -k_{17} \frac{B_o g H^2}{ch} ag{3.44}$$

where k_{17} is the coefficient

h) The cross-sectional area of roller, A, may also depend on the shape of water surface. The wave shape parameter B_{σ} is employed as a dimensionless parameter to represent the shape of water surface. Therefore, the formulas of A in the Eqs. (3.35), (3.39) and (3.42) may be modified as follows

$$A = k_{18} B_o H^2 (3.45)$$

$$A = k_{19} B_{\scriptscriptstyle o} HL \tag{3.46}$$

$$A = k_{20} B_o \frac{H^3}{h} ag{3.47}$$

here k_{18} , k_{19} , and k_{20} are the coefficients.

Substituting Eqs. (3.45), (3.46) and (3.47) into Eq. (3.34), respectively, lead to

$$U_{r} = -k_{18}B_{o}\frac{H^{2}}{Th} \tag{3.48}$$

$$U_{r} = -k_{19}B_{o}\frac{cH}{h} \tag{3.49}$$

$$U_r = -k_{20}B_o \frac{H^3}{Th^2} \tag{3.50}$$

Based on the above previous studies (with some modifications) from a) to h), we will try to find out an appropriate formula for computing U_r . From Eqs. (3.36), (3.37), (3.38), (3.40), (3.41), (3.43), (3.44), (3.48), (3.49) and (3.50), we see that there are ten possible forms for computing U_r .

The measured data that used in this section is the same as that of in section 3.1.2. The regression analysis is performed with the measured $U_m + 0.76 \frac{B_o g H^2}{ch}$ (at the breaking point and inner surf zone) vs. each possible formula of U_r . The results of regression analysis (the best-fit value of k_n and regression coefficient R^2) are shown in the second and third column of Table 3.4. Using the best fit value of k_n , the error ER of each possible formula (comparing with the laboratory data at the breaking point and inner surf zone) is shown in the fourth column of Table 3.4. Through Table 3.4, we see that the form of Eq. (3.49) has the best prediction on the mean velocity. Therefore, the formula for computing U_r in the present study is

$$U_r = -1.12B_o \frac{cH}{h} {(3.51)}$$

This means that the cross-sectional area of roller, A, should be equal to $1.12B_oHL$. Up to here, we can conclude that the following formula is suitable for computing U_{\perp} .

$$U_{m} = \begin{cases} -0.76 \frac{B_{o}gH^{2}}{ch} - 1.12 \frac{B_{o}cH}{h} & inner\ zone \\ -0.76 \frac{B_{o}gH^{2}}{ch} & breaking\ point \end{cases}$$
(3.52)

Since there is no surface roller in the offshore zone, the value of the mean velocity caused by surface roller is zero. The formula for computing the mean velocity in the offshore zone is the same as that of at the breaking point.

Table 3.4: Results of regression analysis of U_r and rms relative error (ER) of the ten possible forms of U_r (using measured data at the breaking point and inner surf zone).

Formulas		Best-fit k,	R²	ER (%)
Eq. (3.36):	$U_r = -k_{12} \frac{H^2}{Th}$	$k_{12} = 2.01$	0.31	33.24
Eq. (3.37):	$U_r = -k_9 H \sqrt{\frac{g}{h}}$	$k_9 = 0.10$	0.74	20.34
Eq. (3.38):	$U_r = -k_{13} \frac{cH}{d}$	$k_{13} = 0.08$	0.73	20.58
Eq. (3.40):	$U_r = -k_{14} \frac{cH}{h}$	$k_{14} = 0.10$	0.74	20.35
F -	$U_r = -k_{15} \frac{H^2}{dT}$	$k_{15} = 1.56$	0.34	32.55
Eq. (3.43):	$U_r = -k_{16} \frac{H^3}{Th^2} -$	$k_{16} = 2.61$	0.10	37.89
Eq. (3.44):	$U_r = -k_{17} \frac{B_n g H^2}{ch}$	$k_{17} = 1.58$	0.74	20.48
Eq. (3.48):	$U_r = -k_{18}B_o \frac{H^2}{Th}$	$k_{18} = 23.02$	0.38	31.54
Eq. (3.49):	$U_r = -k_{19}B_o \frac{cH}{h}$	$k_{19} = 1.12$	0.75	20.06
Eq. (3.50):	$U_r = -k_{20}B_{\nu}\frac{H^3}{Th^2}$	$k_{20} = 31.03$	0.21	35.59

Considering at the transition zone: the structure of the flow field in this zone has not yet been described in sufficient details to make it possible to identify the characteristic of the flow field. Okayasu et al. (1986) suggested the cross-sectional area of surface roller, A, grows linearly with distance from zero at the plunging point. Also, Basco and Yamashita (1986) suggested linear increasing of A (with distance) from zero at the breaking point for the case of spilling breaker and from zero at the plunging point for the case of plunging breaker. However, if we follow the previous researcher's assumptions, we need to define the position of the plunging point which will make the model to be more complicated. From the trial of many possible parameters, finally, we assume A increases linearly with one over square root of wave height (A is zero at the breaking point and it is fully developed at the transition point). Eq. (3.52), therefore, can be written as

$$U_{_{PN}} = -0.76 \frac{B_{_{o}}gH^{2}}{ch} - 1.12b_{_{3}} \frac{B_{_{o}}cH}{h}$$
 (3.53)

where b_3 is the coefficient and expressed as

$$b_{3} = \begin{cases} 0 & offshore zone \\ \frac{1/\sqrt{H} - 1/\sqrt{H_{b}}}{1/\sqrt{H_{t}} - 1/\sqrt{H_{b}}} & transition zone \\ 1 & inner zone \end{cases}$$

where subscript b indicates the value at the breaking point, and subscript t indicates the value at the transition point.

The comparison between measured $U_{\it m}$ and computed $U_{\it m}$ from Eq. (3.53) is shown in Fig. 3.5. The examples of cross-shore variations of measured and computed $U_{\it m}$ are shown in Fig. 3.6. We can see from Figs. 3.5 and 3.6 that the mean velocities are predicted well in general cases, but the variation of computed $U_{\it m}$ is rather smoother than the measured $U_{\it m}$. However, for the experiment of Hansen and Svendsen (1984), the present formula gives over estimations for all points of the measurements. This may indicate the limitation of the capability of present formula. Since the experimental condition of Hansen and Svendsen (1984) is not significantly different from that of Nadaoka et al. (1982), Okayasu et al. (1988) and Cox et al. (1994), the limitation of present formula can not be identified at the present. More analysis is necessary to find out the limitation.

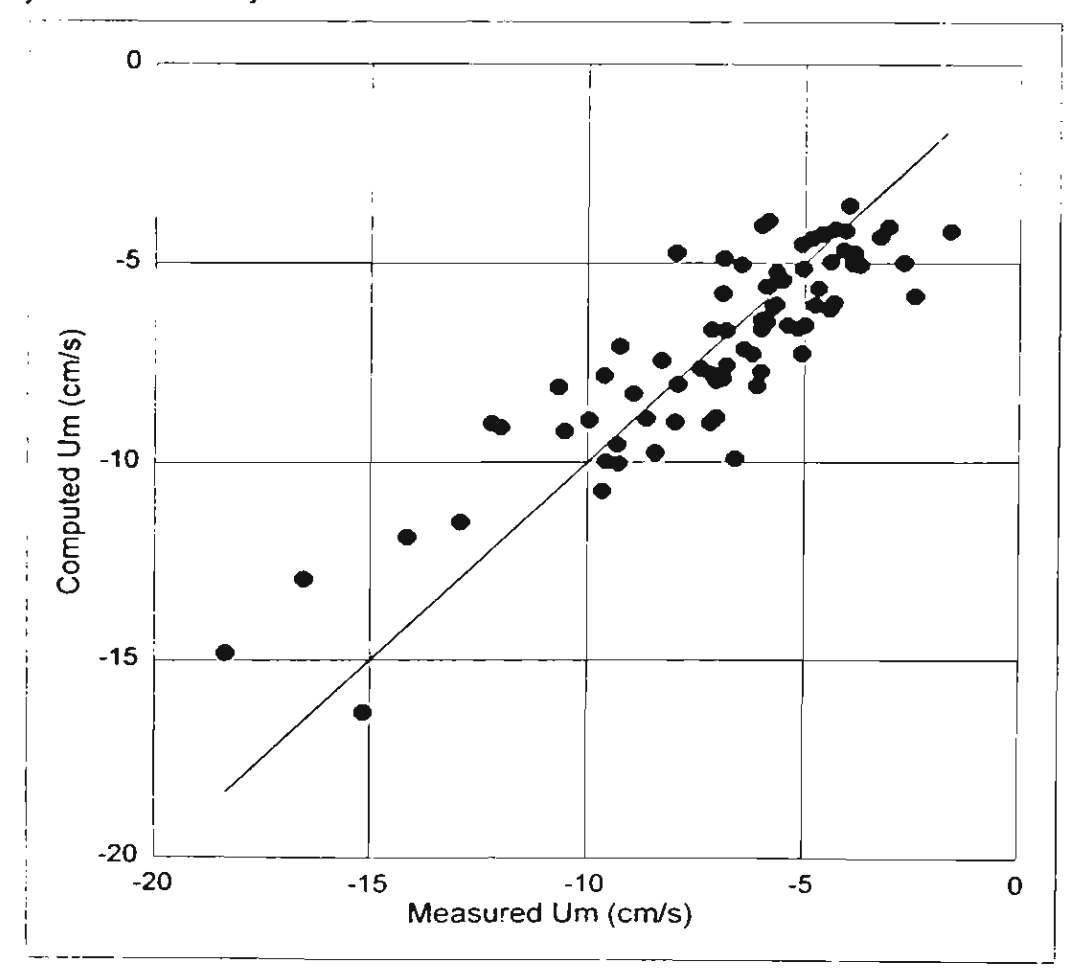


Figure 3.5: Comparison between measured and computed mean velocity $U_{\it m}$ inside the surf zone (measured data from 4 sources as shown in Table 3.2).

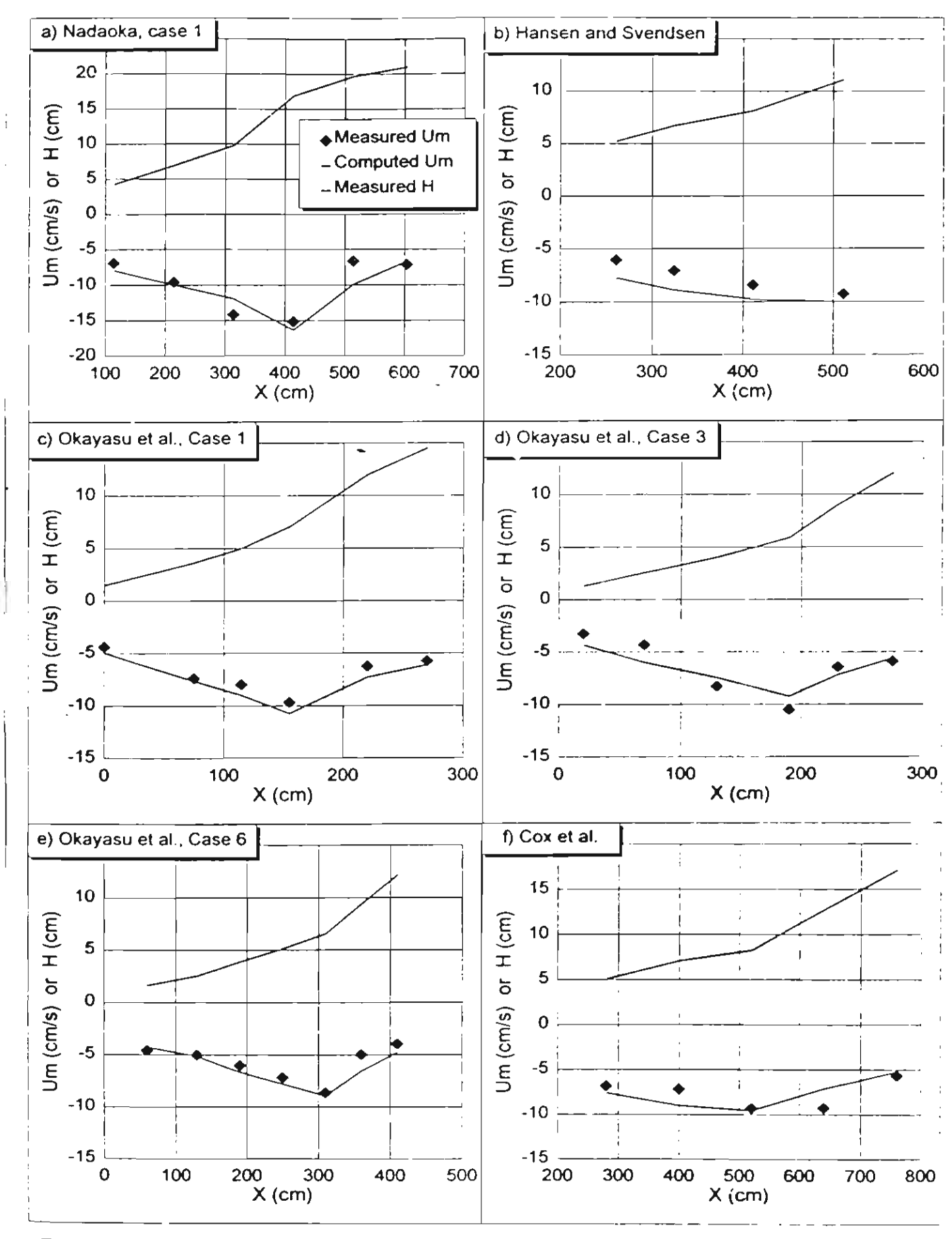


Figure 3.6: Examples of cross-shore variations of measured and computed mean velocity, $U_{\rm m}$, inside the surf zone (measured data from 4 sources as shown in Table 3.2).

3.1.4 Recommended procedure for computation of undertow profile

The recommended procedure for computing undertow profile, is summarized as follows:

- 1) Given X, z, h, H, T, d, X_b , X_t and m_b .
- 2) Compute c using linear wave theory.
- 3) Compute B_o , U_m and U from Eqs. (3.17), (3.53) and (3.14), respectively. Although, the present model is developed for predicting the undertow profile inside the surf zone, application of the present model to the offshore zone is possible. By assuming that the turbulence in the offshore zone (above the bottom boundary layer) is very small and is negligible, the coefficients b_1 and b_2 in Eq. (3.14) equal to zero. Therefore, Eq. (3.14) for the offshore zone becomes $U = U_m$.

3.1.5 Model verification

In order to examine the overall performance of the model, the model has been applied to the wide range of laboratory data covering small-scale and large-scale experiments, i.e., the experiments of Nadaoka et al. (1982), Hansen and Svendsen (1984), Okayasu et al. (1988), Cox et al. (1994), CRIEPI (Kajima et al., 1983) and SUPERTANK (Kraus and Smith, 1994). Brief summary of each experiment is given below.

The experiment of Nadaoka et al. (1982) was conducted to reveal the structure of velocity field inside and near the surf zone. A 16.8-m-long wooden plane beach of slope 1:20 was set in a small wave flume of 44.5 m long, 0.5 m wide and 1.0 m deep. The experiments were carried out under regular wave actions for 12 cases. In most cases (except cases 1 and 5) velocities were measured at elevation 0.5 m above the bottom. Only in cases 1 and 5, the velocity profiles were measured at 7 locations (P1-P7) in cross-shore direction. The measured velocities below the trough level of cases 1 and 5 are used in this study. For case 1, the measuring locations in the offshore zone, breaking point, transition zone and inner surf zone were P7, P6, P5 and P4-P1, respectively. For case 5, the measuring locations in the offshore zone, breaking point, transition zone and inner surf zone were P7-P6, P5, P4 and P3-P1, respectively. The experimental conditions are shown in Table 3.5.

The experiment of Hansen and Svendsen (1984) was conducted to measure velocity field inside and near the surf zone over the 1:34.3 concrete plane slope. The experiment was carried out under regular wave action in a small wave flume of 32.0 m long, 0.6 m wide and 0.6 m deep. The measured velocities below the trough level are used in this study. The velocity profiles were measured at 6 locations (L1-L6) in cross-shore direction. The first and second measuring positions (L1 and L2) were set in the offshore zone. The third measuring

position (L3) was set in the transition zone. The other positions (L4-L6) were located in the inner surf zone. Only the velocity profiles at L3-L6 are available. The experimental condition is shown in Table 3.5.

The experiment of Okayasu et al. (1988) was constructed to measure the velocity field and to determine the Reynolds stress and eddy viscosity in the surf zone including the area close to the bottom. The experiments were carried out under regular wave actions in a small wave flume of 23.0 m long, 0.8 m wide and 1.0 m deep. Ten wave conditions were performed on 1:20 and 1:30 slopes of rubber and stainless plane beach. Only in case 5, the measuring points were taken close to the bottom and will not be used in this study. The measured velocities below the trough level of cases 1-10, except case 5, are used in this study. The velocity profiles were measured at 6 or 7 locations (L1-L7) in cross-shore direction. The first measuring position (L1) was set on the wave breaking point. The second measuring position (L2) was set in the transition zone. The other positions (L3-L7) were located in the inner surf zone. The experimental conditions are shown in Table 3.5.

The experiment of Cox et al. (1994) was conducted to measure velocity field inside and near the surf zone over a rough bottom. A single layer of sand grains with $d_{50} = 0.10$ cm was glued on the 1:35 plane beach to increase the bottom roughness. The experiment was carried out under regular wave action in a small wave flume of 33.0 m long, 0.6 m wide and 1.5 m deep. The measured velocities between the upper edge of bottom boundary layer and the trough level are used in this study. The velocity profiles were measured at 6 locations (L1-L6) in cross-shore direction. The first measuring position (L1) was set on the wave breaking point. The second measuring position (L2) was set in the transition zone. The other positions (L3-L6) were located in the inner surf zone. The experimental condition is shown in Table 3.5.

The experiment of CRIEPI was performed by Kajima et al. (1983) at Central Research Institute of Electric Power Industry (CRIEPI). The experiments were performed under the condition of regular wave and movable bed in a large wave flume (205 m \log_2 3.4 m wide and 6 m deep). Coarse sand (D_{50} =0.47 mm) and fine sand (D_{50} =0.27 mm, were used in the experiments. The velocities were measured at various sections along the fume, covering both in offshore and surf zone. However at a few points, the vertical velocities were measured. Table 3.6 shows the CRIEPI experimental conditions that are used in this section.

The experiment of SUPERTANK Laboratory Data Collection Project (Kraus and Smith, 1994) was conducted to investigate cross-shore hydrodynamic and sediment transport processes, during the period of August 5 to September 13, 1992, at Oregon State University, Corvallis, Oregon, USA. A 76-m-long sandy beach was constructed in a large wave tank of

104 m long, 3.7 m wide and 4.6 m deep. The 20 major tests were performed and each major test consisted of several cases. Most of the major tests were performed under the irregular wave actions. However, 5 major tests were performed under regular wave actions, i.e., test No. STEO, STFO, STGO, STHO and STIO. The velocities were measured at various sections along the flume, covering both in offshore and surf zone. However at a few points, the vertical velocities were measured. Table 3.6 shows the SUPERTANK experimental conditions that are used in the verification.

3.1.5.1 Comparison with small-scale experiments

Four sources of the small-scale laboratory data are used to verify the present model, i.e., Nadaoka et al. (1982), Hansen and Svendsen (1984), Okayasu et al. (1988) and Cox et al. (1994). The undertow profiles are computed based on the procedure recommended in section 3.1.4. All coefficients in the model are kept to be constant for all cases. Table 3.5 shows root mean square relative error (ER) of computed undertow U for each data set. The ER of all cases is 24%. The error of each data source is summarized in Table 3.7. Fig. 3.7 shows the comparison between measured and computed undertow for all points of the measurements. Examples of measured and computed undertow profiles are shown in Figs. 3.8-3.9. Through Figs. 3.7-3.9 (except 8d and 8j) and Table 3.5, it can be seen that the present model is quite realistic in the simulation of undertow profile in the surf zone.

The model is also applied to compute the undertow profile in the offshore zone. Figs. 3.8d and 3.8j show the predicted undertow profiles in the offshore zone over the smooth bed and rough bed, respectively. The model could not predict well the velocity near and inside the bottom boundary layer. Fig. 3.8d shows that the model gives under estimation of the velocity near and inside the bottom boundary layer, while Fig. 3.8j shows that the model gives over estimation. It seems to be impossible to use the simple model for predicting the velocity near and inside the bottom boundary layer in the offshore zone. However, the model gives reasonably well prediction in the region out of the bottom boundary layer. It may be accurate enough for using in the computation of suspended sediment transport above the bottom boundary layer.

Table 3.5: Root mean square relative error (ER) of the present model comparing with the small-scale experiments.

Sources	Case	m_{i}	T	H_{i}	h _i	Total No.	ER
	No.		(s)	(cm)	(cm)	of profiles	
Nadaoka et al. (1982)	1	1/20	1.32	21.6	70.0	7	27.17
	5	1/20	2.34	21.9	70.0	7	22.61
Hansen and Svendsen	1	1/34	2.00	12.0	36.0	4	22.60
(1984)							
Okayasu et al. (1988)	1	1/20	2.00	8.50	40.0	6	18.59
	2	1/20	2.00	5.63	40.0	6	28.41
	3	1/20	1.17	9.87	40.0	6	22.23
	4	1/20	0.91	6.69	40.0	6	24.73
	6	1/30	1.61	8.80	40.0	7	16.93
	7	1/30	1 97	6.17	40.0	6	21.00
	8	1/30	1.96	8.22	40.0	7	23.43
	9	1/30	1.12	8.26	40.0	6	28.18
	10	1/30	1.23	6.05	40.0	6	46.07
Cox et al. (1994)	1	1/35	2.20	13.22	28.0	6	22.55
Total						80	24.27

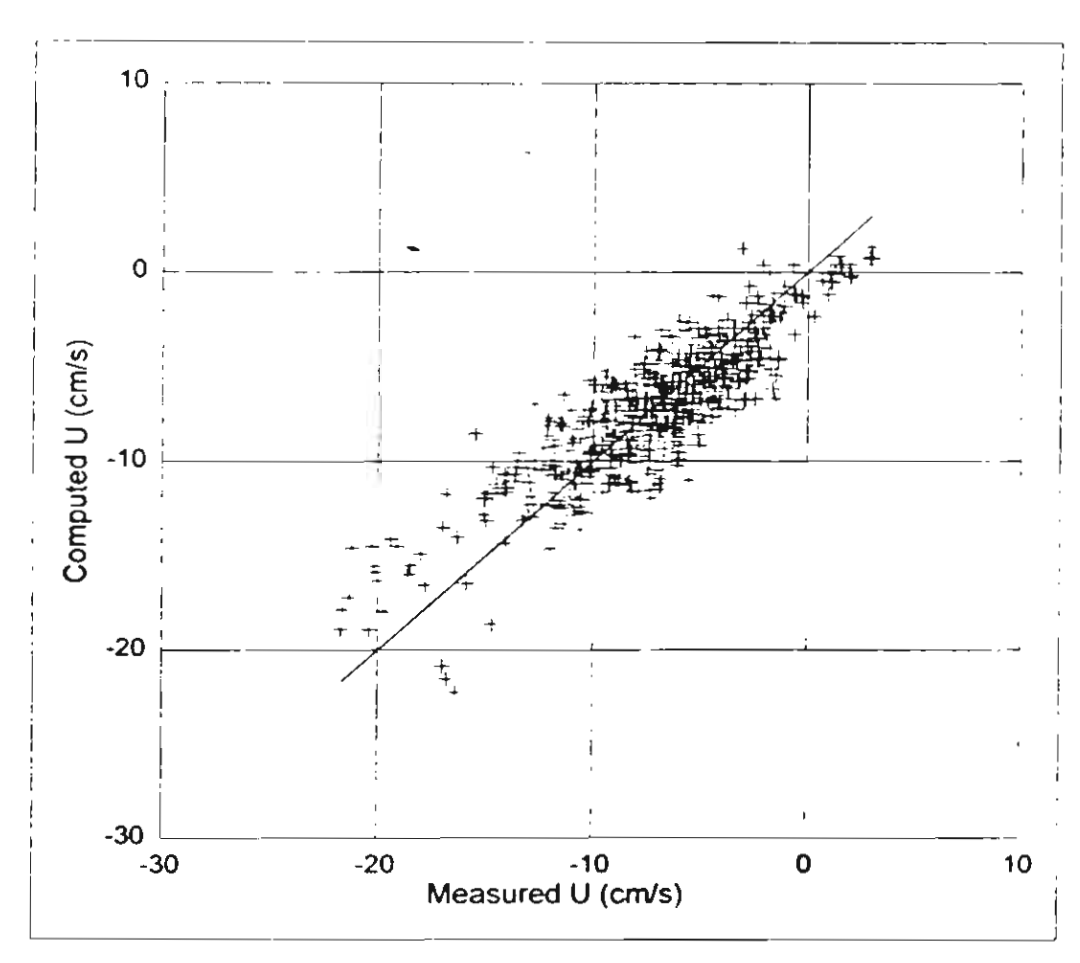


Figure 3.7: Comparison between measured and computed U for all points of the data (measured data from 4 sources of small-scale experiments as shown in Table 3.5).

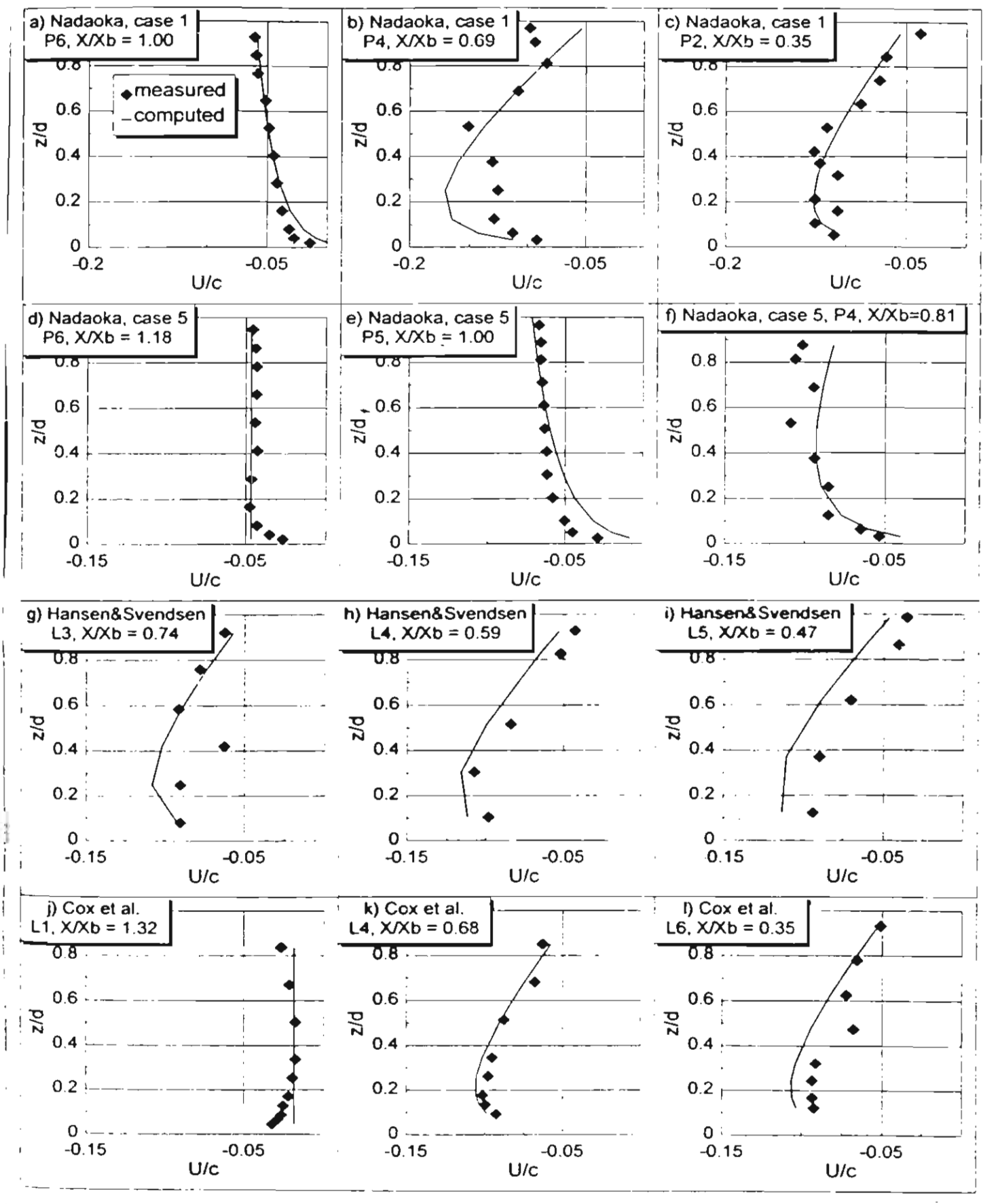


Figure 3.8: Examples of measured and computed undertow profiles (measured data from Nadaoka et al., 1982; Hansen and Svendsen, 1984; and Cox et al., 1994).

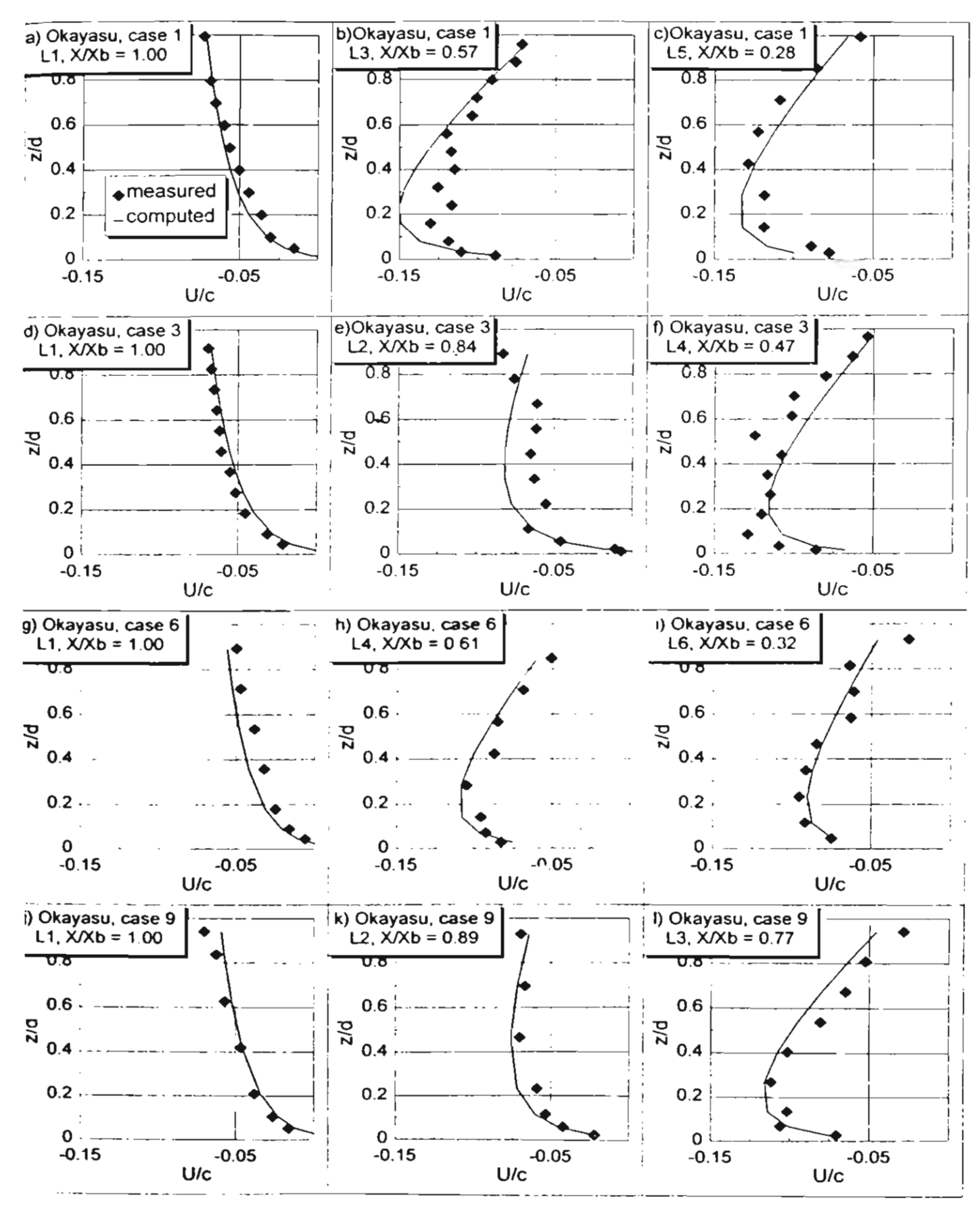


Figure 3.9: Examples of measured and computed undertow profiles (measured data from Okayasu et al., 1988).

3.1.5.2 Comparison with large-scale experiments

Two sources of the large-scale laboratory data are used to verify the model, i.e., CRIEPI (Kajima et al., 1983) and SUPERTANK (Kraus and Smith, 1994). The velocity profiles are computed based on the procedure recommended in section 3.1.4. All coefficients in the model are kept to be constant for all cases in the verification. However, due to the fluctuations of measured wave heights (that is used to determine the coefficient b_3 in Eq. 3.53), the coefficient b_3 become negative which is impossible. To overcome this problem, (only in this subsection) the coefficient b_3 is set to be equal to the coefficient b_2 in Eq. (3.14).

The last column of Table 3.6 shows the rms relative error, ER, of the present model for each case. The rms relative error, ER, for all data sets is 39%. The error of each data source is summarized in Table 3.7. Fig. 3.10 shows the verification results of all measuring points. Fig. 3.10 shows about 82 percent of the predicted results are within 0.5 and 2 times the measured values. Figs. 3.12 and 3.14 show examples of measured and computed undertow profiles. From the general tendency of Figs. 3.10-3.14, we can judge that the present formula gives reasonably well estimations of the time-averaged velocity in the large-scale wave flume.

Table 3.6: Root mean square relative error ($\it ER$) of the present model comparing with the large-scale laboratory data.

Sources	Case	Time	D_{sc}	T	H_{i}	h_i	Total	ER of
	No		(mm)	(s)	(cm)	(cm)	No. of	present
			()				profiles	study
CRIEPI (1983)	2.1	26.0 hr	0.47	6.0	180	350	13	38.95
	2.3	3.1 hr	0.47	3.1	66	350	10	25.95
	3.3	5.7 hr	0.27	12.0	81	450	5	35.62
		24.3 hr	√ 0.27	12.0	81	450	6	32.13
		78.3 hr	0.27	12.0	81	450	5	18.01
	3.4	4.9 hr	0.27	3.1	154	450	. 5	29.51
		23.6 hr	0.27	3.1	154	450	4	42.78
		75.2 hr	0.27	3.1	154	450	4	46.89
	4.1	10.8 hr	0.27	3.5	31	350	5	53.52
		22.9 hr	0.27	3.5	31	350	5	50.36
	4.2	5.2 hr	0.27	4.5	97	400	7	37.23
		24.4 hr	0.27	4.5	97	400	8	47.99
		76.3 hr	0.27	4.5	97	400	7	64.20
	4.3	30.3 hr	0.27	3.1	151	400	25	48.37
		91.0 hr	0.27	3.1	151	400	23	50.94
	5.2	8.0 hr	0.27	3.1	74	350	16	51.85
		29.1 hr	0.27	3.1	74	350	20	45.14
		89.5 hr	0.27	3.1	74	350	21	47.12
	6.1	9.8 hr	0.27	5.0	166	400	5	25.29
	-	53.6 hr	0.27	5.0	166	400	16	31.91
	6.2	6.2 hr	0.27	7.5	112	450	19	36.84
SUPERTANK	STEO	s0315a	0.22	3.0	60	305	3	44.65
(1994)		s0316a	0.22	3.0	80	305	5	36.32
	STFO	s0410a	0.22	8.0	40	274	4	39.07
	STGO	s0415a	0.22	3.0	80	305	5	47.60
		s0416a	0.22	3.0	80	305	5	40.74
	STHO	s0508a	0.22	3.0	80	305	5	37.09
		s0510a	0.22	4.5	70	305	5	31.00
	STIO	s0513a	0.22	8.0	50	305	5	34.26
		s0514a	0.22	8.0	50	305	5	28.09
		s0515a	0.22	8.0	50	305	5	31.47
		s0516a	0.22	8.0	50	305	5	40.37
		s0607a	0.22	8.0	50	305	4	31.61
		s0610a	0.22	8.0	50	305	4	32.63
		s0612a	0.22	8.0	50	305	5	42.98
		s0614a	0.22	8.0	50	305	5	40.82
Total							299	39.03

Table 3.7: Summary of root mean square relative error (ER) of the present model comparing with measured data of each data source.

Sources	Apparatus	Total No. of	Total No. of	ER
		profiles	data points	
Nadaoka et al. (1982)	small-scale	14	149	24.6
Hansen and Svendsen (1984)	small-scale	4	22	22.6
Okayasu et al. (1988)	small-scale	56	465	25.0
Cox et al. (1994)	small-scale	6	53	22.6
CRIEPI (1983)	large-scale	229	667	39.0
SUPERTANK (1994)	large-scale	70	119	39.6
Total	-	379	1475	

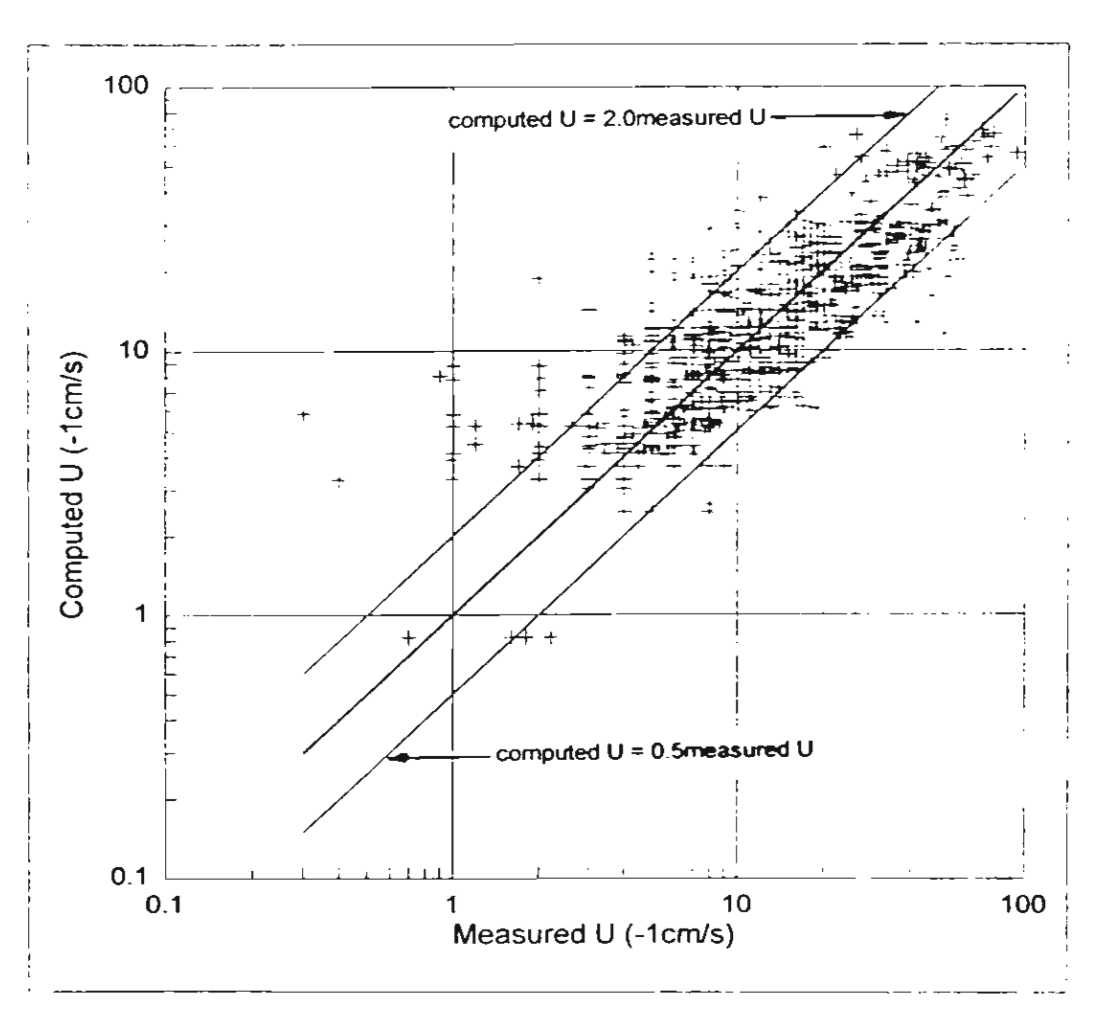


Figure 3.10: Comparison between measured and computed U for all points of the measurements (measured data from 2 sources of large-scale experiments as shown in Table 3.6).

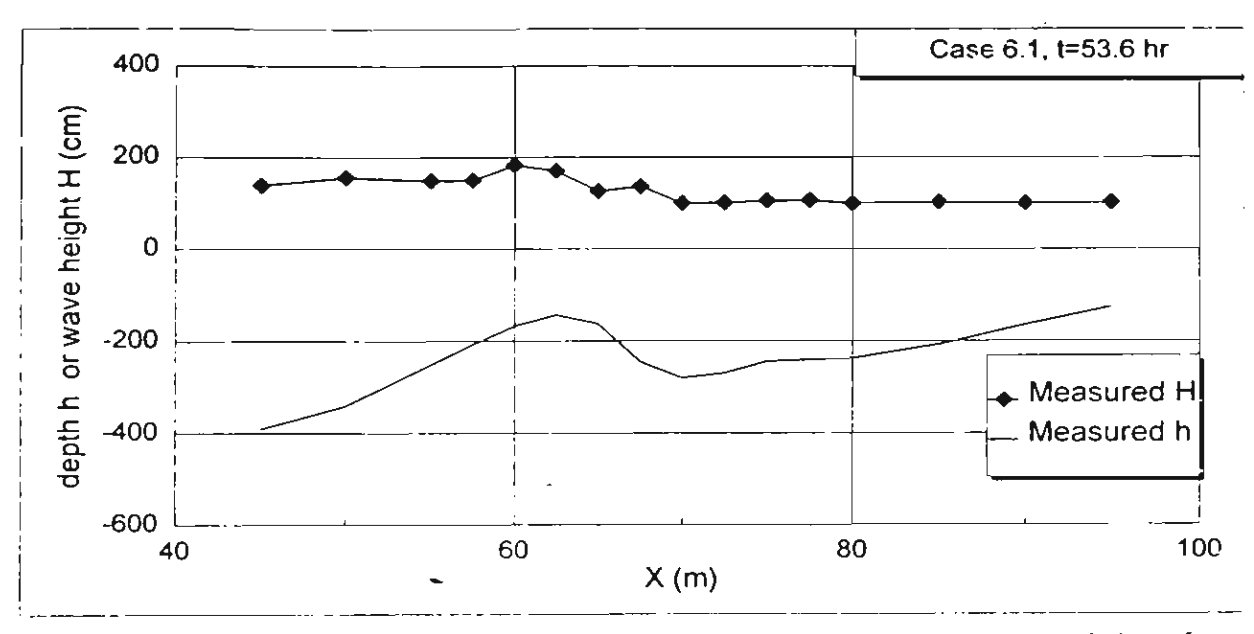


Figure 3.11: Measured bottom topography and wave height variation (measured data from CRIEPI, 1983, case 6.1, time = 53.6 hr).

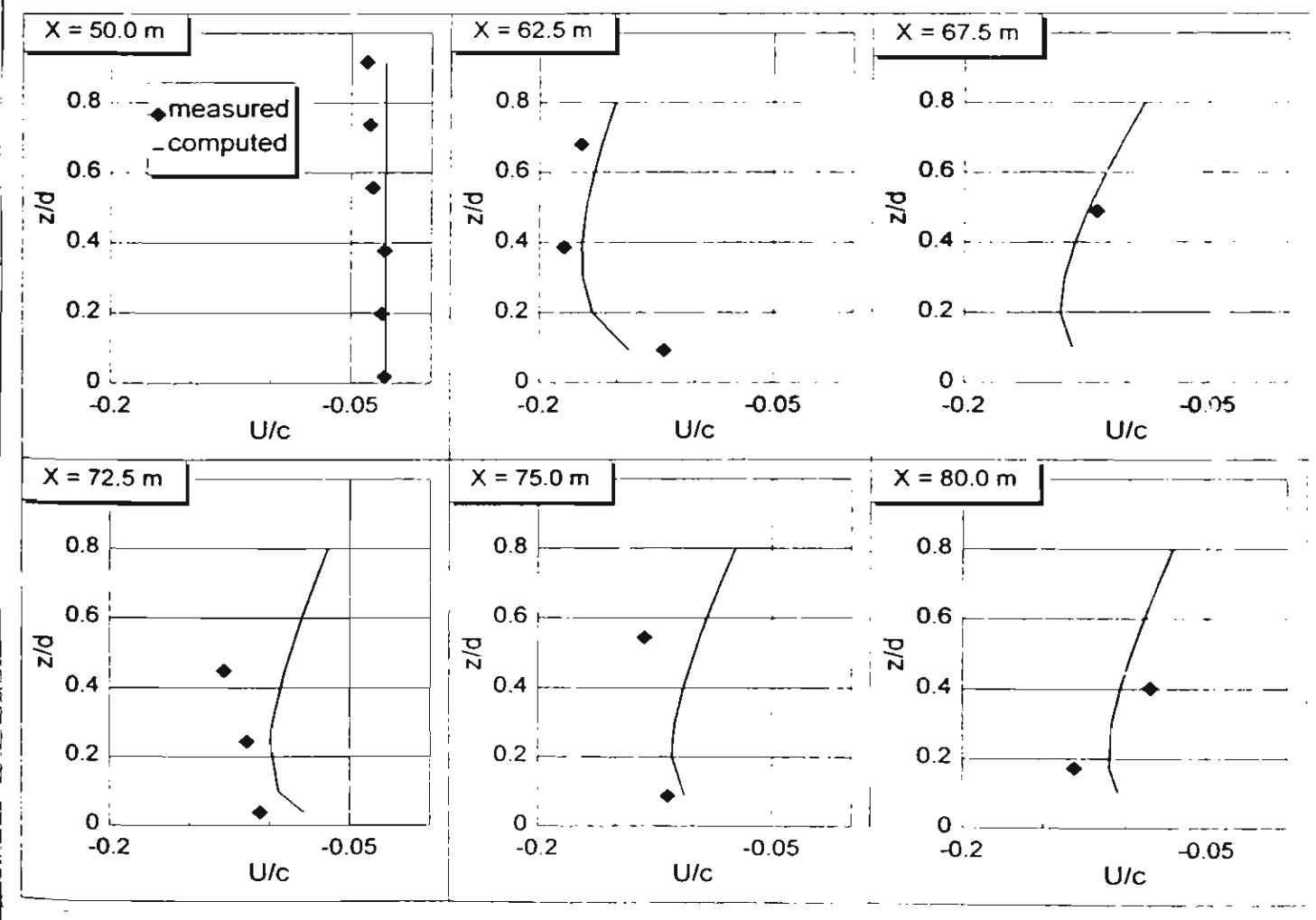


Figure 3.12: Computed and measured undertow profiles (measured data from CRIEPI, 1983, case 6.1, time = 53.6 hr).

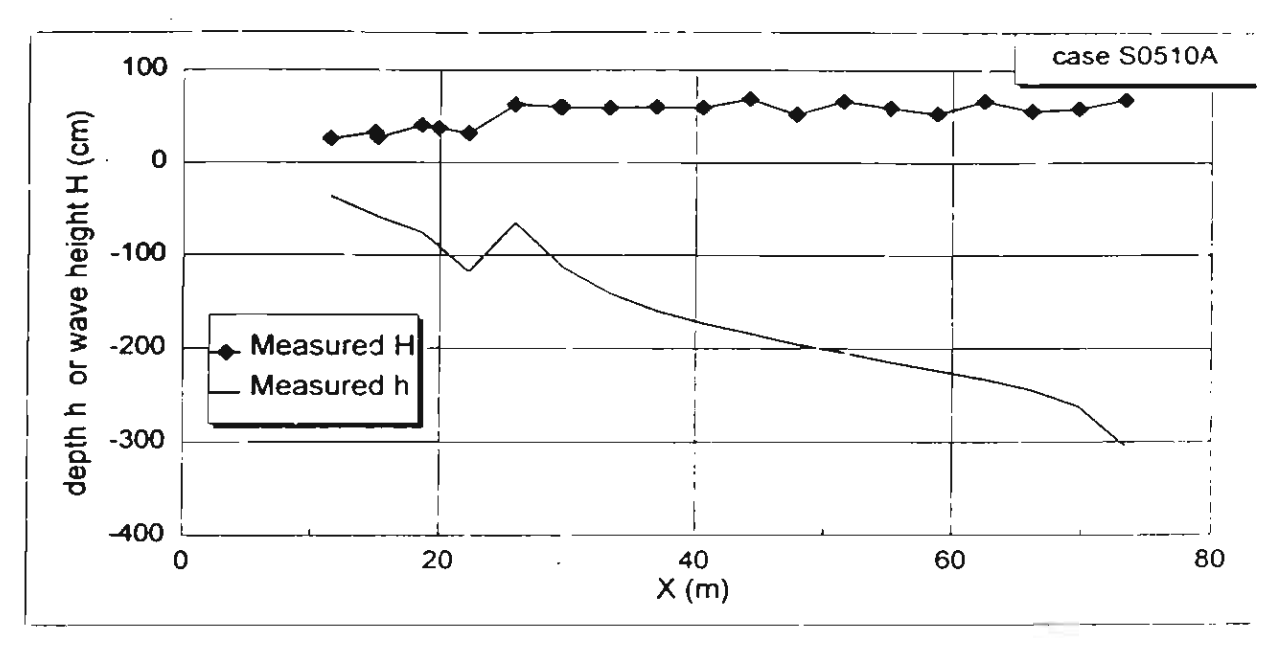


Figure 3.13: Measured bottom topography and wave height variation (measured data from SUPERTANK, 1994, case s0510a).

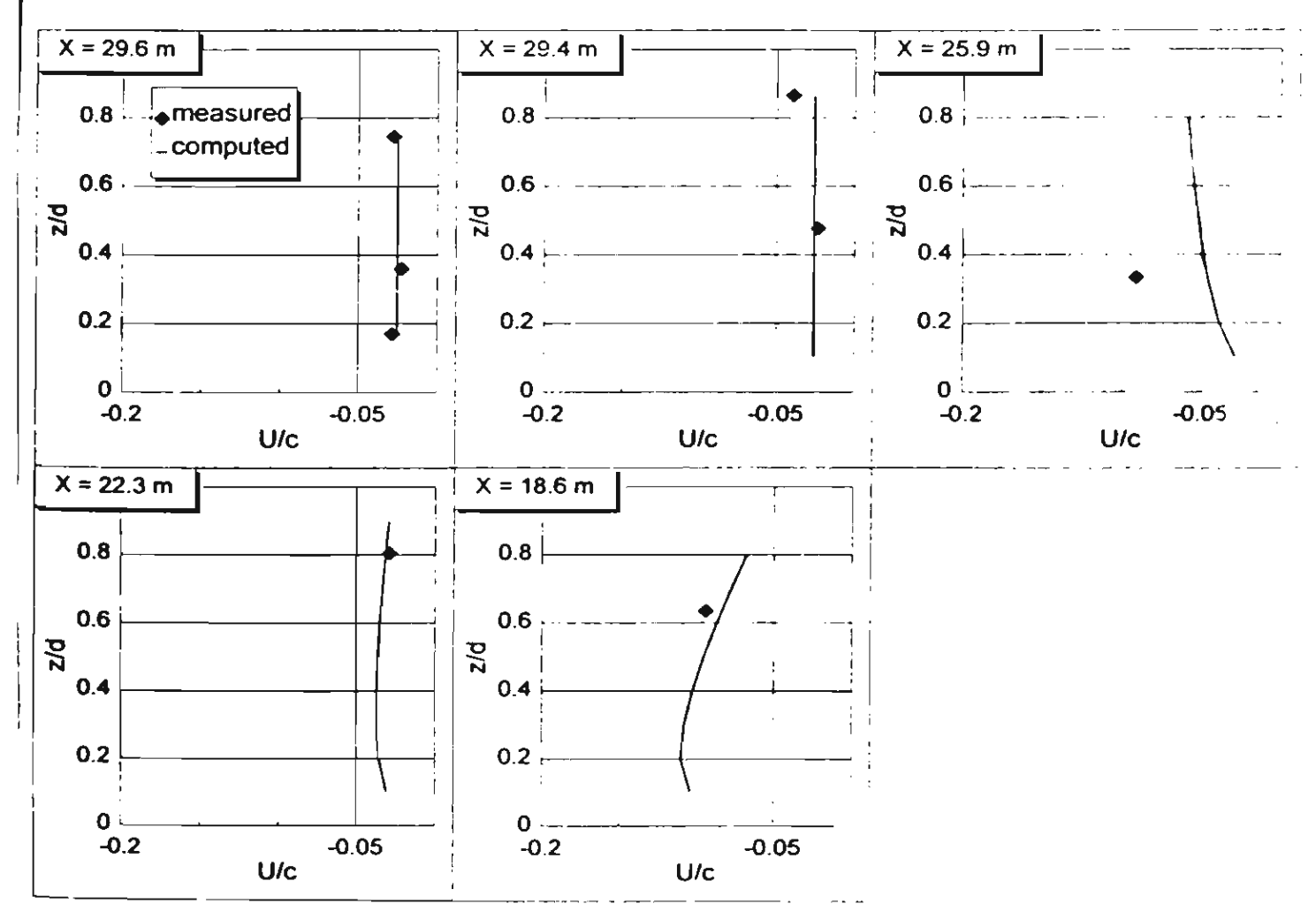


Figure 3.14: Computed and measured undertow profiles (measured data from SUPERTANK, 1994, case s0510a).

3.2 Undertow Velocity Induced by Irregular Waves

Cross-shore time-averaged velocity below wave trough, or undertow, is important in the computation of suspended sediment transport rate and consequently, beach deformation.

Recently, Cox and Kobayashi (1997) developed a simple model for computing the profile (vertical distribution) of undertow induced by regular waves. The model combines a logarithmic profile in the bottom boundary layer with a parabolic profile in the middle layer. Their model was applied by Kennedy et al. (1998) to predict the profile of undertow induced by irregular waves. Their model is simple and easy to use but the empirical coefficients in the model are not really constant. The coefficients have to be adjusted at each measured profile. This may be difficult to use in the practical work.

This section concentrates on the derivation of a simple formula for predicting the profile of undertow induced by irregular waves based on the formula for regular wave as described in sec. 3.1. All coefficients in the present formulas will be kept to be constant for all cases of the computation.

Published experimental data of undertow profiles from 5 sources, including 675 undertow profiles, have been collected for calibration of the present formulas. These include small-scale, large-scale, and field experimental data obtained from a variety of wave and bottom conditions. A summary of the collected experimental data is given in Table 3.8.

Table 3.8: Summary of collected experimental data.

Sources	Apparatus	Bed condition	Wave	Total No.
			condition	of profiles
Dette and Uliczka (1986)	Large-scale	sandy beach	irregular	4
Okayasu and Katayama	Small-scale	plane beach	irregular	6
(1992)	ı			
SUPERTANK (1994)	Large-scale	sandy beach	irregular	643
Shimisu and Ikeno (1996)	Large-scale	sandy beach	irregular	14
Rodriguez et al. (1994)	field	sandy beach	irregular	8
Total	_			675

3.2.1 Profile of undertow velocity

Irregular wave breaking is more complex than regular wave breaking. In contrast to regular waves there is no well-defined breaking point for irregular waves. The highest wave tends to break at greatest distance from the shore. Thus the turbulence, induced by irregular breaking waves, occurs over a considerably greater area than that of regular waves. Since the width of surf zone and the transition zone varies with each individual wave, the influence of the transition zone is not significantly observed in the irregular wave surf zone (Nairn et al., 1990). To make the formula simple, the influence of the transition zone for irregular wave is excluded in this study. Therefore Eq. (3.10) is applied for computing the undertow profile of irregular waves.

$$U = D_B^{1/3} \left[k_{21} \left(\frac{z}{d} - \frac{1}{2} \right) + k_{22} \left(\ln \frac{z}{d} + 1 \right) \right] + U_m$$
 (3.54)

where k_{21} and k_{22} are the coefficients.

Using the concept of Battjes and Janssen (1978), the energy dissipation rate, $D_{\it B}$, of the irregular breaking waves can be expressed as

$$D_B = \frac{Q_h \rho g H_{rms}^3}{4Th} \tag{3.55}$$

where H_{rm} is the root mean square wave height, Q_b is the fraction of breaking wave which can be computed from the derivation of Battjes and Janssen (1978) as

$$\frac{1 - Q_h}{-\ln Q_h} = \left(\frac{H_{mix}}{H_h}\right)^2 \tag{3.56}$$

where H_{h} is the breaking wave height that can be computed by using breaking criteria of Goda (1970):

$$H_{b} = 0.1L_{o} \left\{ 1 - \exp \left[-1.5 \frac{\pi h}{L_{o}} \left(1 + 15 m_{o}^{4/3} \right) \right] \right\}$$
 (3.57)

where L_a is the deep-water wavelength, and m_a is the average bottom slope. The coefficient 0.1 is used according to Rattanapitikon and Shibayama (1998).

Substituting Eq. (3.55) into Eq. (3.54), the undertow profile can be expressed as

$$U = \left(\frac{Q_h g H_{mis}^3}{4Th}\right)^{1/3} \left[k_{21} \left(\frac{z}{d} - \frac{1}{2}\right) + k_{22} \left(\ln \frac{z}{d} + 1\right)\right] + U_m \tag{3.58}$$

The coefficients k_{21} and k_{22} can be determined from the formula calibration. The measured undertow profile data, under irregular wave actions, from 5 sources (see Table 3.8) are used to calibrate the formula.

The undertow profile is computed from Eq. (3.58) by using measured U_m as the input data. Trial simulations indicated that $k_{21}=0.30\,\mathrm{and}\ k_{22}=0.12$ give good agreement

between measured and computed undertows. Fig. 3.15 shows the verification results of all measuring points. Fig. 3.16 shows the examples of measured and computed undertow profiles. Table 3.9 shows the rms relative error, ER, for each case. Table 3.10 shows the rms relative error, ER, for irregular wave data is 21%. From Fig. 3.15-3.16 and Table 3.10, we can judge that the Eq. (3.58) is accurate enough to be used for computing the profile (or shape) of undertows induced by irregular waves.

Table 3.9: Root mean square relative error (ER) of the Eq. (3.58) comparing with the experiment performed under irregular wave actions.

Sources	Test	Case No.	T	H_i	h,	Total	ER
	No		(s)	(cm)	(cm)	No. of	of Eq.
					(31.2)	profiles	(3.58)
Dette and Uliczka		dune without	6.0	106.1	500	4	26.2
(1986)		foreshore					
Okayasu and		2	1.26	5.9	35	6	21.9
Katayama (1992)							
Shimisu and		L2	5.0	76.4	205	3	19.6
Ikeno (1996)							
		L3	5.0	83.4	205	3	31.0
		L5	3.0	73.5	200	4	23.1
		L6	3.0	77.1	200	4	20.6
Rodriguez et al.		C3	6.1	60	750	3	15.3
(1994)							
		C4	5.6	44.3	750	5	21.3
SUPERTANK	ST10	a0509a, a0510a,	3.0	56.6	305	53	23.9
(1994)		a0512a, a0515a,					Ì
		a0517a, a0608a,					
		a0609a, a0611a,			ľ		į
		a0615a					i
		a0617a, a1618a	3.0	56.6	290	12	31.5
		a0710a, a0711a,	4.5	56.6	305	60	25.6
	<u> </u>	a0713a, a0715a,				1	
		a0717a, a0808a,			1		
		a0809a, a0812a,					
		a0814a, a0815a					
		a0908a	6.0	56.6	305	6	18.3
		a0910a	5.0	35.4	305	6	20.5
		a0911a	3.0	49.5	305	6	30.0
		a0912a	3.0	63.6	305	6	31.3
	<u> </u>	a0914a	4.5	63.6	305	6	27.3

Table 3.9 (cont.): Root mean square relative error (ER) of the Eq. (3.58) comparing with the experiment performed under irregular wave actions.

Sources	Test	Case No.	T	H_i	h,	Total	ER
	No		(s)	(cm)	(cm)	No. of	of Eq.
					(****)	profiles	(3.58)
SUPERTANK (1994)	ST20	a1212a	8.0	28.3	305	6	11.0
		a1215a	8.0	42.4	305	7	20.5
		a1217a	8.0	56.6	305	6	23.3
		a1310a	3.0	28.3	305	5	11.2
		a1313a	3.0	42.4	305	7	27.7
		a1315a	3.0	56.6	305	7	32.2
	ST30	a1408a, a1409a, a1410a, a1411a, a1413b	8.0	28.3	305	31	8.9
		al415a, al416a, al417a	8.0	35.4	305	21	15.2
		a1507b, a1508a, a1510a, a1511a, a1513b	9.0	28.3	305	32	10.0
		a1515a, a1516a	9.0	35.4	290	14	20.4
		a1607b	6.0	28.3	305	7	10.8
		a1608a	7.0	35.4	305	7	12.2
		a1610a	7.0	28.3	305	7	15.0
		a1611a	10.0	28.3	305	7	13.5
	ST40	a1909b	3.0	28.3	305	5	12.0
		а2007ь	5.0	49.5	305	5	18.9
		a2008a	5.0	49.5	305	5	21.6
		a2015a	5/8	35.4	305	5	7.7
		a2017a	8.0	35.4	305	5	13.6
		a2018a	5.0	35.4	305	5	16.8
		a2107b	5/8	49.5	305	5	7.0
<u></u>	_	a2108a	5/8	49.5	305	5	8.7
		a2109a	3/7	49.5	305	5	5.8
	_	a2111a	3/7	28.3	305	5	14.3
		a2112a	3/7	49.5	305	5	5.5
	ST50	a2208a, a2209a	3.0	56.6	290	10	5.8
		a2209b	4.5	56.6	290	5	7.9
	_	a2210a	6.0	56.6	290	6	3.3
		a2213b	3.0	56.6	320	7	19.8
		a2214a	4.5	49.5	320	7	18.0
		a2215a	6.0	49.5	320	6	15.6
		a2216a	3/7	35.4	320	7	21.7

Table 3.9 (cont.): Root mean square relative error (ER) of the Eq. (3.58) comparing with the experiment performed under irregular wave actions.

Sources	Test	Case No.	T	H_i	h_i	Total	ER
	No		(s)	(cm)	(cm)	No. of	of Eq.
				, ,		profiles	(3.58)
SUPERTANK	ST60	a2308a, a2308b,	3.0	49.5	320	18	16.5
(1994)		a2309a					
		a2310a, a2311a,	4.5	49.5	320	18	15.3
		a2311b					
		a2313b, a2315a,	6.0	35.4	335	15	21.6
		a2316a					
	ST70	a2609a, a2610a,	4.5	49.5	290	12	5.8
		a2610b					
		a2613a -	4.5	49.5	305	4	9.4
		a2614a, a2615a	4.5	70.7	305	11	6.6
		a2617b	4.5	56.6	335	7	11.7
		a2618a, a2618b	4.5	49.5	335	14	11.7
	ST80	a2708a, a2708b,	4.5	49.5	335	20	31.8
		a2709a					
	ST90	a2809b, a2810a,	3.0	49.5	335	20	22.3
		a2811a					
	STAO	a2816b	3.0	49.5	335	7	17.8
	STCO	s0209b, s0210a,	3.0	56.6	274	12	9.6
		s0211a					
	STDO	s0309a, s0310a,	3.0	49.5	305	15	10.7
		s0311a					
	STJO	s0913a, s0914a,	3.0	49.5	305	18	20.6
		s0915a, s0916a		İ			
		s0917a, s1008a,	8.0	35.4	305	30	14.3
		s1008b, s1009a,			1	ļ	
		si011a, s1013a					
	Total	119				675	20.5

Table 3.10: Summary of rms relative error (ER) of each data source.

Sources	Apparatus	Bed condition	Total No.	ER
			of profiles	
Dette and Uliczka (1986)	large-scale	sandy beach	4	26.2
Okayasu and Katayama (1992)	small-scale	plane beach	6	21.9
SUPERTANK (1994)	large-scale	sandy beach	643	19.1
Shimisu and Ikeno (1996)	large-scale	sandy beach	14	23.1
Rodriguez et al. (1994)	field	sandy beach	8	18.7
Total			675	20.5

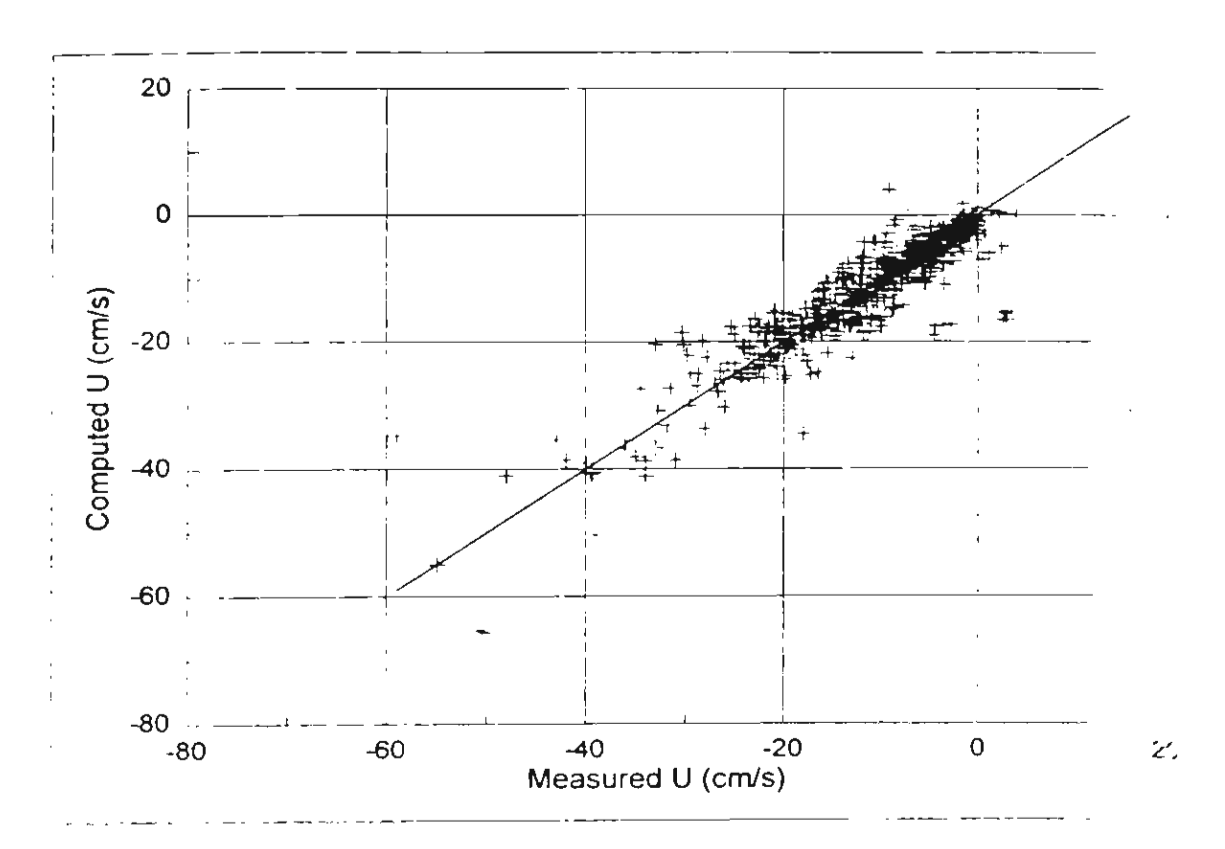


Figure 3.15: Comparison between measured and computed the undertow velocity. / induced by irregular wave actions (measured data from Table 3.8).

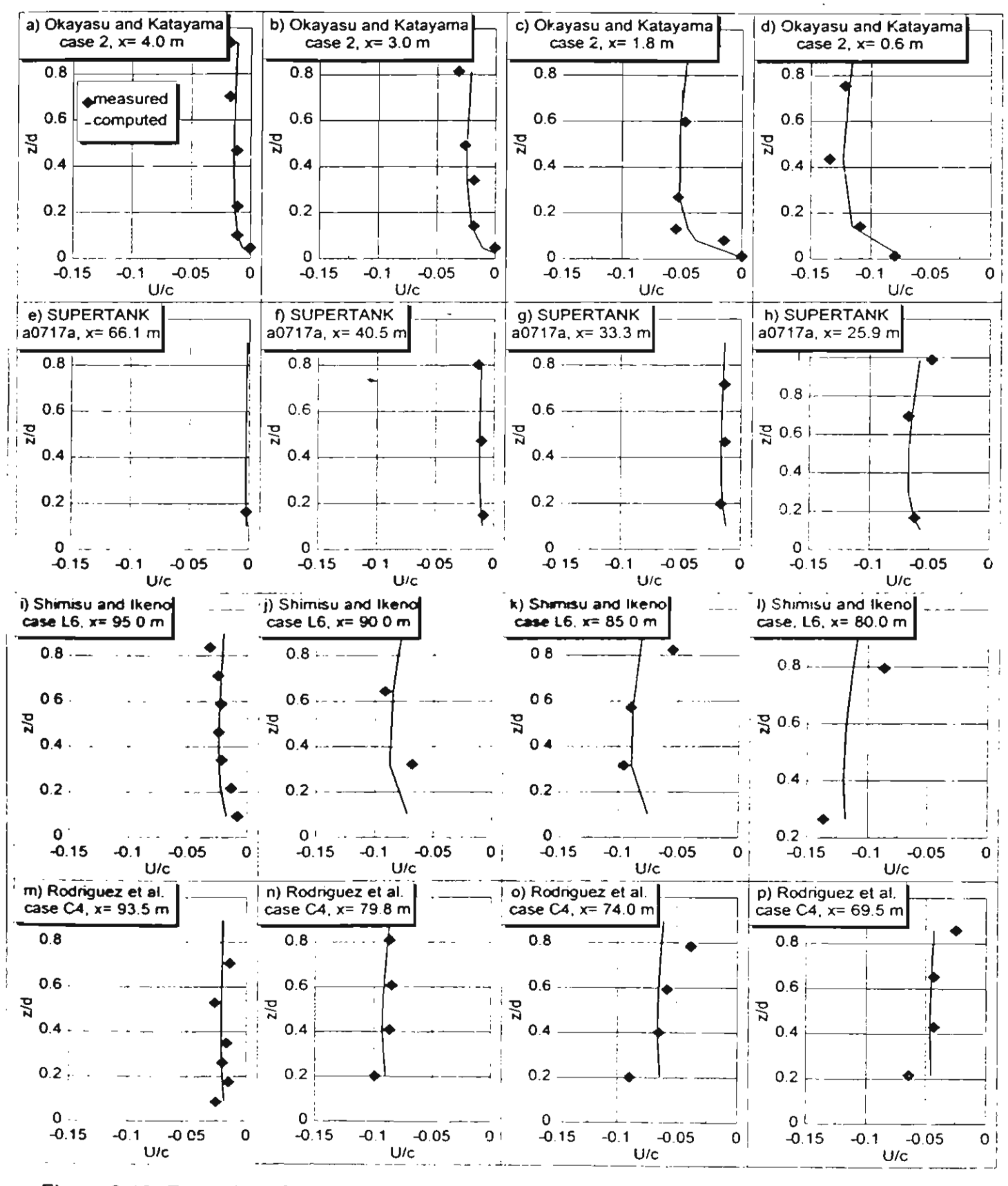


Figure 3.16: Examples of measured and computed undertow profiles induced by irregular wave actions (measured data from Table 3.8).

3.2.2 Mean undertow velocity

Irregular wave breaking is more complex than regular wave breaking. The highest wave tends to break at greatest distance from the shore. Since the width of surf zone and the transition zone varies with each individual wave, the influence of the transition zone is not significantly observed in the surf zone of irregular wave (Nairn et al., 1990). To make the formula simple, the influence of the transition zone for irregular wave is excluded in this study. Therefore Eq. (3.53) is modified to compute U_m of irregular waves.

$$U_{m} = -k_{23} \frac{gH_{mnx}^{2}}{ch} - k_{24} \frac{Q_{h}cH_{mnx}}{h}$$
 (3.59)

where Q_b is the fraction of breaking wave which can be computed from Eqs. (3.56) and (3.57), k_{23} and k_{24} are the coefficients which can be determined by the model calibration.

The measured undertow profile data, under irregular wave actions, from 5 sources (see Table 3.8) are used to calibrate the model.

The undertow profile is computed from Eq. (3.59). Trial simulations indicated that $k_{23} = 0.57$ and $k_{24} = 0.50$ give good agreement between measured and computed undertows. Fig. 3.17 shows the verification results of all measuring points. Figs. 3.18 and 3.19 show the examples of measured and computed the mean undertow velocities.

Table 3.11: Summary of collected experimental data and rms relative error (ER) of the Eq. (3.59).

Sources	Apparatus	Total No.	Total No.	ER of
		of cases	of profiles	Eq. (3.59)
Dette and Uliczka (1986)	large-scale	1	4	27.2
Okayasu and Katayama (1992)	small-scale	1	6	28.8
SUPERTANK (1994)	large-scale	111	643	43.7
Shimisu and Ikeno (1996)	large-scale	4	14	30.3
Rodriguez et al. (1994)	field	2	8	48.9
Total		119	675	42.6

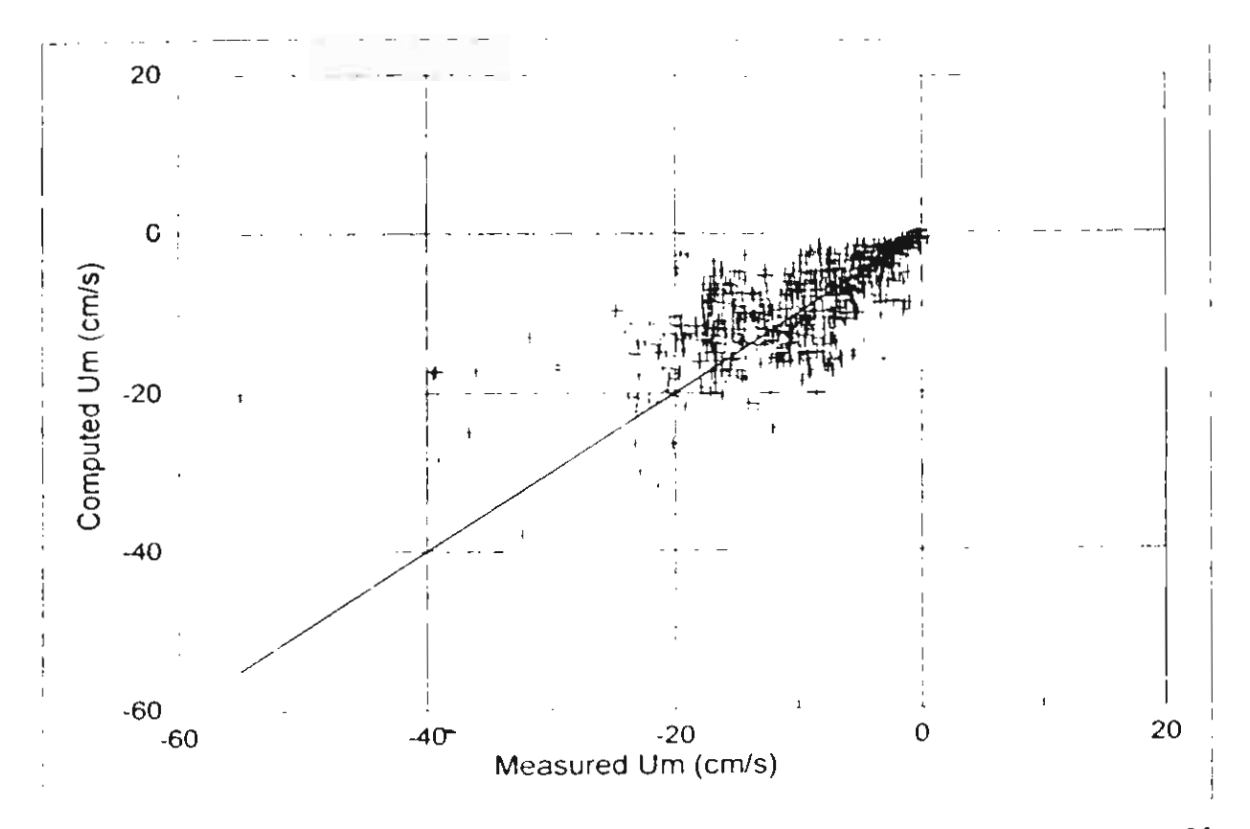


Figure 3.17: Comparison between measured and computed mean undertow velocity, $U_{\it m}$ induced by irregular wave actions (measured data from Table 3.8).

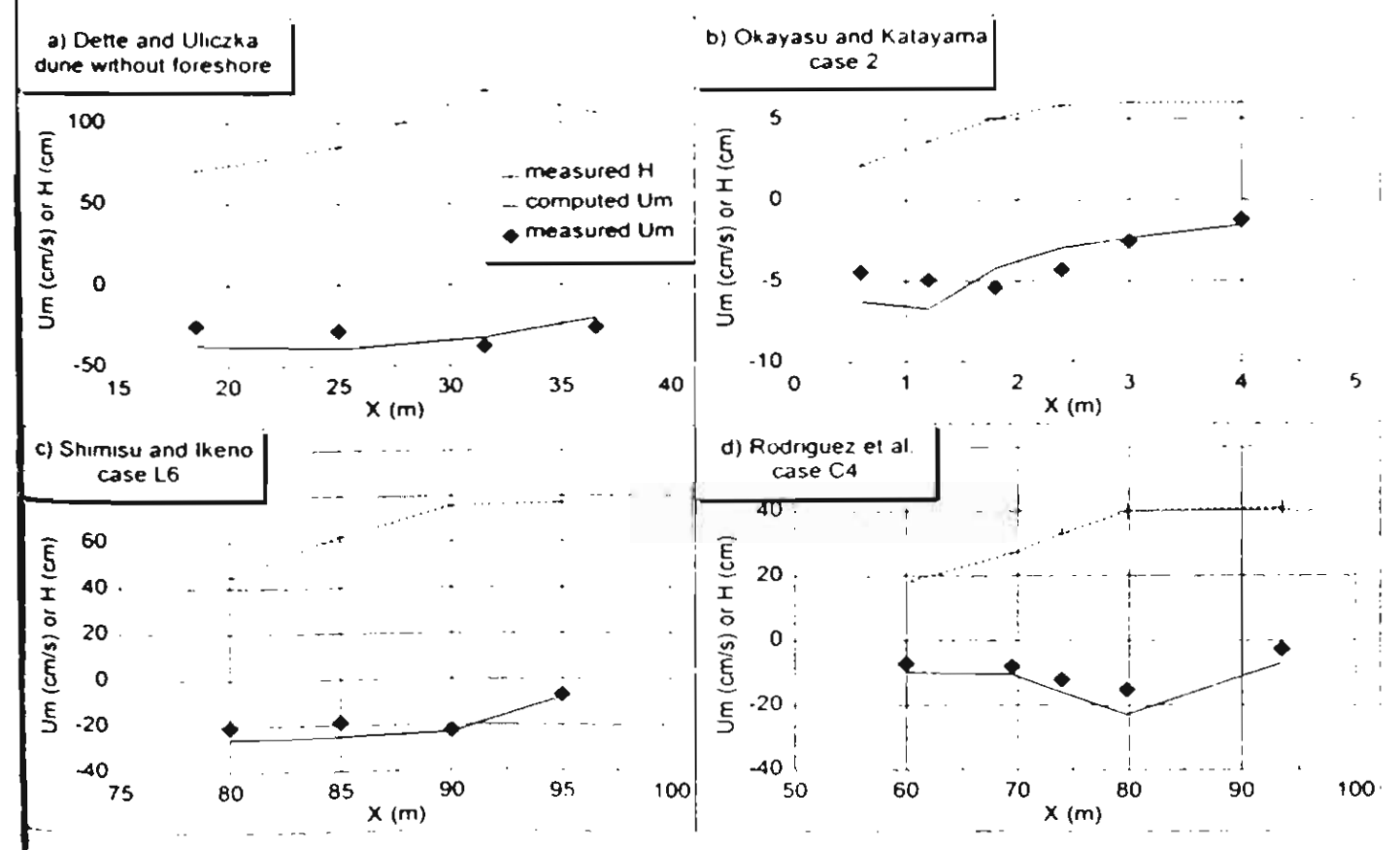


Figure 3.18: Examples of cross-shore variations of measured and computed mean undertow velocity, $U_{\rm m}$, induced by irregular wave actions (measured data from Table 3.8, except SUPERTANK data).

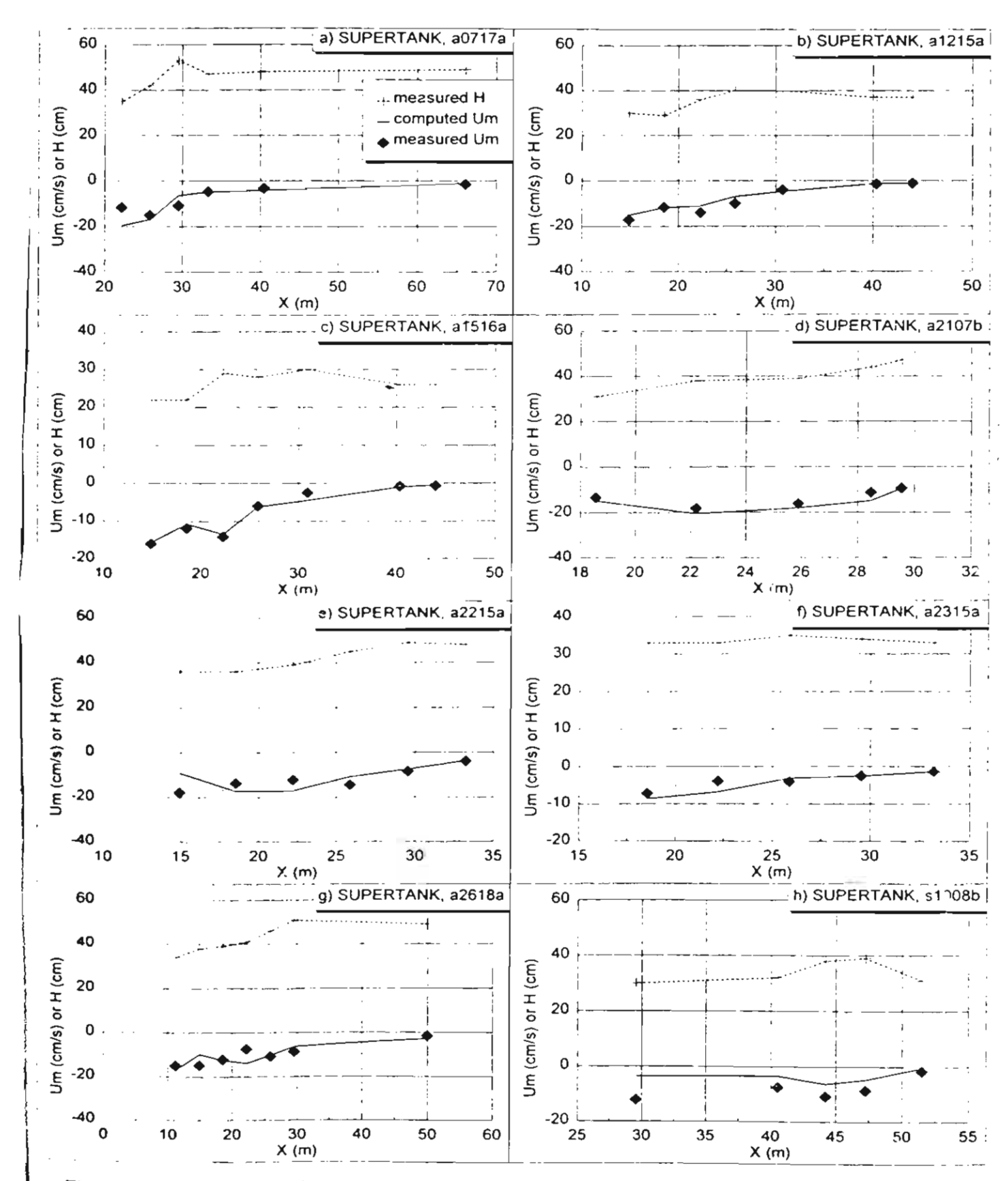


Figure 3.19: Examples of cross-shore variations of measured and computed mean undertow velocity, U_{m} , induced by irregular wave actions (measured data from SUPERTANK, 1994).

Chapter 4: MODELS COMPARISONS

Due to the complication of the wave breaking mechanism, most of the hydrodynamics models have to be based on an empirical or semi-empirical formula calibrated from the laboratory data. Over the past century, many models have been proposed for computing the initiation of breaking wave heights, wave height transformation, and undertow velocity. This often causes confusion in the profession in the selection of models for solving engineering problems. Moreover, no direct literature has been written to describe clearly the applicability and the accuracy of each formula. Hence, the objective of this study is to examine the validity of each model and find out the proper models that predict well for a wide range of experimental conditions.

The comparison of the existing models of breaker height, wave height, and undertow are presented in sections 4.1 to 4.3, respectively.

4.1 Breaker Height Formulas

The initiation of breaking wave height is an essential requirement for computing wave height transformation. It is also important to the design of coastal structures. Over the past century, many breaker height formulas have been proposed for computing the initiation of breaking wave heights. Hence, the objective of this study is to examine the validity of each formula and find out a proper breaker height formula that predicts well for a wide range of experimental conditions.

Laboratory data of broken wave heights from 24 sources, including 574 cases, have been collected for examination of the formulas. The data cover a wide range of wave and bottom slope conditions (deepwater wave steepness ranging between 0.001 and 0.100, and bottom slope ranging between 0 and 0.44). The data include 3 types of beach conditions, i.e., plane beach, barred beach, and stepped beach. All experiments were performed under regular wave actions and the wave propagates normally to the beach. The experiments were performed in both small-scale and large-scale wave flumes. The experiment of Maruyama et al. (1983) was performed in large-scale wave flume and other experiments were performed in small-scale wave flumes. A summary of the collected experimental data is given in Table 4.1.

This section is divided into two main parts. The first part presents the existing breaker height formulas. The second part is an examination of the all formulas to identify the best one.

4.1.1 Description of the breaker height formulas

The majority of the existing formulas represent a relationship between the breaking wave height (H_b) and the variables at the breaking or deepwater conditions, i.e., water depth at breaking (h_b) , wavelength at breaking (L_b) , bottom siope (m), deepwater wavelength (L_a) , and deepwater wave height (H_a) . A total of 23 existing breaker height formulas are examined in this study. A brief review of the 23 breaker wave height formulas, that may be used in general cases, are described as follows.

a) McCowan (1894), hereafter referred to as MC94, derived a limit of breaking wave in water of constant depth based on solitary wave theory and proposed that the breaking will occur when

$$H_b = 0.78h_b {(4.1)}$$

where H_b is the breaking wave height, h_b is the water depth at the breaking point.

b) Miche (1944), hereafter referred to as MI44, developed the semi-theoretical breaking criterion for periodic waves in finite water depth and proposed the limiting wave steepness as a function of water depth to wavelength ratio.

$$H_b = 0.142L_b \tanh\left(\frac{2\pi h_b}{L_b}\right) \tag{4.2}$$

where L_b is the wavelength at the breaking point. Danel (1952) suggested changing the coefficient from 0.142 to be 0.12 when applying to the horizontal bottom.

c) Le Mehaute and Koh (1967), hereafter referred to as MK67, proposed an empirical formula based on three sources of the experimental data (Suquet, 1950; Iversen, 1952; and Hamada, 1963). The experiments cover a range of 1/50 < m < 1/5 and 0.002 $< H_o / L_o <$ 0.093.

$$H_b = 0.76H_o \left(\frac{H_o}{L_o}\right)^{-1/4} m^{1/7} \tag{4.3}$$

where H_o is the deepwater wave height, L_o is the deepwater wavelength, and m is the local bottom slope.

Table 4.1: Summary of collected experimental data used to validate the formulas.

Sources	No. of cases	Beach conditions	Bottom slopes (m)	H_o/L_o
Galvin (1969)*	19	plane beach	0.05-0.20	0.001-0.051
Hansen and Svendsen (1979)	17	plane beach	0.03	0.002-0.069
Hattori and Aono (1985)	3	stepped beach	0.00	0.006-0.021
Harikawa and Kua (1066)	98	plane beach	0.01-0.05	0.006-0.073
Horikawa and Kuo (1966)	60	stepped beach	0.00	0.007-0.100
Hwung et al. (1992)	2	plane beach	0.07	0.026-0.048
Iversen (1952)*	63	plane beach	0.02-0.10	0.003-0.080
lwagaki et al. (1974)	39	plane beach	0.03-0.10	0.005-0.074
Maruyama et al. (1983)*	1	plane beach	0.03	0.091
Mizuguchi (1980)*	1	plane beach	0.10	0.045
Nadaoka et al. (1982)	12	plane beach	0.05	0.013-0.080
	1	plane beach	0.05	0.027
Nagayama (1983)	5	barred beach	0.05	0.025-0.051
	6	stepped beach	0.00-0.05	0.025-0.055
Okayasu et al. (1986)	2	plane beach	0.05	0.023-0.025
Okayasu et al. (1988)	10	plane beach	0.03-0.05	0.009-0.054
Ozaki et al. (1977)	20	plane beach	0.10	0.005-0.060
Saeki and Sasaki (1973)*	2	plane beach	0.02	0.005-0.039
Sato et al. (1988)	3	plane beach	0.05	0.031-0.050
Sato et al. (1989)	2	plane beach	0.03	0.019-0.036
Sato et al. (1990)	7	plane beach	0.05	0.003-0.073
Singamsetti and Wind (1980)*	95	plane beach	0.03-0.20	0.018-0.079
Smith and Vasua (1000)*	5	plane beach	0.03	0.009-0.092
Smith and Kraus (1990)*	75	barred beach	0.03-0.44	0.008-0.096
Stive (1984)	2	plane beach	0.03	0.010-0.032
Ting and Kirby (1994)	2	plane beach	0.03	0.002-0.020
Visser (1982)*	7	plane beach	0.05-0.10	0.014-0.079
Walker (1974)*	15	plane beach	0.03	0.001-0.037
Total	574		0.00-0.44	0.001-0.100

^{*} data from Smith and Kraus (1990)